DIRECT TORQUE CONTROL OF PERMANENT MAGNET SYNCHRONOUS MOTORS WITH NON-SINUSOIDAL BACK-EMF

A Dissertation

by

SALIH BARIS OZTURK

Submitted to the Office of Graduate Studies of
Texas A&M University
in partial fulfillment of the requirements for the degree of

DOCTOR OF PHILOSOPHY

May 2008

Major Subject: Electrical Engineering

DIRECT TORQUE CONTROL OF PERMANENT MAGNET SYNCHRONOUS MOTORS WITH NON-SINUSOIDAL BACK-EMF

A Dissertation

by

SALIH BARIS OZTURK

Submitted to the Office of Graduate Studies of
Texas A&M University
in partial fulfillment of the requirements for the degree of

DOCTOR OF PHILOSOPHY

Approved by:

Chair of Committee,	Hamid A. Toliyat
Committee Members,	Prasat N. Enjeti
	S. P. Bhattacharyya
	Reza Langari
Head of Department,	Costas N. Georghiades

May 2008

Major Subject: Electrical Engineering

ABSTRACT

Direct Torque Control of Permanent Magnet Synchronous Motors With Non-Sinusoidal Back-EMF. (May 2008)

Salih Baris Ozturk, B.S., Istanbul Technical University, Istanbul, Turkey;

M.S., Texas A&M University, College Station

Chair of Advisory Committee: Dr. Hamid A. Toliyat

This work presents the direct torque control (DTC) techniques, implemented in four- and six-switch inverter, for brushless dc (BLDC) motors with non-sinusoidal back-EMF using two and three-phase conduction modes. First of all, the classical direct torque control of permanent magnet synchronous motor (PMSM) with sinusoidal back-EMF is discussed in detail. Secondly, the proposed two-phase conduction mode for DTC of BLDC motors is introduced in the constant torque region. In this control scheme, only two phases conduct at any instant of time using a six-switch inverter. By properly selecting the inverter voltage space vectors of the two-phase conduction mode from a simple look-up table the desired quasi-square wave current is obtained. Therefore, it is possible to achieve DTC of a BLDC motor drive with faster torque response while the stator flux linkage amplitude is deliberately kept almost constant by ignoring the flux control in the constant torque region.

Third, the avarege current controlled boost power factor correction (PFC) method is applied to the previously discussed proposed DTC of BLDC motor drive in the constant torque region. The test results verify that the proposed PFC for DTC of BLDC

motor drive improves the power factor from 0.77 to about 0.9997 irrespective of the load.

Fourth, the DTC technique for BLDC motor using four-switch inverter in the constant torque region is studied. For effective torque control in two phase conduction mode, a novel switching pattern incorporating the voltage vector look-up table is designed and implemented for four-switch inverter to produce the desired torque characteristics. As a result, it is possible to achieve two-phase conduction DTC of a BLDC motor drive using four-switch inverter with faster torque response due to the fact that the voltage space vectors are directly controlled..

Finally, the position sensorless direct torque and indirect flux control (DTIFC) of BLDC motor with non-sinusoidal back-EMF has been extensively investigated using three-phase conduction scheme with six-switch inverter. In this work, a novel and simple approach to achieve a low-frequency torque ripple-free direct torque control with maximum efficiency based on dq reference frame similar to permanent magnet synchronous motor (PMSM) drives is presented.

To my mother and father

ACKNOWLEDGMENTS

This dissertation, while an induvidual work, would not be possible without the kind assistance, encouragement and support of countless people, whom I want to thank.

I would like to thank, first and foremost, my advisor, Prof. Hamid A. Toliyat, for his support, continuous help, patience, understanding and willingness throughout the period of the research to which this dissertation relates. Moreover, spending his precious time with me is appreciated far more than I have words to express. I am very grateful to work with such a knowledgeable and insightful professor. Before pursuing graduate education in the USA I spent a great amount of time finding a good school, and more importantly a quality professor to work with. Even before working with Prof. Toliyat I realized that the person you work with is more important than the prestige of the university you attend. The education he provided me at Texas A&M University is priceless.

I would also like to thank the members of my graduate study committee, Prof. Prasad Enjeti, Prof. S.P. Bhattacharyya, and Prof. Reza Langari for accepting my request to be a part of the committee even though they had a very busy schedule.

I would like to express my deepest gratitude to my fellow colleagues in the Advanved Electric Machine and Power Electronics Laboratory: Dr. Bilal Akin, Dr. Namhun Kim, Jeihoon Baek, Salman Talebi, Nicolas Frank, Steven Campbell, Anand Balakrishnan, Robert Vartanian, Anil Chakali. I cherish their friendship and the good memories I have had with them since my arrival at Texas A&M University.

Also, I would like to thank to the people who are not participants of our lab but who are my close friends and mentors who helped, guided, assisted and advised me during the completion of this dissertation: Amir Toliyat, Dr. Oh Yang, David Tarbell, and many others whom I may forget to mention here.

I would also like to acknowledge the Electrical Engineering department staff at Texas A&M University: Ms. Tammy Carda, Ms. Linda Currin, Ms. Gayle Travis and many others for providing an enjoyable and educational atmosphere.

Last but not least, I would like to thank my parents for their patience and endless financial, and more importantly, moral support throughout my life. First, I am very grateful to my dad for giving me the opportunity to study abroad to earn a good education. Secondly, I am very grateful to my mother for her patience which gave me a glimpse of how strong she is. Even though they do not show their emotion when I talk to them, I can sense how much they miss me when I am away from them. No matter how far away from home I am, they are always there to support and assist me. Finally, to my parents, no words can express my gratitude for you and sacrifices you have made for me.

TABLE OF CONTENTS

Page

ABSTRACT iii

DEDICATION v

ACKNOWLEDGMENTS vi

TABLE OF CONTENTS viii

LIST OF FIGURES xi

LIST OF TABLES xvii

CHAPTER

I INTRODUCTION: DIRECT TORQUE CONTROL OF PERMANENT MAGNET SYNCHRONOUS MOTOR WITH SINUSOIDAL BACK-EMF 1

1.1 Introduction and Literature Review 1
1.2 Principles of Classical DTC of PMSM Drive 11
1.2.1 Torque Control Strategy in DTC of PMSM Drive 11
1.2.2 Flux Control Strategy in DTC of PMSM Drive 16
1.2.3 Voltage Vector Selection in DTC of PMSM Drive 19
1.3 Control Strategy of DTC of PMSM Drive 24

II DIRECT TORQUE CONTROL OF BRUSHLESS DC MOTOR WITH NON-SINUSOIDAL BACK-EMF USING TWO-PHASE CONDUCTION MODE 29

2.1 Introduction 29
2.2 Principles of the Proposed Direct Torque Control (DTC) Technique 35
2.2.1 Control of Electromagnetic Torque by Selecting the Proper Stator Voltage Space Vector 43
2.3 Simulation Results 48
2.4 Experimental Results 56
2.5 Conclusion 59

CHAPTER Page

III POWER FACTOR CORRECTION OF DIRECT TORQUE CONTROLLED BRUSHLESS DC MOTOR WITH NON-SINUSOIDAL BACK-EMF USING TWO-PHASE CONDUCTION MODE 60

3.1 Introduction 60
3.2 The Average Current Control Boost PFC with Feed-Forward Voltage Compensation 63
3.2.1 Calculation of Feed-Forward Voltage Component *C* and Multiplier Gain K_m 64
3.3 Experimental Results 67
3.4 Conclusion 74

IV DIRECT TORQUE CONTROL OF FOUR-SWITCH BRUSHLESS DC MOTOR WITH NON-SINUSOIDAL BACK-EMF USING TWO-PHASE CONDUCTION MODE 75

4.1 Introduction 75
4.2 Topology of the Conventional Four-Switch Three-Phase AC Motor Drive 78
4.2.1 Principles of the Conventional Four-Switch Inverter Scheme 78
4.2.2 Applicability of the Conventional Method to the BLDC Motor Drive 80
4.3 The Proposed Four-Switch Direct Torque Control of BLDC Motor Drive 82
4.3.1 Principles of the Proposed Four-Switch Inverter Scheme 82
4.3.2 Control of Electromagnetic Torque by Selecting the Proper Stator Voltage Space Vectors 88
4.3.3 Torque Control Strategies of the Uncontrolled Phase-*c* 91
4.4 Simulation Results 96
4.5 Experimental Results 103
4.6 Conclusion 106

V SENSORLESS DIRECT TORQUE AND INDIRECT FLUX CONTROL OF BRUSHLESS DC MOTOR WITH NON-SINUSOIDAL BACK-EMF USING THREE-PHASE CONDUCTION MODE 108

5.1 Introduction 108
5.2 The Proposed Line-to-Line Clarke and Park Transformations in 2x2 Matrix Form 115
5.2.1 Conventional Park Transformation for Balanced Systems 115

CHAPTER Page

5.2.2 The Proposed Line-to-Line Clarke and Park Transformations for Balanced Systems 117
5.3 The Proposed Sensorless DTC of BLDC Drive Using Three-Phase Conduction 120
5.3.1 Principles of the Proposed Method 120
5.3.2 Electromagnetic Torque Estimation in *dq* and *ba–ca* Reference Frames 127
5.3.3 Control of Stator Flux Linkage Amplitude 128
5.3.4 Control of Stator Flux Linkage Rotation and Voltage Vector Selection for DTC of BLDC Motor Drive 131
5.3.5 Estimation of Electrical Rotor Position 132
5.4 Simulation Results 134
5.5 Experimental Results 144
5.6 Conclusion 150

VI SUMMARY AND FUTURE WORK 152

REFERENCES 157

APPENDIX A 165

APPENDIX B 167

APPENDIX C 170

APPENDIX D 172

APPENDIX E 174

VITA 177

LIST OF FIGURES

FIGURE Page

1.1. Eight possible voltage space vectors obtained from VSI 2

1.2. Circular trajectory of stator flux linkage in the stationary DQ–plane 3

1.3. Phasor diagram of a non-saliet pole synchronous machine in the motoring mode 12

1.4. Electrical circuit diagram of a non-salient synchronous machine at constant frequency (speed) 12

1.5. Rotor and stator flux linkage space vectors (rotor flux is lagging stator flux) 15

1.6. Incremental stator flux linkage space vector representation in the DQ-plane 16

1.7. Representation of direct and indirect components of the stator flux linkage vector 18

1.8. Voltage Source Inverter (VSI) connected to the R-L load 20

1.9. Voltage vector selection when the stator flux vector is located in sector *i* 22

1.10. Basic block diagram for DTC of PMSM drive 25

2.1. Actual (solid curved line) and ideal (straight dotted line) stator flux linkage trajectories, representation of two-phase voltage space vectors in the stationary $\alpha\beta$–axes reference frame 42

2.2. Representation of two-phase switching states of the inverter voltage space vectors for a BLDC motor 44

2.3. Overall block diagram of the two-phase conduction DTC of a BLDC motor drive in the constant torque region. 46

FIGURE Page

2.4. Simulated open-loop stator flux linkage trajectory under the two-phase conduction DTC of a BLDC motor drive at no load torque (speed + torque control) 49

2.5. Simulated open-loop stator flux linkage trajectory under the two-phase conduction DTC of a BLDC motor drive at 1.2835 N·m load torque (speed + torque control) 50

2.6. Simulated phase–*a* voltage under 1.2 N·m load when zero voltage vector is used to decrease the torque (only torque control is performed) 51

2.7. Simulated stator flux linkage locus with non-ideal trapezoidal back-EMF under full load (speed + torque + flux control) 52

2.8. Simulated phase–*a* current when flux control is obtained using (2.20) under full load (speed + torque + flux control) 53

2.9. Simulated phase–*a* current when just torque is controlled without flux control under 1.2 N·m load with non-ideal trapezoidal back-EMF (reference torque is 1.225 N·m)....54

2.10. Simulated electromagnetic torque when just torque is controlled without flux control under 1.2 N·m load with non-ideal trapezoidal back-EMF (reference torque is 1.225 N·m)....54

2.11. Simulated phase–*a* voltage when just torque is controlled without flux control under 1.2 N·m load with non-ideal trapezoidal back-EMF (reference torque is 1.225 N·m)....55

2.12. Experimental test-bed. (a) Inverter and DSP control unit. (b) BLDC motor coupled to dynamometer and position encoder (2048 pulse/rev)....57

2.13. (a) Experimental phase–*a* current and (b) electromagnetic torque under 0.2292 N·m (0.2 pu) load 58

3.1. Overall block diagram of the two-phase conduction DTC of a BLDC motor drive with boost PFC in the constant torque region 62

3.2. Experimental test-bed. (a) Inverter, DSP control unit, and boost PFC board. (b) BLDC motor coupled to dynamometer and position encoder (2048 pulse/rev.)....69

FIGURE Page

3.3. Measured steady-state phase–*a* current of two-phase DTC of BLDC motor drive using boost PFC under 0.371 N·m load with 0.573 N·m reference torque. Current: 1.25 A/div. Time base: 7 ms/div.....70

3.4. Measured output dc voltage V_o, line voltage V_{line}, and line current I_{line} without PFC under no load with 0.4 N·m reference torque. (Top) Output dc voltage V_o = 80 V. (Middle) Line voltage V_{line} = 64.53 V_{rms}. (Bottom) Line current I_{line} = 1.122 A. V_o: 20 V/div; I_{line}: 2 A/div; V_{line}: 50 V/div. Time base: 5 ms/div.....71

3.5. Measured steady-state output dc voltage V_o, line voltage V_{line}, and line current I_{line} with PFC under no load with 0.4 N·m reference torque. (Top) Output dc voltage V_o = 80 V. (Middle) Line voltage V_{line} = 25.43 V_{rms}. (Bottom) Line current I_{line} = 2.725 A. V_o: 20 V/div; I_{line}: 5 A/div; V_{line}: 50 V/div. Time base: 5 ms/div.....72

3.6. Measured steady-state output dc voltage V_o, line voltage V_{line}, and line current I_{line} with PFC under 0.371 N·m load torque with 0.573 N·m reference torque. (Top) Output dc voltage V_o = 80 V. (Middle) Line voltage V_{line} = 25.2 V_{rms}. (Bottom) Line current I_{line} = 4.311 A. V_o: 20 V/div; I_{line}: 5 A/div; V_{line}: 50 V/div. Time base: 5 ms/div.....73

4.1. Conventional four-switch voltage vector topology. (a) (0,0) vector, (b) (1,1) vector, (c) (1,0) vector, and (d) (0,1) vector 79

4.2. Actual (realistic) phase back-EMF, current, and phase torque profiles of the three-phase BLDC motor drive with four-switch inverter.....81

4.3. Actual (solid curved lines) and ideal (straight dotted lines) stator flux linkage trajectories, representation of the four-switch two-phase voltage space vectors, and placement of the three hall-effect sensors in the stationary $\alpha\beta$–axes reference frame ($V_{dc\_link} = V_{dc}$).....86

4.4. Representation of two-phase switching states of the four-switch inverter voltage space vectors for a BLDC motor 86

4.5. Proposed four-switch voltage vector topology for two-phase conduction DTC of BLDC motor drives. (a) V_1(1000) vector, (b) V_2(0010) vector, (c) V_3(0110) vector, (d) V_4(0100) vector, (e) V_5(0001) vector, (f) V_6(1001), (g) V_7(0101), and (h) V_0(1010) 87

FIGURE Page

4.6. Individual phase–*a* and –*b* torque control, T_{ea} and T_{eb} , in Sectors 2 and 5 93

4.7. Overall block diagram of the four-switch two-phase conduction DTC of a BLDC motor drive in the constant torque region....94

4.8. Simulated open-loop stator flux linkage trajectory under the four-switch two-phase conduction DTC of a BLDC motor drive at no load torque (speed + torque control) 98

4.9. Simulated open-loop stator flux linkage trajectory under the four-switch two-phase conduction DTC of a BLDC motor drive at 1.2835 N·m load torque (speed + torque control) 98

4.10. Simulated stator flux linkage locus whose reference is chosen from (4.3) under full load (speed + torque + flux control) 99

4.11. Simulated electromagnetic torque using actual *αβ*–axes motor back-EMFs under full load (speed + torque + flux control) 99

4.12. Simulated abc frame phase currents when stator flux reference is obtained from (4.3) under full load (speed + torque + flux control)....101

4.13. Simulated *abc* frame phase currents when just torque is controlled without flux control under 0.5 N·m load using actual back-EMFs (reference torque is 0.51 N·m)....102

4.14. Simulated electromagnetic torque when just torque is controlled without flux control under 0.5 N·m load using actual back-EMFs (reference torque is 0.51 N·m)....103

4.15. Experimental test-bed. (a) Four-switch inverter and DSP control unit. (b) BLDC motor coupled to dynamometer and position encoder (2048 pulse/rev)....104

4.16. Top: Steady-state and transient experimental electromagnetic torque in per-unit under 0.5 N·m load torque (0.5 N·m/div). Bottom: Steady-state and transient experimental *abc* frame phase currents (2 A/div) and time base: 16.07 ms/div....106

5.1. Rotor and stator flux linkages of a BLDC motor in the stationary *αβ*–plane and synchronous *dq*–plane 125

FIGURE Page

5.2. Decagon trajectory of stator flux linkage in the stationary $\alpha\beta$–plane 131

5.3. BLDC motor stator flux linkage estimation with an amplitude limiter 134

5.4. Overall block diagram of the sensorless direct torque and indirect flux control of BLDC motor drive using three-phase conduction mode 135

5.5. Simulated indirectly controlled stator flux linkage trajectory under the sensorless three-phase conduction DTC of a BLDC motor drive at 0.5 N·m load torque ($i_{ds}^{r*} = 0$) 136

5.6. Simulated indirectly controlled stator flux linkage trajectory under the sensorless three-phase conduction DTC of a BLDC motor drive when i_{ds}^{r} is changed from 0 A to -5 A at 0.5 N·m load torque 137

5.7. Steady-state and transient behavior of (a) simulated *ba–ca* frame currents, (b) actual electromagnetic torque, and (c) estimated electromagnetic torque under 0.5 N·m load torque.....138

5.8. Steady-state and transient behavior of (a) estimated electrical rotor position, (b) actual electrical rotor position under 0.5 N·m load torque 141

5.9. Actual *ba–ca* frame back-EMF constants versus electrical rotor position ($k_{ba}(\theta_e)$ and $k_{ca}(\theta_e)$) 142

5.10. Actual *q*– and *d*–axis rotor reference frame back-EMF constants versus electrical rotor position ($k_q(\theta_e)$ and $k_d(\theta_e)$) 143

5.11. Steady-state and transient behavior of the simulated *q*– and *d*–axis rotor reference frame currents when $i_{ds}^{r*} = 0$ under 0.5 N·m load torque.....143

5.12. Experimental test-bed. (a) Inverter and DSP control unit. (b) BLDC motor coupled to dynamometer and position encoder is not used 145

5.13. Steady-state and transient behavior of the experimental (a) *ba–ca* frame currents, and (b) estimated electromagnetic torque under 0.5 N·m load torque. 146

5.14. Experimental indirectly controlled stator flux linkage trajectory under the sensorless three-phase conduction DTC of a BLDC motor drive when $i_{ds}^{r*} = 0$ at 0.5 N·m load torque. 148

FIGURE Page

5.15. Steady-state and transient behavior of the experimental q– and d–axis rotor reference frame currents when $i_{ds}^{r^*} = 0$ under 0.5 N·m load torque. 148

5.16. Steady-state and transient behavior of the actual and estimated electrical rotor positions from top to bottom under 0.5 N·m load torque. 149

A.1. (a) Actual line-to-line back-EMF constants ($k_{ab}(\theta_e)$, $k_{bc}(\theta_e)$ and $k_{ca}(\theta_e)$) and (b) stationary reference frame back-EMF constants ($k_\alpha(\theta_e)$and $k_\beta(\theta_e)$) .165

E.1. Line-to-line back-EMF waveforms (e_{ab}, e_{bc}, and e_{ca}) 174

E.2. α–axis back-EMF (e_α) waveform 176

LIST OF TABLES

TABLE		Page
I	Switching Table for DTC of PMSM Drive	23
II	Two-phase Voltage Vector Selection for BLDC Motor	43
III	Electromagnetic Torque Equations for the Operating Regions	84
IV	Two-Phase Four-Switch Voltage Vector Selection for DTC of BLDC Motor Drive (CCW)	89
V	Voltage Vector Selection in Sectors II and V for Four-Switch DTC of BLDC Motor Drive (CCW)	89
VI	Switching Table for DTC of BLDC Motor Using Three-Phase Conduction	132

CHAPTER I

INTRODUCTION: DIRECT TORQUE CONTROL OF PERMANENT MAGNET SYNCHRONOUS MOTOR WITH SINUSOIDAL BACK-EMF

1.1. Introduction and Literature Review

Today there are basically two types of instantaneous electromagnetic torque-controlled ac drives used for high-performance applications: vector and direct torque control (DTC) drives. The most popular method, vector control was introduced more than 25 years ago in Germany by Hasse [1], Blaske [2], and Leonhard. The vector control method, also called Field Oriented Control (FOC) transforms the motor equations into a coordinate system that rotates in synchronism with the rotor flux vector. Under a constant rotor flux amplitude there is a linear relationship between the control variables and the torque. Transforming the ac motor equations into field coordinates makes the FOC method resemble the decoupled torque production in a separately excited dc motor. Over the years, FOC drives have achieved a high degree of maturity in a wide range of applications. They have established a substantial worldwide market which continues to increase [3].

No later than 20 years ago, when there was still a trend toward standardization of control systems based on the FOC method, direct torque control was introduced in Japan

---

This dissertation follows the style and format of *IEEE Transactions on Industry Applications.*

by Takahashi and Nagochi [4] and also in Germany by Depenbrock [5], [6], [7]. Their innovative studies depart from the idea of coordinate transformation and the analogy with dc motor control. These innovators proposed a method that relies on a bang-bang control instead of a decoupling control which is the characteristic of vector control. Their technique (bang-bang control) works very well with the on-off operation of inverter semiconductor power devices.

After the innovation of the DTC method it has gained much momentum, but in areas of research. So far only one form of a DTC of ac drive has been marketed by an industrial company, but it is expected very soon that other manufacturers will come out with their own DTC drive products [8].

The basic concept behind the DTC of ac drive, as its name implies, is to control the electromagnetic torque and flux linkage directly and independently by the use of six or eight voltage space vectors found in lookup tables. The possible eight voltage space vectors used in DTC are shown in Fig. 1.1 [8].

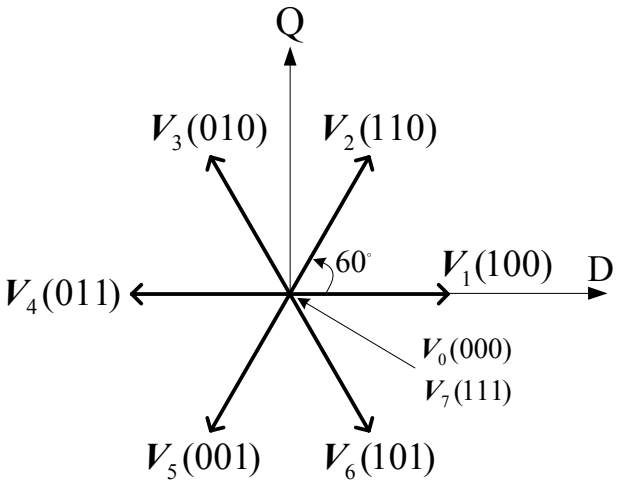

Fig. 1.1. Eight possible voltage space vectors obtained from VSI.

The typical DTC includes two hysteresis controllers, one for torque error correction and one for flux linkage error correction. The hysteresis flux controller makes the stator flux rotate in a circular fashion along the reference trajectory for sinewave ac machines as shown in Fig. 1.2. The hysteresis torque controller tries to keep the motor torque within a pre-defined hysteresis band.

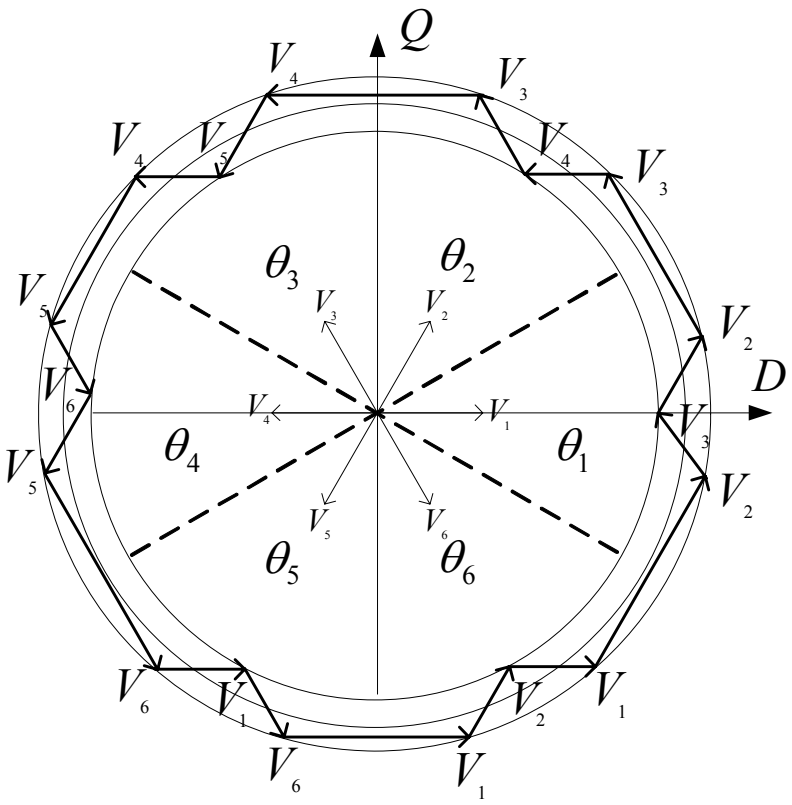

Fig. 1.2. Circular trajectory of stator flux linkage in the stationary DQ−plane.

At every sampling time the voltage vector selection block decides on one of the six possible inverter switching states (S_a, S_b, S_c) to be applied to the motor terminals. The possible outputs of the hysteresis controller and the possible number of switching states in the inverter are finite, so a look-up table can be constructed to choose the

appropriate switching state of the inverter. This selection is a result of both the outputs of the hysteresis controllers and the sector of the stator flux vector in the circular trajectory.

There are many advantages of direct torque control over other high-performance torque control systems such as vector control. Some of these are summarized as follows:

- The only parameter that is required is stator resistance
- The switching commands of the inverter are derived from a look-up table, simplifying the control system and also decreasing the processing time unlike a PWM modulator used in vector control
- Instead of current control loops, stator flux linkage vector and torque estimation are required so that simple hysteresis controllers are used for torque and stator flux linkage control
- Vector transformation is not applied because stator quantities are enough to calculate the torque and stator flux linkage as feedback quantities to be compared with the reference values
- The rotor position, which is essential for torque control in a vector control scheme, is not required in DTC (for induction and synchronous reluctance motor DTC drives)

Once the initial position of the rotor magnetic flux problem is solved for PMSM drives by some initial rotor position estimation techniques or by bringing the rotor to the known position, DTC of the PMSM can be as attractive as DTC of an induction motor. It is also easier to implement and as cost-effective (no position sensor is required) when

compared to vector controlled PMSM drives. The DTC scheme, as its name indicates, is focused on the control of the torque and the stator flux linkage of the motor, therefore, a faster torque response is achieved over vector control. Furthermore, due to the fact that DTC does not need current controller, the time delay caused by the current loop is eliminated.

Even though the DTC technique was originally proposed for the induction machine drive in the late 1980's, its concept has been extended to the other types of ac machine drives recently, such as switched reluctance and synchronous reluctance machines. In the late 90s, DTC techniques for the interior permanent magnet synchronous machine appeared, as reported in [9], [10].

Although there are several advantages of the DTC scheme over vector control, it still has a few drawbacks which are explained below:

- A major drawback of the DTC scheme is the high torque and stator flux linkage ripples. Since the switching state of the inverter is updated once every sampling time, the inverter keeps the same state until the outputs of each hysteresis controller changes states. As a result, large ripples in torque and stator flux linkage occur.
- The switching frequency varies with load torque, rotor speed and the bandwidth of the two hysteresis controllers.
- Stator flux estimation is achieved by integrating the difference between the input voltage and the voltage drop across the stator resistance (by the back-EMF integration as given in (1.9)). The applied voltage on the motor terminal can be

obtained either by using a dc-link voltage sensor, or two voltage sensors connected to the any two phases of the motor terminals. For current sensing there should be two current sensors connected on any two phases of the motor terminals. Offset in the measurements of dc-link voltage and the stator currents might happen, because for current and voltage sensing, however, temperature sensitive devices, such as operational amplifiers, are normally used which can introduce an unwanted dc offset. This offset may introduce large drifts in the stator flux linkage computation (estimation) thus creating an error in torque estimation (torque is proportional to the flux value) which can make the system become unstable.

- The stator flux linkage estimation has a stator resistance, so any variation in the stator resistance introduces error in the stator flux linkage computation, especially at low frequencies. If the magnitude of the applied voltage and back-EMF are low, then any change in the resistance will greatly affect the integration of the back-EMF.
- Because of the constant energy provided from the permanent magnet on the rotor the rotor position of motor will not necessarily be zero at start up. To successfully start the motor under the DTC scheme from any position (without locking the motor at a known position), the initial position of the rotor magnetic flux must be known. Once it is started properly, however, the complete DTC scheme does not explicitly require a position sensor.

From the time the DTC scheme was discovered for ac motor drives, it was always inferior to vector control because of the disadvantages associated with it. The goal is to bring this technology as close to the performance level of vector control and even exceed it while keeping its simple control strategy and cost-effectiveness. As a result, many papers have been presented by several researchers to minimize or overcome the drawbacks of the DTC scheme. Here are some of the works that have been done by researchers to overcome the drawbacks for the most recent ac drive technology using direct torque control:

- Recently, researchers have been working on the torque and flux ripple reduction, and fixing the switching frequency of the DTC system, as reported in [11]–[16]. Additionally, they came up with a multilevel inverter solution in which there are more voltage space vectors available to control the flux and torque. As a consequence, smoother torque can be obtained, as reported in [14] and [15], but by doing so, more power switches are required to achieve a lower ripple and an almost fixed switching frequency, which increases the system cost and complexity. In the literature, a modified DTC scheme with fixed switching frequency and low torque and flux ripple was introduced in [13] and [16]. With this design, however, two PI regulators are required to control the flux and torque and they need to be tuned properly. Very recently Rahman [17] proposed a method for torque and flux ripple reduction in interior permanent magnet synchronous machines under an almost fixed switching frequency without using

any additional regulators. This method is a modified version of the previously discovered method for the induction machine by the authors in [18].

- Stator flux linkage estimation by the integration of the back-EMF should be reset regularly to reduce the effect of the dc offset error. There has been a few compensation techniques related to this phenomenon proposed in the literature [19]–[21] and [22]. Chapuis et al. [19] introduced a technique to eliminate the dc offset, but a constant level of dc offset is assumed which is usually not the case. In papers [19]–[21] and [22], low-pass filters (LPFs) have been introduced to estimate the stator flux linkage. In [19], a programmable cascaded LPF was proposed instead of the single-stage integrator to help decrease the dc offset error more than the single-stage integrator for induction motor drives. More recently, Rahman [23] has reached an approach like [19] with further investigation and implementation for the compensation of dc offset error in a direct controlled interior permanent magnet (IPM) synchronous motor drive. It has been claimed and proven with simulation and experimental results that programmable cascaded LPFs can also be adopted to replace the single-stage integrator and compensate for the effect of dc offsets in a direct-torque-controlled IPM synchronous motor drive, improving the performance of the drive.
- The voltage drop in the stator resistance is very large when the motor runs at low frequency such that any small deviations in stator resistance from the one used in the estimation of the stator flux linkage creates large errors between the reference and actual stator flux linkage vector. This also affects the torque estimation as

well. Due to these errors, the drive can easily go unstable when operating at low speeds. The worst case scenario might happen at low speed under a very high load. A handful of researchers have recently pointed to the issue of stator resistance variation for the induction machine. For example, fuzzy and proportional-integral (PI) stator resistance estimators have been developed and compared for a DTC induction machine based on the error between the reference current and the actual one by Mir et al. [24]. On the other hand, they did not show any detail on how to obtain the reference current for the stator resistance estimation. Additionally, some stability problems of the fuzzy estimator were observed when the torque reference value was small. As reported in [25], fuzzy logic based stator resistance observers are introduced for induction motor. Even though it is an open-loop controller based on fuzzy rules, the accuracy of estimating the stator resistance is about 5% and many fuzzy rules are necessary. This resulted in having to conduct handful numbers of extensive experiments to create the fuzzy rules resulting in difficulty in implementation. Lee and Krishnan [26] contributed a work related to the stator resistance estimation of the DTC induction motor drive by a PI regulator. An instability issue caused by the stator estimation error in the stator resistance, the mathematical relationships between stator current, torque and flux commands, and the machine parameters are also analyzed in their work. The stator configuration of all ac machines is almost the same, so the stator resistance variation problem still exists for permanent magnet synchronous motors. Rahman et al. [27] reported a method, for stator resistance

estimation by PI regulation based on the error in flux linkage. It is claimed that any variation in the stator resistance of the PM synchronous machine will cause a change in the amplitude of the actual flux linkage. A PI controller works in parallel with the hysteresis flux controller of the DTC such that it tracks the stator resistance by eliminating the error in the command and the actual flux linkage. One problem with this method was that the rotor position was necessary to calculate the flux linkage. Later on the same author proposed a similar method but this time the PI stator resistance estimator was able to track the change of the stator resistance without requiring any position information.

- The back-EMF integration for the stator flux linkage calculation, which runs continuously, requires a knowledge of the initial stator flux position, $\lambda_{s|_{t=0}}$, at start up. In order to start the motor without going in the wrong direction, assuming the stator current is zero at the start, only the rotor magnetic flux linkage should be considered as an initial flux linkage value in the integration formula. The next step is to find its position in the circular trajectory. The initial position of the rotor is not desired to be sensed by position sensors due to their cost and bulky characteristics, therefore some sort of initial position sensing methods are required for permanent magnet synchronous motor DTC applications. A number of works, [28]–[39], have been proposed recently for the detection of the initial rotor position estimation at standstill for different types of PM motors. Common problems of these methods include: most of them fail at standstill because the rotor magnet does not induce any voltage, so no

information of the magnetization is available; position estimation is load dependent; excessive computation and hardware are required; instead of a simple voltage vector selection method used in the DTC scheme, those estimation techniques need one or more pulse width-modulation (PWM) current controllers. Recently, a better solution was introduced for the rotor position estimation. It is accomplished by applying high-frequency voltage to the motor, as reported in [37]–[39]. This approach is adapted to the DTC of interior permanent magnet motors for initial position estimation by Rahman et. al. [23].

1.2. Principles of Classical DTC of PMSM Drive

The basic idea of direct torque control is to choose the appropriate stator voltage vector out of eight possible inverter states (according to the difference between the reference and actual torque and flux linkage) so that the stator flux linkage vector rotates along the stator reference frame (DQ frame) trajectory and produces the desired torque. The torque control strategy in the direct torque control of a PM synchronous motor is explained in Section 1.2.1. The flux control is discussed following the torque control section.

1.2.1. Torque Control Strategy in DTC of PMSM Drive

Before going through the control principles of DTC for PMSMs, an expression for the torque as a function of the stator and rotor flux will be developed. The torque equation used for DTC of PMSM drives can be derived from the phasor diagram of permanent magnet synchronous motor shown in Fig. 1.3.

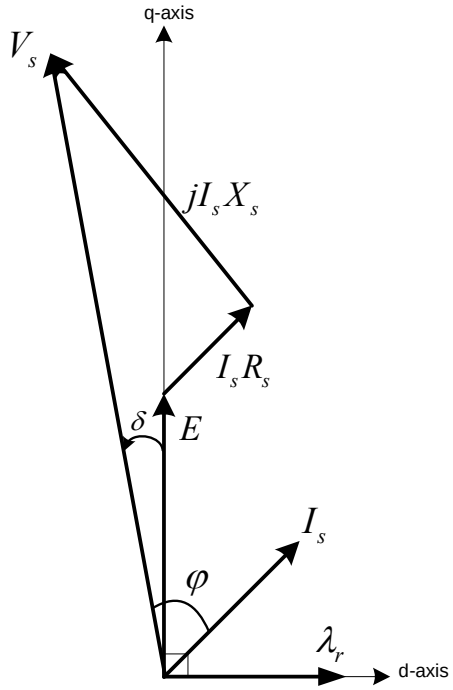

Fig. 1.3. Phasor diagram of a non-salient pole synchronous machine in the motoring mode.

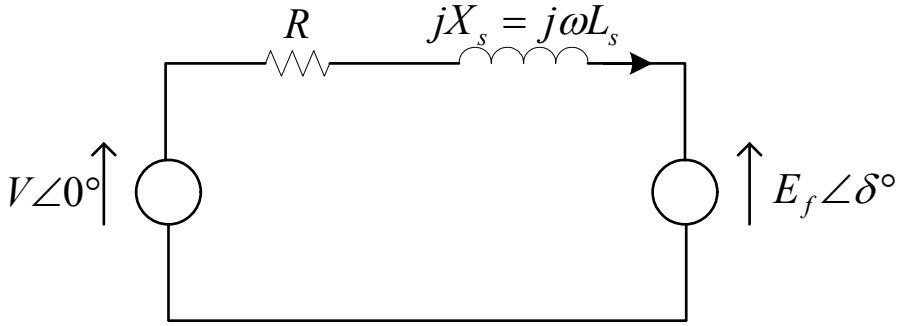

Fig. 1.4. Electrical circuit diagram of a non-salient synchronous machine at constant frequency (speed).

When the machine is loaded through the shaft, the motor will take real power. The rotor will then fall behind the stator rotating field. From the circuit diagram, shown in Fig. 1.4, the motor current expression can be written as

$$I_s = \frac{V_s\angle 0 - E\angle\delta}{R_s + jX_s} = \frac{V_s\angle 0 - E\angle\delta}{|Z_s|\angle\varphi} \tag{1.1}$$

where $|Z_s| = \sqrt{R_s^{\,2} + X_s^{\,2}}$, also $X_s = \omega_e L_s$

and $\varphi = \tan^{-1}\left(\frac{X_s}{R_s}\right)$

Assuming a reasonable speed such that the X_s term is higher than the resistance R_s such that R_s can be neglected, then $|Z_s| \approx X_s$ and $\varphi \approx \frac{\pi}{2}$. I_s can then be rewritten as

$$I_s = \frac{V_s\angle 0}{X_s} - \frac{E\angle\delta - \frac{\pi}{2}}{X_s} \tag{1.2}$$

Such that the real part of I_s is

$$\begin{aligned} \mathrm{Re}[I_s] = I_s\cos\varphi &= \frac{V_s}{X_s}\cos\left(-\frac{\pi}{2}\right) - \frac{E}{X_s}\cos\left(\delta - \frac{\pi}{2}\right) \\ &= -\frac{E}{X_s}\cos\left(\delta - \frac{\pi}{2}\right) = -\frac{E}{X_s}\sin\delta \end{aligned} \tag{1.3}$$

The developed power is given by

$$P_i = 3V_s\,\mathrm{Re}[I_s] = 3V_s I_s\cos\varphi \tag{1.4}$$

Substituting (1.3) into (1.4) yields

$$P_i = -3\frac{V_s E}{X_s}\sin\delta \quad \text{[Watts/phase]} \tag{1.5}$$

This power is positive when δ negative, meaning that when the rotor field lags the stator field the machine is operating in the motoring region. When $\delta > 0$ the machine is operating in the generation region. The negative sign in (1.5) can be dropped, assuming that for motoring operation a negative δ is implied.

If the losses of the machine are ignored, the power P_i can be expressed as the shaft (output) power as well

$$P_i = P_o = \frac{2}{P}\omega_e T_{em} \tag{1.6}$$

When combining (1.5) and (1.6), the magnitude of the developed torque for a non-salient synchronous motor (or surface-mounted permanent magnet synchronous motor) can be expressed as

$$\begin{aligned} T_{em} &= 3\left(\frac{P}{2}\right)\frac{|\boldsymbol{V}_s|}{\omega_e}\frac{|\boldsymbol{E}|}{|X_s|}\sin\delta \\ &= 3\left(\frac{P}{2}\right)\frac{|\boldsymbol{\lambda}_s||\boldsymbol{\lambda}_r|}{L_s}\sin\delta \end{aligned} \tag{1.7}$$

where δ is the torque angle between flux vectors $\boldsymbol{\lambda}_s$ and $\boldsymbol{\lambda}_r$. If the rotor flux remains constant and the stator flux is changed incrementally by the stator voltage $\boldsymbol{V}_s$ then the torque variation ΔT_{em} expression can be written as

$$\Delta T_{em} = 3\left(\frac{P}{2}\right)\frac{|\boldsymbol{\lambda}_s + \Delta\boldsymbol{\lambda}_s||\boldsymbol{\lambda}_r|}{L_s}\sin\Delta\delta \tag{1.8}$$

where the bold terms in the above expressions indicate vectors.

As it can be seen from (1.8), if the load angle δ is increased then torque variation is increased. To increase the load angle δ the stator flux vector should turn faster than rotor flux vector. The rotor flux rotation depends on the mechanical speed of the rotor, so to decrease load angle δ the stator flux should turn slower than rotor flux. Therefore, according to the torque (1.7), the electromagnetic torque can be controlled effectively by controlling the amplitude and rotational speed of stator flux vector $\boldsymbol{\lambda}_s$. To achieve the

above phenomenon, appropriate voltage vectors are applied to the motor terminals. For counter-clockwise operation, if the actual torque is smaller than the reference value, then the voltage vectors that keep the stator flux vector $\boldsymbol{\lambda}_s$ rotating in the same direction are selected. When the load angle δ between $\boldsymbol{\lambda}_s$ and $\boldsymbol{\lambda}_r$ increases the actual torque increases as well. Once the actual torque is greater than the reference value, the voltage vectors that keep stator flux vector $\boldsymbol{\lambda}_s$ rotating in the reverse direction are selected instead of the zero voltage vectors. At the same time, the load angle δ decreases thus the torque decreases. The reason the zero voltage vector is not chosen in the DTC of PMSM drives will be discussed later in this chapter. A more detailed look at the selection of the voltage vectors and their effect on torque and flux results will be discussed later as well. Referring back to the discussion above, however, torque is controlled via the stator flux rotation speed, as shown in Fig. 1.5. If the speed of the stator flux is high then faster torque response is achieved.

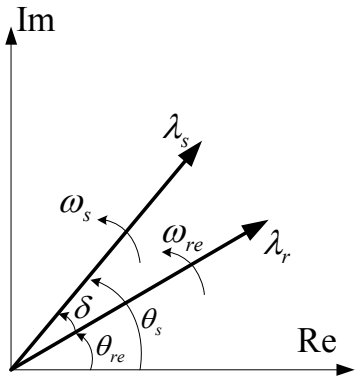

Fig. 1.5. Rotor and stator flux linkage space vectors (rotor flux lagging stator flux) [21].

1.2.2. Flux Control Strategy in DTC of PMSM Drive

If the resistance term in the stator flux estimation algorithm is neglected, the variation of the stator flux linkage (incremental flux expression vector) will only depend on the applied voltage vector as shown in Fig. 1.6 [40].

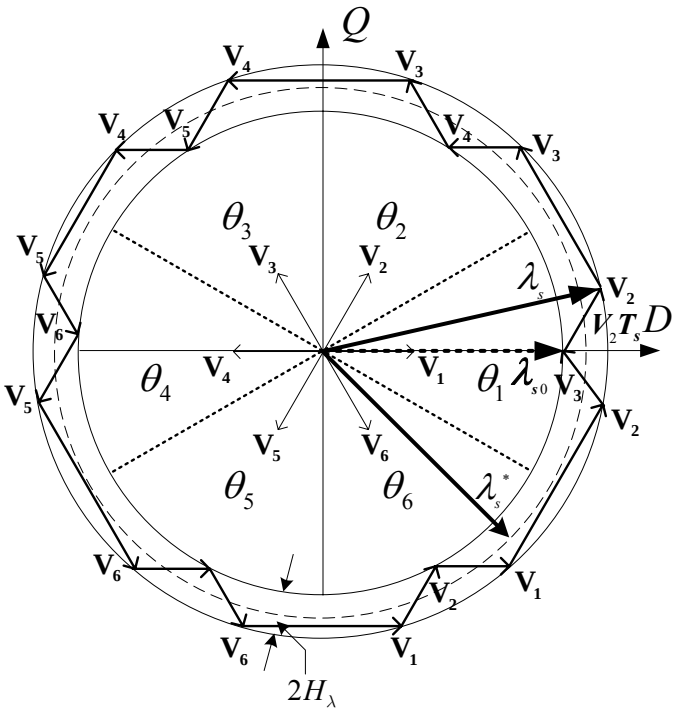

Fig. 1.6. Incremental stator flux linkage space vector representation in the DQ−plane.

For a short interval of time, namely the sampling time $T_s = \Delta t$ the stator flux linkage $\boldsymbol{\lambda}_s$ position and amplitude can be changed incrementally by applying the stator voltage vector $\boldsymbol{V}_s$. As discussed above, the position change of the stator flux linkage vector $\boldsymbol{\lambda}_s$ will affect the torque. The stator flux linkage of a PMSM that is depicted in the stationary reference frame is written as

$$\boldsymbol{\lambda}_s = \int (\boldsymbol{V}_s - R_s \boldsymbol{i}_s) dt \tag{1.9}$$

During the sampling interval time or switching interval, one out of the six voltage vectors is applied, and each voltage vector applied during the pre-defined sampling interval is constant, therefore (1.9) can be rewritten as

$$\boldsymbol{\lambda}_s = \boldsymbol{V}_s t - R_s \int \boldsymbol{i}_s dt + \lambda_{s|t=0} \tag{1.10}$$

where $\lambda_{s|t=0}$ is the initial stator flux linkage at the instant of switching, $\boldsymbol{V}_s$ is the measured stator voltage, $\boldsymbol{i}_s$ is the measured stator current, and R_s is the estimated stator resistance. When the stator term in stator flux estimation is removed implying that the end of the stator flux vector $\boldsymbol{\lambda}_s$ will move in the direction of the applied voltage vector, as shown in Fig. 1.6, we obtain

$$\boldsymbol{V}_s = \frac{d}{dt}(\boldsymbol{\lambda}_s) \tag{1.11}$$

or

$$\Delta\boldsymbol{\lambda}_s = \boldsymbol{V}_s \Delta t \tag{1.12}$$

The goal of controlling the flux in DTC is to keep its amplitude within a pre-defined hysteresis band. By applying a required voltage vector stator flux linkage amplitude can be controlled. To select the voltage vectors for controlling the amplitude of the stator flux linkage the voltage plane is divided into six regions, as shown in Fig. 1.2.

In each region two adjacent voltage vectors, which give the minimum switching frequency, are selected to increase or decrease the amplitude of stator flux linkage, respectively. For example, according to the Table I, when the voltage vector $\boldsymbol{V}_2$ is applied in Sector 1, then the amplitude of the stator flux increases when the flux vector

rotates counter-clockwise. If V_3 is selected then stator flux linkage amplitude decreases. The stator flux incremental vectors corresponding to each of the six inverter voltage vectors are shown in Fig. 1.1.

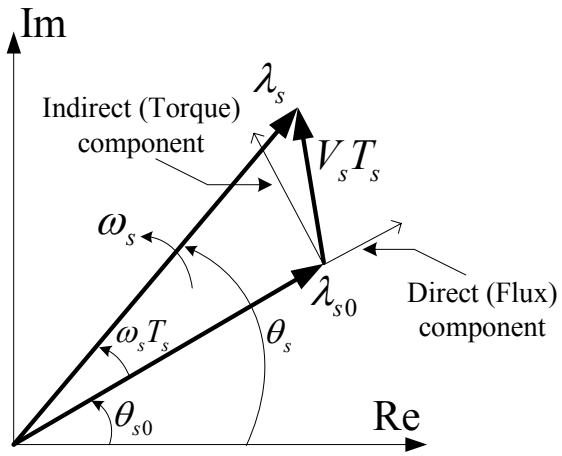

Fig. 1.7. Representation of direct and indirect components of the stator flux linkage vector [21].

Fig. 1.7 is a basic graph that shows how flux and torque can be changed as a function of the applied voltage vector. According to the figure, the direct component of applied voltage vector changes the amplitude of the stator flux linkage and the indirect component changes the flux rotation speed which changes the torque. If the torque needs to be changed abruptly then the flux does as well, so the closest voltage vector to the indirect component vector is applied. If torque change is not required, but flux amplitude is increased or decreased then the voltage vector closest to the direct component vector is chosen. Consequently, if both torque and flux are required to change then the appropriate resultant mid-way voltage vector between the indirect and direct components is applied [21]. It seems obvious from (1.9) that the stator flux linkage vector will stay at its original position when zero voltage vectors $S_a(000)$ and $S_a(111)$ are applied. This is

true for an induction motor since the stator flux linkage is uniquely determined by the stator voltage. On the other hand, in the DTC of a PMSM, the situation of applying the zero voltage vectors is not the same as in induction motors. This is because the stator flux linkage vector will change even when the zero voltage vectors are selected since the magnets rotate with the rotor. As a result, the zero voltage vectors are not used for controlling the stator flux linkage vector in a PMSM. In other words, the stator flux linkage should always be in motion with respect to the rotor flux linkage vector [10].

1.2.3. Voltage Vector Selection in DTC of PMSM Drive

As discussed before, the stator flux is controlled by properly selected voltage vectors, and as a result the torque by stator flux rotation. The higher the stator vector rotation speed the faster torque response is achieved.

The estimation of the stator flux linkage components described previously requires the stator terminal voltages. In a DTC scheme it is possible to reconstruct those voltages from the dc-link voltage V_{dc} and the switching states (S_a, S_b, S_c) of a six-step voltage-source inverter (VSI) rather than monitoring them from the motor terminals. The primary voltage vector $\boldsymbol{v}_s$ is defined by the following equation:

$$\boldsymbol{v}_s = \frac{2}{3}(v_a + v_b e^{j(2/3)\pi} + v_c e^{j(4/3)\pi}) \tag{1.13}$$

where v_a, v_b, and v_c are the instantaneous values of the primary line-to-neutral voltages. When the primary windings are fed by an inverter, as shown in Fig. 1.8, the primary voltages v_a, v_b and v_c are determined by the status of the three switches S_a, S_b, and

S_c. If the switch is at state 0 that means the phase is connected to the negative and if it is at 1 it means that the phase is connected to the positive leg.

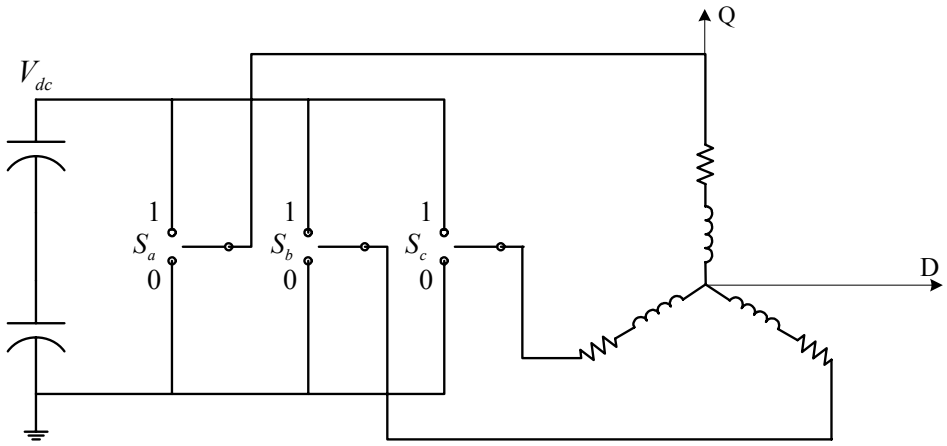

Fig. 1.8. Voltage Source Inverter (VSI) connected to the R-L load [5].

For example, v_a is connected to V_{dc} if S_a is one, otherwise v_a is connected to zero. This is similar for v_b and v_c. The voltage vectors that are obtained this way are shown in Fig. 1.1. There are six nonzero voltage vectors: $\boldsymbol{V}_1(100)$, $\boldsymbol{V}_2(110)$, …, and $\boldsymbol{V}_6(101)$ and two zero voltage vectors: $\boldsymbol{V}_7(000)$ and $\boldsymbol{V}_8(111)$. The six nonzero voltage vectors are 60° apart from each other as in Fig. 1.1.

The stator voltage space vector (expressed in the stationary reference frame) representing the eight voltage vectors can be shown by using the switching states and the dc-link voltage V_{dc} as

$$\boldsymbol{v}_s(S_a,S_b,S_c)=\frac{2}{3}V_{dc}(S_a+S_b e^{j(2/3)\pi}+S_c e^{j(4/3)\pi}) \tag{1.14}$$

where V_{dc} is the dc-link voltage and the coefficient of 2/3 is the coefficient comes from the Park Transformation. Equation (1.14) can be derived by using the line-to-line

voltages of the ac motor which can be expressed as $v_{ab} = V_{dc}(S_a - S_b)$, $v_{bc} = V_{dc}(S_b - S_c)$, and $v_{ca} = V_{dc}(S_c - S_a)$. The stator phase voltages (line-to-neutral voltages) are required for (1.14). They can be obtained from the line-to-line voltages as $v_a = (v_{ab} - v_{ca})/3$, $v_b = (v_{bc} - v_{ab})/3$, and $v_c = (v_{ca} - v_{bc})/3$. If the line-to-line voltages in terms of the dc-link voltage V_{dc} and switching states are substituted into the stator phase voltages it gives

$$v_a = \frac{1}{3}V_{dc}(2S_a - S_b - S_c)$$

$$v_b = \frac{1}{3}V_{dc}(-S_a + 2S_b - S_c) \tag{1.15}$$

$$v_c = \frac{1}{3}V_{dc}(-S_a - S_b + 2S_c)$$

Equation (1.15) can be summarized by combining with (1.13) as

$$v_a = \mathrm{Re}(\boldsymbol{v}_s) = \frac{1}{3}V_{dc}(2S_a - S_b - S_c)$$

$$v_b = \mathrm{Re}(\boldsymbol{v}_s) = \frac{1}{3}V_{dc}(-S_a + 2S_b - S_c) \tag{1.16}$$

$$v_c = \mathrm{Re}(\boldsymbol{v}_s) = \frac{1}{3}V_{dc}(-S_a - S_b + 2S_c)$$

To determine the proper applied voltage vectors, information from the torque and flux hysteresis outputs, as well as stator flux vector position, are used so that circular stator flux vector trajectory is divided into six symmetrical sections according to the non zero voltage vectors as shown in Fig. 1.2.

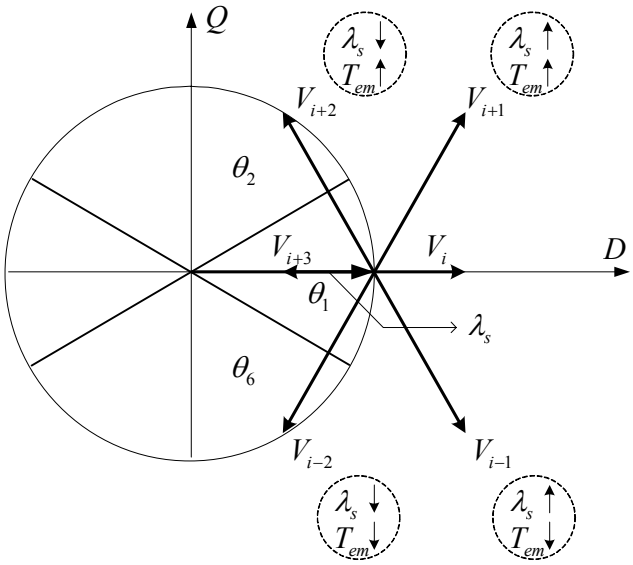

Fig. 1.9. Voltage vector selection when the stator flux vector is located in sector *i* [21].

According to Fig. 1.9, while the stator flux vector is situated in sector *i*, voltage vectors V_{i+1} and V_{i-1} have positive direct components, increasing the stator flux amplitude, and V_{i+2} and V_{i-2} have negative direct components, decreasing the stator flux amplitude. Moreover, V_{i+1} and V_{i+2} have positive indirect components, increasing the torque response, and V_{i-1} and V_{i-2} have negative indirect components, decreasing the torque response. In other words, applying V_{i+1} increases both torque and flux but applying V_{i+1} increases torque and decreases flux amplitude [21].

The switching table for controlling both the amplitude and rotating direction of the stator flux linkage is given in Table I.

TABLE I

SWITCHING TABLE FOR DTC OF PMSM DRIVE

φ	τ	θ					
		θ(1)	θ(2)	θ(3)	θ(4)	θ(5)	θ(6)
$\varphi=1$	$\tau=1$	$\mathbf{V}_2(110)$	$\mathbf{V}_3(010)$	$\mathbf{V}_4(001)$	$\mathbf{V}_5(101)$	$\mathbf{V}_6(110)$	$\mathbf{V}_1(110)$
	$\tau=0$	$\mathbf{V}_6(101)$	$\mathbf{V}_1(100)$	$\mathbf{V}_2(010)$	$\mathbf{V}_3(011)$	$\mathbf{V}_4(110)$	$\mathbf{V}_5(110)$
$\varphi=0$	$\tau=1$	$\mathbf{V}_3(010)$	$\mathbf{V}_4(011)$	$\mathbf{V}_5(101)$	$\mathbf{V}_6(100)$	$\mathbf{V}_1(110)$	$\mathbf{V}_2(110)$
	$\tau=0$	$\mathbf{V}_5(001)$	$\mathbf{V}_6(101)$	$\mathbf{V}_1(110)$	$\mathbf{V}_2(010)$	$\mathbf{V}_3(110)$	$\mathbf{V}_4(110)$

The voltage vector plane is divided into six sectors so that each voltage vector divides each region into two equal parts. In each sector, four of the six non-zero voltage vectors may be used. Zero vectors are also allowed. All the possibilities can be tabulated into a switching table. The switching table presented by Rahman et al [10] is shown in Table I. The output of the torque hysteresis comparator is denoted as τ, the output of the flux hysteresis comparator as φ and the flux linkage sector is denoted as θ. The torque hysteresis comparator is a two valued comparator; $\tau=0$ means that the actual value of the torque is above the reference and out of the hysteresis limit and $\tau=1$ means that the actual value is below the reference and out of the hysteresis limit. The flux hysteresis comparator is a two valued comparator as well where $\varphi=1$ means that the actual value of the flux linkage is below the reference and out of the hysteresis limit and $\varphi=0$ means that the actual value of the flux linkage is above the reference and out of the hysteresis limit. Rahman et al [10] have suggested that no zero vectors should be used with a PMSM. Instead, a non zero vector which decreases the absolute value of the torque is used. Their argument was that the application of a zero vector would make the change in torque subject to the rotor mechanical time constant which may be rather long

compared to the electrical time constants of the system. This results in a slow change of the torque. This reasoning does not make sense, since in the original switching table the zero vectors are used when the torque is inside the torque hysteresis (i.e. when the torque is wanted to be kept as constant as possible). This indicates that the zero vector must be used. If the torque ripple needs to be kept as small as with the original switching table, a higher switching frequency must be used if the suggestion of [10] is obeyed [3].

We define φ and τ to be the outputs of the hysteresis controllers for flux and torque, respectively, and $\theta(1)-\theta(6)$ as the sector numbers to be used in defining the stator flux linkage positions. In Table I, if $\varphi = 1$, then the actual flux linkage is smaller than the reference value. On the other hand, if $\varphi = 0$, then the actual flux linkage is greater than the reference value. The same is true for the torque.

1.3. Control Strategy of DTC of PMSM

Fig. 1.10 illustrates the schematic of the basic DTC controller for PMSM drives. The command stator flux λ_s^* and torque T_{em}^* magnitudes are compared with their respective estimated values. The errors are then processed through the two hysteresis comparators, one for flux and one for torque which operate independently of each other. The flux and torque controller are two-level comparators. The digital outputs of the flux controller have following logic:

$$d_\lambda = 1 \quad \text{for } |\lambda_s| < \lambda_s^* - H_\lambda \tag{1.17}$$

$$d_\lambda = 0 \quad \text{for } |\lambda_s| < \lambda_s^* + H_\lambda \tag{1.18}$$

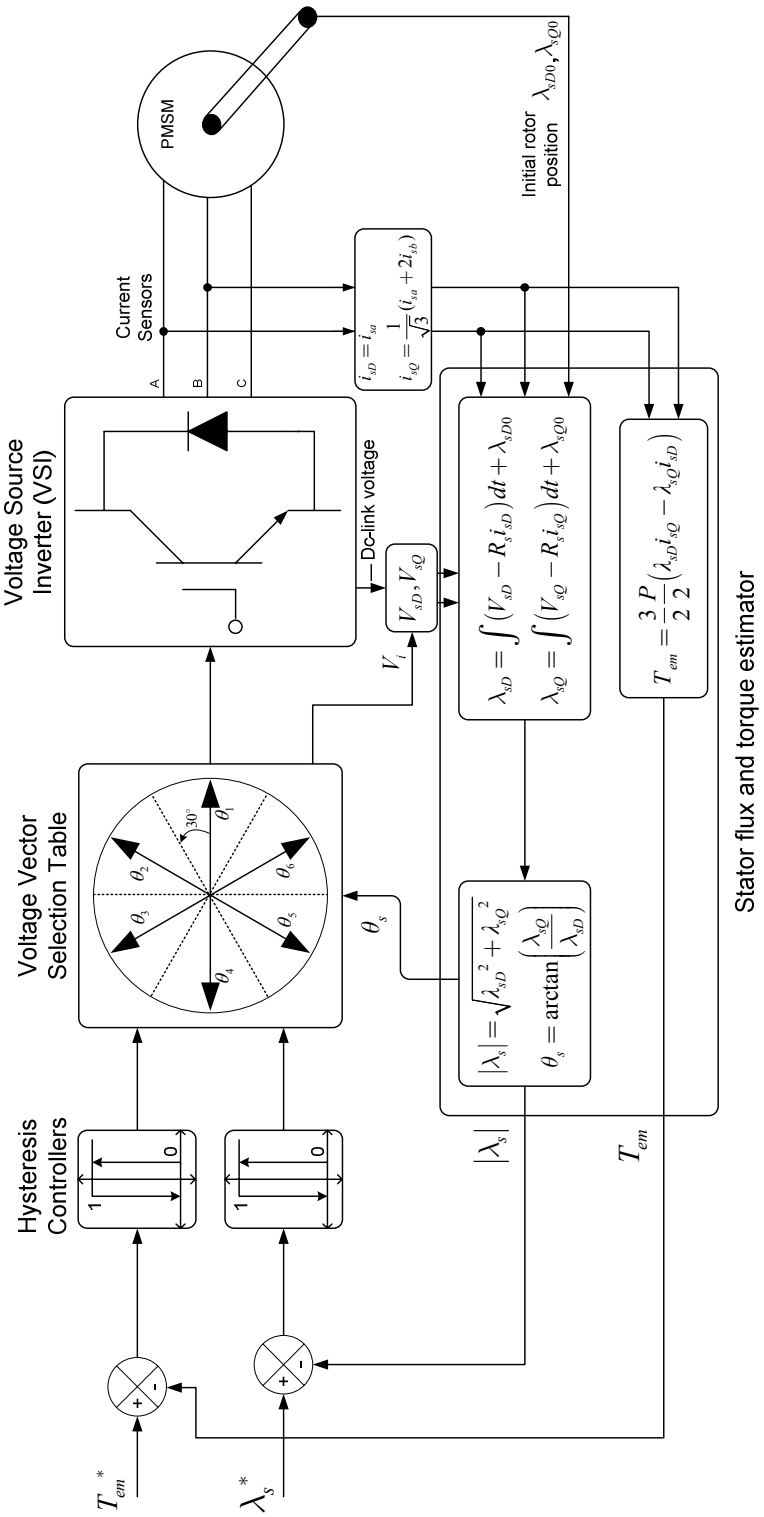

Fig. 1.10. Basic block diagram for DTC of PMSM drive.

where $2H_\lambda$ is the total hysteresis-band width of the flux comparator, and d_λ is the digital output of the flux comparator.

By applying the appropriate voltage vectors the actual flux vector $\boldsymbol{\lambda_s}$ is constrained within the hysteresis band and it tracks the command flux λ_s^* in a zigzag path without exceeding the total hysteresis-band width. The torque controller has also two levels for the digital output, which have the following logic:

$$d_{T_{em}} = 1 \quad \text{for } T_{em} < T_{em}^* - H_{T_{em}} \tag{1.19}$$

$$d_{T_{em}} = 0 \quad \text{for } T_{em} < T_{em}^* + H_{T_{em}} \tag{1.20}$$

where $2H_{T_{em}}$ is the total hysteresis-band width of the torque comparator, and $d_{T_{em}}$ is the digital output of the torque comparator.

$$\begin{bmatrix} f_D \\ f_Q \\ f_0 \end{bmatrix} = \begin{bmatrix} 1 & -\frac{1}{2} & -\frac{1}{2} \\ 0 & \frac{\sqrt{3}}{2} & -\frac{\sqrt{3}}{2} \\ \frac{1}{2} & \frac{1}{2} & \frac{1}{2} \end{bmatrix} \begin{bmatrix} f_a \\ f_b \\ f_c \end{bmatrix} \tag{1.21}$$

Knowing the output of these comparators and the sector of the stator flux vector, the look-up table can be built such that it applies the appropriate voltage vectors via the inverter in a way to force the two variables to predefined trajectories. If the switching states of the inverter, the dc-link voltage of the inverter and two of the motor currents are known then the stator voltage and current vectors of the motor in the DQ stationary frame are obtained easily by a simple transformation. This transformation is called the Clarke Transformation [4] (1.21) as shown in Fig. 1.10. The DQ frame voltage and

current information can then be used to estimate the corresponding D– and Q–axis stator flux linkages λ_D and λ_Q which are given by

$$\lambda_D(k) = \lambda_D(k-1) + \left\{ v_D(k-1) - R_s \bar{i}_D(k) \right\} T_s \tag{1.22}$$

$$\lambda_Q(k) = \lambda_Q(k-1) + \left\{ v_Q(k-1) - R_s \bar{i}_Q(k) \right\} T_s \tag{1.23}$$

where k and $k-1$ are present and previous sampling instants, respectively, v_D and v_Q are the stator voltages in DQ stationary reference frame, $\bar{i}_D(k) = (i_D(k-1) + i_D(k))/2$ and $\bar{i}_Q(k) = (i_Q(k-1) + i_Q(k))/2$ are the average values of stator currents i_D and i_Q derived from the present $i_{DQ}(k)$ and previous $i_{DQ}(k-1)$ sampling interval values of the stator currents, R_s is the stator resistance, and T_s is the sampling time. The stator flux linkage vector can be written as

$$\boldsymbol{\lambda}_s(k) = \sqrt{\lambda_D(k)^2 + \lambda_Q(k)^2} \angle \tan^{-1}\left(\frac{\lambda_Q(k)}{\lambda_D(k)} \right) \tag{1.24}$$

where $\sqrt{\lambda_D(k)^2 + \lambda_Q(k)^2}$ is the magnitude of the stator flux linkage vector and $\tan^{-1}\left(\frac{\lambda_Q(k)}{\lambda_D(k)} \right)$ is the angle of stator flux linkage vector with respect to the stationary D–axis in DQ frame (or *a*–axis in *abc* frame). The developed stationary DQ reference frame electromagnetic torque in terms of the DQ frame stator flux linkages and currents is given by

$$T_{em}(k) = \frac{3}{2} P \left\{ \lambda_Q(k) i_D(k) - \lambda_D(k) i_Q(k) \right\} \tag{1.25}$$

where P is the number of pole pairs.

As it can be seen form (1.22) and (1.23) the stator resistance is the only machine parameter to be known in the flux, and consequently torque, estimation. Even though the stator is the direct parameter seen in (1.22) and (1.23), there is an indirect (hidden) motor parameter for DTC of PMSM drives. This parameter is the rotor flux magnitude which constructs the initial values of the D– and Q–axis stator fluxes. If the rotor flux vector $\boldsymbol{\lambda}_r$ is assumed to be aligned with the D–axis of the stationary reference frame, then $\lambda_D(k-1)$ equals the rotor flux amplitude $\sqrt{2}\lambda_r$. If the rotor magnetic flux $\boldsymbol{\lambda}_r$ resides on the D–axis (the rotor magnetic flux can be intentionally brought to the known position by applying the appropriate voltage vector for a certain amount of time), then the initial value of the Q–axis flux $\lambda_Q(k-1)$ is considered to be zero, therefore there will not be any initial starting problem for the motor. On the other hand, if the rotor is in a position other than the zero reference degree then both the $\lambda_D(k-1)$ and $\lambda_Q(k-1)$ values should be known to start the motor properly in the correct direction without oscillation. Moreover, if the initial values of the DQ frame integrators are not estimated correctly then those incorrect initial flux values will be seen as dc components in the integration calculations of the DQ frame fluxes. This will cause the stator flux linkage space vector to drift away from the origin centered circular path and if they are not corrected quickly while motor is running then instability in the system will result quickly.

CHAPTER II

DIRECT TORQUE CONTROL OF BRUSHLESS DC MOTOR WITH NON-SINUSOIDAL BACK-EMF USING TWO-PHASE CONDUCTION MODE

2.1. Introduction

Permanent magnet synchronous motor (PMSM) with sinusoidal shape back-EMF and brushless dc (BLDC) motor with trapezoidal shape back-EMF drives have been extensively used in many applications. They are used in applications ranging from servo to traction drives due to several distinct advantages such as high power density, high efficiency, large torque to inertia ratio, and better controllability [41]. Brushless dc motor (BLDC) fed by two-phase conduction scheme has higher power/weight, torque/current ratios. It is less expensive due to the concentrated windings which shorten the end windings compared to three-phase feeding permanent magnet synchronous motor (PMSM) [42]. The most popular way to control BLDC motors is by PWM current control in which a two-phase feeding scheme is considered with variety of PWM modes such as soft switching, hard-switching, and etc. If the back-EMF waveform is ideal trapezoidal with 120 electrical degrees flat top, three hall-effect sensors are usually used as position sensors to detect the current commutation points that occur at every 60 electrical degrees. Therefore, a relatively low cost drive is achieved when compared to a PMSM drive with expensive high-resolution position sensor, such as optical encoder.

Several current and torque control methods have been employed for BLDC motor drives to minimize the torque pulsations mainly caused by commutation and non-ideal shape of back-EMF. The optimum current excitation method, considering the unbalanced three-phase stator windings as well as non-identical and half-wave asymmetric back-EMF waveforms, is reported in [43]. Each phase back-EMF versus rotor position data is stored in a look-up table. Then, they are transformed to the *dq*–axes synchronous reference frame. The *d*–axis current is assumed to be zero and the *q*–axis current is obtained from the desired reference torque, motor speed, and the *q*–axis back-EMF. Consequently, inverse park transformation is applied to the *dq*–axes currents to obtain the *abc* frame optimum reference current waveforms. Minimum torque ripple and maximum efficiency are achieved at low speeds for a BLDC motor. However, three hysteresis current controllers with PWM generation which increases the complexity of the drive are used to drive the BLDC motor. Several transformations are required in order to get the *abc* frame optimum reference current waveforms. These transformations complicate the control algorithm and the scheme could not directly control the torque, therefore fast torque response cannot be achieved.

In [44], estimating the electromagnetic torque from the rate of change of coenergy with respect to position is described. However, the stator flux linkage, the coenergy, and the torque versus the estimated position look-up tables are needed to generate the optimized current references for the desired torque, therefore more complicated control algorithm is inevitable. Moreover, open-loop position estimation

using voltages and currents may create drift on the stator flux linkage locus, therefore wrong position estimation might occur.

In [45], electromagnetic torque is calculated from the product of the instantaneous back-EMF and current both in two-phase and in the commutation period, Then, the pre-stored phase back-EMF values which are obtained using mid-precision position sensor. As a result, torque pulsations due to the commutation are considerably reduced compared to the conventional PI current controller even for BLDC motor with non-ideal trapezoidal back-EMF. However, phase resistance is neglected and the torque estimation depends on parameters such as dc-link voltage and phase inductance. Moreover, instead of a simple voltage selection look-up table technique more complicated PWM method is used to drive the BLDC motor.

In [46], the stator flux linkage is estimated by the model reference adaptive system (MRAS) technique and the torque is calculated using estimated flux and measured current. Then, the torque is instantaneously controlled by the torque controller using the integral variable structure control (VSC) and the space-vector pulse-width modulation (SVPWM). Thus, good steady-state performance and switching characteristics are obtained. Torque and speed pulsations are effectively reduced. Nevertheless, this technique increases the complexity of the control system and is applied only to a PMSM drive employing three-phase conduction instead of a BLDC motor with two-phase conduction. In addition, since the stator flux linkage is estimated on-line using MRAS technique, the values of the resistance and inductance are regarded

as important parameters in determining the estimation and control performance. Therefore, the effects on the parameter variations should have been considered.

In [47], the instantaneous torque is directly controlled by variable structure strategy (VSS) in *dq*–axes synchronous reference frame in which the torque pulsations mainly caused by a conventional sinusoidal current control are minimized. Torque estimation algorithm operates well down to zero speed, but depends on pre-knowledge of the harmonic torque coefficients of the machine, which are subject to motor parameter variations. In addition, knowledge of the motor parameters such as phase inductance and resistance as well as rotor position is required. Also, three-phase conduction scheme instead of a more usual two-phase conduction mode is considered for the BLDC motor.

Torque coefficients in [47] are updated using an on-line recursive least square estimator in [48], however it is computationally intensive and difficult to implement because it requires differentiation of the motor current. Real-time harmonics flux estimator to calculate the sixth-harmonic current that must be injected to cancel the sixth- and twelfth-harmonic pulsating torque components rather than depending on stored coefficients is reported in [49]. Unfortunately, the flux estimation algorithm still depends on pre-knowledge of the motor resistance and inductance. Also, the parameter sensitivity issue is not clarified.

In [50], predetermination of optimal current wave shapes using Park like *dq*–axes reference frame is obtained by adding some harmonics to the fundamental current to cancel specific torque harmonic components. However, these optimal current references are not constant and require very fast controllers especially when the motor operates at

high speed. Moreover, the bandwidth of the classical proportional plus integral (PI) controllers does not allow tracking all of the reference current harmonics.

Problems in [50] are claimed to be solved in [51] such that a new torque control strategy using the *ba–ca* reference frame is proposed in which easily accessible line-to-line back-EMFs are measured and stored in a look-up table. Smooth and maximum torque is obtained, however this technique presents a steady-state torque error compared to the *dq*–axes reference frame scheme in [50] and the motor is driven by digital scalar modulation technique which operates like a SVPWM, therefore a more complicated control is inevitable.

Since the Park Transformation and its extensions proposed in [50] do not linearize completely the non-linear model of the machine, state feedback linearization technique is applied in order to obtain the desired high performance torque control in [52]. However, this DTC technique has the same drawbacks as the torque control in the synchronous reference frame for the PMSM with sinusoidal back-EMF drives. Additionally, more tedious computations are needed to be performed compared to [50], which complicates the real-time implementation of the control strategy.

Direct torque control scheme was first proposed by Takahashi [53] and Depenbrock [54] for induction motor drives in the mid 1980s. More than a decade later, in the late 1990s, DTC techniques for both interior and surface-mounted synchronous motors (PMSM) were analyzed [55]. More recently, application of DTC scheme is extended to BLDC motor drives to minimize the low-frequency torque ripples and torque response time as compared to conventional PWM current controlled BLDC motor

drives [56]. In [56], the voltage space vectors in a two-phase conduction mode are defined and a stationary reference frame electromagnetic torque equation is derived for surface-mounted permanent magnet synchronous machines with non-sinusoidal back-EMF (BLDC, and etc.). It is claimed that the electromagnetic torque and the stator flux linkage amplitude of the DTC of BLDC motor under two-phase conduction mode can be controlled simultaneously.

In this section, the DTC of a BLDC motor drive operating in two-phase conduction mode, proposed in [56], is further studied and simplified to just a torque controlled drive by intentionally keeping the stator flux linkage amplitude almost constant by eliminating the flux control in the constant torque region. Since the flux control is removed, fewer algorithms are required for the proposed control scheme. Specifically, it is shown that in two-phase conduction DTC of BLDC motor drive rather than attempting to control the stator flux amplitude, only torque is controlled. It will be explained in detail that due to the sharp changes which occur every 60 electrical degrees flux amplitude control is quite difficult. Moreover, there is no need to control the stator flux linkage amplitude of a BLDC motor in the constant torque region. The stator flux linkage position in the trajectory is helpful to find the right sector for the torque control in sensorless applications of BLDC motor drives. Therefore, the torque is controlled while the stator flux linkage amplitude is kept almost constant on purpose. Furthermore, simulations show that using the zero inverter voltage space vector suggested in [56] only to decrease the electromagnetic torque could have some disadvantages, such as generating more frequent and larger spikes on the phase voltages that deteriorate the

trajectory of the stator flux-linkage locus, increase the switching losses, and contributes to the large common-mode voltages that can potentially damage the motor bearings [57]. To overcome these problems, a new simple two-phase inverter voltage space vector look-up table is developed. Simulated and experimental results are presented to illustrate the validity and effectiveness of the proposed two-phase conduction DTC of a BLDC motor drive in the constant torque region.

2.2. Principles of the Proposed Direct Torque Control (DTC) Technique

The key issue in the DTC of a BLDC motor drive in the constant torque region is to estimate the electromagnetic torque correctly. The derivation of the electromagnetic torque equation for BLDC motor with non-sinusoidal back-EMF is given in the following:

The general electromagnetic torque equation of a PMSM with sinusoidal/non-sinusoidal back-EMF in the synchronously rotating *dq* reference frame when the influence of the mutual coupling between *d*– and *q*–axis winding inductance neglected can be expressed as [49], [54]–[56].

$$T_{em} = \frac{3P}{4}\left[\left(\frac{dL_{ds}}{d\theta_e}i_{sd} + \frac{d\varphi_{rd}}{d\theta_e} - \varphi_{sq}\right)i_{sd} + \left(\frac{dL_{qs}}{d\theta_e}i_{sq} + \frac{d\varphi_{rq}}{d\theta_e} + \varphi_{sd}\right)i_{sq}\right] \tag{2.1}$$

where

$$\varphi_{sd} = L_{ds}i_{sd} + \varphi_{rd} \tag{2.2}$$

$$\varphi_{sq} = L_{qs}i_{sq} + \varphi_{rq} \tag{2.3}$$

and P is the number of poles, θ_e is the electrical rotor angle, i_{sd} and i_{sq} are the synchronous reference frame (dq–axes) currents, L_{ds} and L_{qs} are the d– and q–axis inductances, respectively, and φ_{rd}, φ_{rq}, φ_{sd}, and φ_{sq} are the d– and q–axis rotor and stator flux linkages, respectively.

The motors with high-coercive PM material higher order harmonics in the stator winding inductance can be neglected because the torque pulsations are mainly associated with the flux harmonics [56]. Therefore, it can be assumed that L_{ds} and L_{qs} are constant. Then, the final synchronous reference frame electromagnetic torque equation for a salient pole PMSM becomes

$$T_{em} = \frac{3P}{4}\left[\left(\frac{d\varphi_{rd}}{d\theta_e} - \varphi_{rq}\right)i_{sd} + \left(\frac{d\varphi_{rq}}{d\theta_e} + \varphi_{rd}\right)i_{sq} + (L_{ds} - L_{qs})i_{sd}i_{sq}\right] \tag{2.4}$$

When the stator flux linkage due to the permanent magnets varies sinusoidally, $\varphi_{rd} = \varphi_m$, and $\varphi_{rq} = 0$ where φ_m is the peak rotor flux linkage. Therefore, $d\varphi_{rd}/d\theta_e = d\varphi_{rq}/d\theta_e = 0$. As a result, the electromagnetic torque equation for an either salient or non-salient PMSM including BLDC motor with sinusoidal back-EMF can then be simplified as

$$T_{em} = \frac{3P}{4}\left(\varphi_{sd}i_{sq} - \varphi_{sq}i_{sd}\right) = \frac{3P}{4}\left(\varphi_{s\alpha}i_{s\beta} - \varphi_{s\beta}i_{s\alpha}\right) \tag{2.5}$$

where i_{sd}, i_{sq}, φ_{sd}, φ_{sq}, $i_{s\alpha}$, $i_{s\beta}$, $\varphi_{s\alpha}$, and $\varphi_{s\beta}$ are the synchronous and stationary reference frame currents and flux linkages, respectively. Therefore, the left hand side of (2.5) is the electromagnetic torque equation in synchronous reference frame and the right hand side of (2.5) represents the stationary reference frame electromagnetic torque equation.

For classical DTC scheme the one on the right hand side in (2.5) is used as electromagnetic torque estimation algorithm because it does not require rotor position information.

For nonsalient-pole machines ($L_{ds} = L_{qs} = L_s$), when the stator flux linkage due to the permanent magnets varies non-sinusoidally, therefore $d\varphi_{rd}/d\theta_e \neq d\varphi_{rq}/d\theta_e \neq 0$, which is the case for BLDC motor. As a result, the electromagnetic torque equation in synchronous reference frame for both surface-mounted PMSM and BLDC motor with non-sinusoidal back-EMF can be simplified using (2.4) in below:

$$T_{em} = \frac{3P}{4}\left[\left(\frac{d\varphi_{rd}}{d\theta_e} - \varphi_{rq}\right)i_{sd} + \left(\frac{d\varphi_{rq}}{d\theta_e} + \varphi_{rd}\right)i_{sq}\right] \tag{2.6}$$

It is desired to obtain electromagnetic torque equation in stationary reference frame instead of synchronous frame for DTC of BLDC motor drive operation. The following is the derivation of the electromagnetic torque equation in stationary reference frame for both surface-mounted PMSM and BLDC motor with non-sinusoidal back-EMF using (2.6):

Stationary reference frame rotor flux linkages $\varphi_{r\alpha}$ and $\varphi_{r\beta}$ can be represented in terms of synchronous reference frame components and the electrical rotor position as

$$\varphi_{r\alpha} = \varphi_{rd}\cos\theta_e - \varphi_{rq}\sin\theta_e \tag{2.7}$$

$$\varphi_{r\beta} = \varphi_{rd}\sin\theta_e + \varphi_{rq}\cos\theta_e \tag{2.8}$$

Derivatives of the stationary $\alpha\beta$–axes reference frame rotor flux linkages given in (2.7) and (2.8) over electrical rotor position respectively yield

$$\begin{aligned}\frac{d\varphi_{r\beta}}{d\theta_e} &= \frac{d}{d\theta_e}\left[\varphi_{rd}\cos\theta_e - \varphi_{rq}\sin\theta_e\right] \\ &= \frac{d\varphi_{rd}}{d\theta_e}\cos\theta_e - \sin\theta_e\varphi_{rd} - \left[\frac{d\varphi_{rd}}{d\theta_e}\sin\theta_e + \cos\theta_e\varphi_{rq}\right]\end{aligned} \tag{2.9}$$

and

$$\begin{aligned}\frac{d\varphi_{r\beta}}{d\theta_e} &= \frac{d}{d\theta_e}\left[\varphi_{rd}\sin\theta_e + \varphi_{rq}\cos\theta_e\right] \\ &= \frac{d\varphi_{rd}}{d\theta_e}\sin\theta_e + \cos\theta_e\varphi_{rd} + \left[\frac{d\varphi_{rd}}{d\theta_e}\cos\theta_e - \sin\theta_e\varphi_{rq}\right]\end{aligned} \tag{2.10}$$

Stationary reference frame currents $i_{s\alpha}$ and $i_{s\beta}$ can also be represented in terms of synchronous reference frame components and the electrical rotor position as

$$i_{s\alpha} = i_{sd}\cos\theta_e - i_{sq}\sin\theta_e \tag{2.11}$$

$$i_{s\beta} = i_{sd}\sin\theta_e + i_{sq}\cos\theta_e \tag{2.12}$$

Multiplications of (2.9) and (2.10) by (2.11) and (2.12) respectively result

$$\begin{aligned}\frac{d\varphi_{r\alpha}}{d\theta_e}i_{s\alpha} = {} & \frac{d\varphi_{rd}}{d\theta_e}i_{sd}\sin^2\theta_e + \cos\theta_e\sin\theta_e\varphi_{rd}i_{sd} + \\ & \frac{d\varphi_{rq}}{d\theta_e}i_{sd}\cos\theta_e\sin\theta_e - \sin^2\theta_e\varphi_{rq}i_{sd} + \\ & \frac{d\varphi_{rd}}{d\theta_e}i_{sq}\cos\theta_e\sin\theta_e + \cos^2\theta_e\varphi_{rd}i_{sq} + \\ & \frac{d\varphi_{rq}}{d\theta_e}i_{sq}\cos^2\theta_e - \cos\theta_e\sin\theta_e\varphi_{rq}i_{sq}\end{aligned} \tag{2.13}$$

and

$$\begin{aligned}\frac{d\varphi_{r\beta}}{d\theta_e}i_{s\beta} = &\frac{d\varphi_{rd}}{d\theta_e}i_{sd}\cos^2\theta_e - \cos\theta_e\sin\theta_e\varphi_{rd}i_{sd} - \\ &\frac{d\varphi_{rq}}{d\theta_e}i_{sd}\cos\theta_e\sin\theta_e - \cos^2\theta_e\varphi_{rq}i_{sd} - \\ &\frac{d\varphi_{rd}}{d\theta_e}i_{sq}\cos\theta_e\sin\theta_e + \sin^2\theta_e\varphi_{rd}i_{sq} + \\ &\frac{d\varphi_{rq}}{d\theta_e}i_{sq}\sin^2\theta_e + \cos\theta_e\sin\theta_e\varphi_{rq}i_{sq}\end{aligned} \tag{2.14}$$

The final electromagnetic torque equation for BLDC motor with non-sinusoidal back-EMF in stationary reference frame which is equivalent to (2.6) is obtained by combining (2.13) and (2.14) with the required coefficients as

$$T_{em} = \frac{3}{2}\frac{P}{2}\left[\frac{d\varphi_{r\alpha}}{d\theta_e}i_{s\alpha} + \frac{d\varphi_{r\beta}}{d\theta_e}i_{s\beta}\right] \tag{2.15}$$

where $\frac{d\varphi_{r\alpha}}{d\theta_e} = \frac{e_\alpha}{\omega_e}$ and $\frac{d\varphi_{r\beta}}{d\theta_e} = \frac{e_\beta}{\omega_e}$.

As a result, for a surface-mounted BLDC motor the back-EMF waveform is non-sinusoidal (trapezoidal), irrelevant to conducting mode (two or three-phase), therefore (2.16) which is given in the stationary reference frame should be used for the electromagnetic torque calculation [50, 56].

$$T_{em} = \frac{3}{2}\frac{P}{2}\left[\frac{e_\alpha}{\omega_e}i_{s\alpha} + \frac{e_\beta}{\omega_e}i_{s\beta}\right] = \frac{3}{2}\frac{P}{2}\left[k_\alpha(\theta_e)i_{s\alpha} + k_\beta(\theta_e)i_{s\beta}\right] \tag{2.16}$$

where ω_e is the electrical rotor speed, and $k_\alpha(\theta_e)$, $k_\beta(\theta_e)$, e_α, e_β are the stationary reference frame ($\alpha\beta$–axes) back-EMF constants according to electrical rotor position, motor back-EMFs, respectively. Since the second equation in (2.16) does not involve the rotor speed in the denominator there will be no problem estimating the torque at zero and near zero

speeds. Therefore, it is used in the proposed control system instead of the one on the left in (2.16).

In (2.16), it is not necessary to know the line-to-neutral back-EMFs. If the neutral point of the motor is not accessible, the phase back-EMFs cannot easily be obtained by direct measurements [43], therefore line-to-line back-EMF waveforms e_{ab}, e_{bc}, and e_{ca} should be used. As a result, Line-to-Line Clarke Transformation is performed to derive (2.16) as given by

$$\frac{1}{3}\begin{bmatrix} 1 & -2 & 1 \\ \sqrt{3} & 0 & -\sqrt{3} \end{bmatrix} \tag{2.17}$$

$$\begin{aligned} V_{s\alpha} &= R_s i_{s\alpha} + L_s \frac{di_{s\alpha}}{dt} + \frac{d\varphi_{r\alpha}}{dt} \\ V_{s\beta} &= R_s i_{s\beta} + L_s \frac{di_{s\beta}}{dt} + \frac{d\varphi_{r\beta}}{dt} \end{aligned} \tag{2.18}$$

Given the $\alpha\beta$–axes the machine equations in (2.18) where $V_{s\alpha}$, $V_{s\beta}$, R_s, and L_s are the $\alpha\beta$–axes stator voltages, phase resistance and inductance, respectively, the $\alpha\beta$–axes rotor flux linkages $\varphi_{r\alpha}$ and $\varphi_{r\beta}$ are obtained by taking the integral of both sides of (2.18) as follows:

$$\begin{aligned} \varphi_{s\alpha} - L_s i_{s\alpha} &= \varphi_{r\alpha} \\ \varphi_{s\beta} - L_s i_{s\beta} &= \varphi_{r\beta} \end{aligned} \tag{2.19}$$

where $\varphi_{s\alpha}$ and $\varphi_{s\beta}$ are the α– and β–axis stator flux linkages, respectively. By using (2.19), reference stator flux linkage command $|\varphi_s(\theta_e)|^*$ for DTC of BLDC motor drive in the constant torque region can be obtained similar to the DTC of a PMSM drive as

$$\left|\varphi_s(\theta_e)\right|^* = \left|\varphi_r(\theta_e)\right| = \sqrt{\varphi_{r\alpha}(\theta_e)^2 + \varphi_{r\beta}(\theta_e)^2} \tag{2.20}$$

where $|\varphi_s(\theta_e)|^*$ varies with the electrical rotor position θ_e unlike a PMSM with sinusoidal back-EMF.

A BLDC motor is operated ideally when the phase current is injected at the flat top portion of the line-to-neutral back-EMF. The back-EMF is usually flat for 120 electrical degrees and in transition for 60 electrical degrees during each half cycle. In the constant torque region (below base speed) when the line-to-line back-EMF voltage is smaller than the dc bus voltage there is no reason to change the amplitude of stator flux linkage. Above base speed, however, the motor performance will significantly deteriorate because the back-EMF exceeds the dc bus voltage, and the stator inductance X_s will not allow the phase current to develop quickly enough to catch up to the flat top of the trapezoidal back-EMF. Beyond the base speed, the desired torque cannot be achieved unless other techniques such as phase advancing, 180 degree conduction, etc [58] are used. Operation of the DTC of a BLDC motor above the base speed is not in the scope of this work.

Conventional two-phase conduction quasi-square wave current control causes the locus of the stator flux linkage to be unintentionally kept in hexagonal shape if the unexcited open-phase back-EMF effect and the free-wheeling diodes are neglected, as shown in Fig. 2.1 with the straight dotted lines forming a hexagon flux trajectory. If the free-wheeling diode effect which is caused by commutation is ignored, more circular flux trajectory can be obtained similar to a PMSM drive.

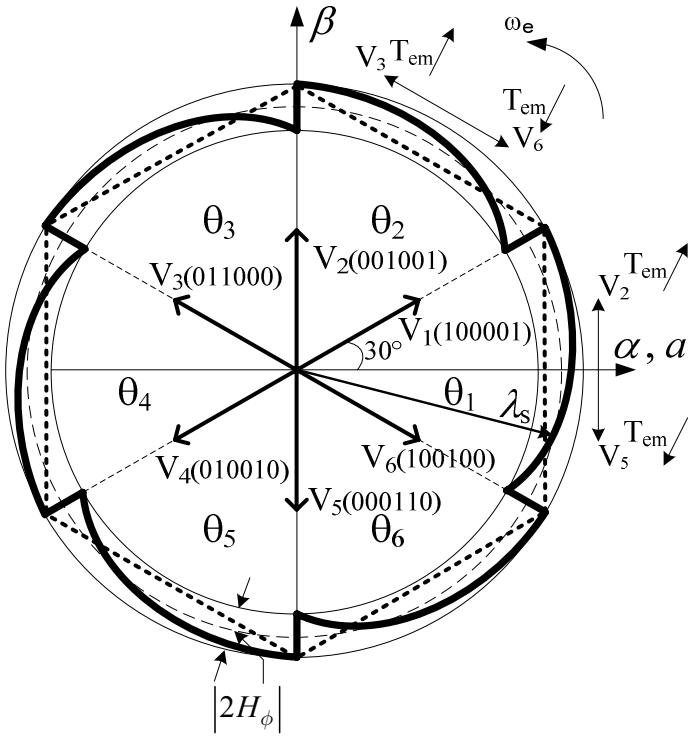

Fig. 2.1. Actual (solid curved lines) and ideal (straight dotted lines) stator flux linkage trajectories, representation of two-phase voltage space vectors in the stationary *αβ*–axes reference frame.

It has also been observed from the stator flux linkage trajectory that when conventional two-phase PWM current control is used, sharp dips occur every 60 electrical degrees. This is due to the operation of the freewheeling diodes. The same phenomenon has been noticed when the DTC scheme for a BLDC motor is used, as shown in Fig. 2.1. Due to the sharp dips in the stator flux linkage space vector at every commutation (60 electrical degrees) and the tendency of the currents to match with the flat top part of the phase back-EMF for smooth torque generation, there is no easy way to control the stator flux linkage amplitude. On the other hand, rotational speed of the stator flux linkage can be easily controlled therefore fast torque response is obtained.

The size of the sharp dips is quite unpredictable and depends on several factors which will be explained in the later part of this section and the related simulations are provided in the Section 2.3. The best way to control the stator flux linkage amplitude is to know the exact shape of it, but it is considered too cumbersome in the constant torque region. Therefore, in the DTC of a BLDC motor drive with two-phase conduction scheme, the flux error φ in the voltage vector selection look-up table is always selected as zero and only the torque error τ is used depending on the error level of the actual torque from the reference torque. If the reference torque is bigger than the actual torque, within the hysteresis bandwidth, the torque error τ is defined as "1," otherwise it is "-1", as shown in Table II.

TABLE II

TWO-PHASE VOLTAGE VECTOR SELECTION FOR BLDC MOTOR

φ	τ	θ					
		θ_1	θ_2	θ_3	θ_4	θ_5	θ_6
1	*1*	*V_1(100001)*	*V_2(001001)*	*V_3(011000)*	*V_4(010010)*	*V_5(000110)*	*V_6(100100)*
	-1	*V_6(100100)*	*V_1(100001)*	*V_2(001001)*	*V_3(011000)*	*V_4(010010)*	*V_5(000110)*
0	**1**	**V_2(001001)**	**V_3(011000)**	**V_4(010010)**	**V_5(000110)**	**V_6(100100)**	**V_1(100001)**
	-1	**V_5(000110)**	**V_6(100100)**	**V_1(100001)**	**V_2(001001)**	**V_3(011000)**	**V_4(010010)**
-1	*1*	*V_3(011000)*	*V_4(010010)*	*V_5(000110)*	*V_6(100100)*	*V_1(100001)*	*V_2(001001)*
	-1	*V_4(010010)*	*V_5(000110)*	*V_6(100100)*	*V_1(100001)*	*V_2(001001)*	*V_3(011000)*

Note: The italic grey area is not used in the proposed DTC of a BLDC motor drive.

2.2.1. Control of Electromagnetic Torque by Selecting the Proper Stator Voltage Space Vector

A change in the torque can be achieved by keeping the amplitude of the stator flux linkage constant and increasing the rotational speed of the stator flux linkage as fast as possible. This allows a fast torque response to be achieved. It is shown in this section that the rotational speed of the stator flux linkage can be controlled by selecting the

proper voltage vectors while keeping the flux amplitude almost constant, in other words eliminating the flux control.

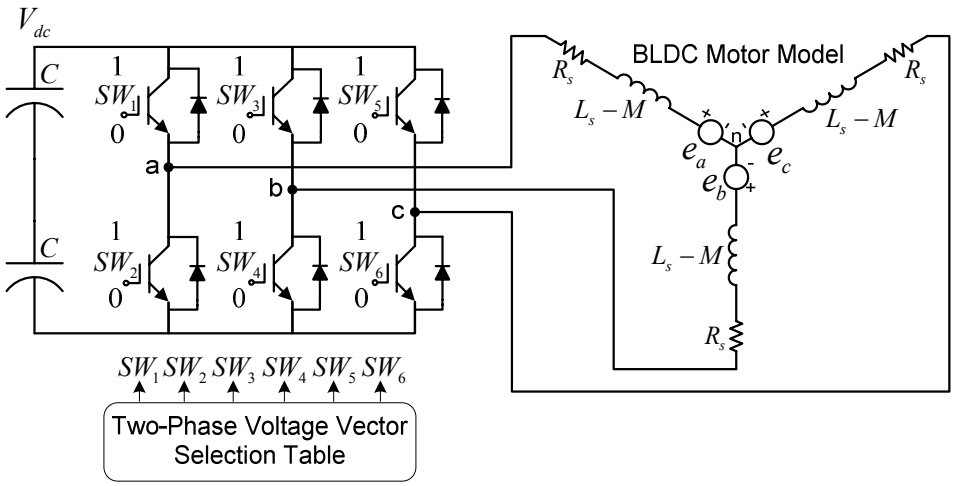

Fig. 2.2. Representation of two-phase switching states of the inverter voltage space vectors for a BLDC motor.

When the primary windings, which are assumed to be symmetric fed by an inverter using two-phase conduction mode, as shown in Fig. 2.2, the primary voltages, V_{an}, V_{bn}, and V_{cn}, are determined by the status of the six switches: SW_1, SW_2, …., and SW_6. For example, if SW_1 is one (turned on), SW_2 is zero (turned off), SW_3 is zero, and SW_4 is one then $V_{an} = V_{dc}/2$ and $V_{bn} = -V_{dc}/2$ (phase–c is open meaning that SW_5 and SW_6 are zero). Since the upper and lower switches in a phase leg may both be simultaneously off, irrespective of the state of the associated freewheeling diodes in two-phase conduction mode, six digits are required for the inverter operation, one digit for each switch [56]. Therefore, there is a total of six non-zero voltage vectors and a zero voltage vector for the two-phase conduction mode which can be represented as $V_{0,1,2,\ldots,6}$ (SW_1, SW_2, …., SW_6), as shown in Fig. 2.1. The six non-zero vectors are 60 degrees

electrically apart from each other, as depicted in Fig. 2.1, but 30 electrical degrees phase shifted from the corresponding three-phase voltage vectors which are used in three-phase conduction DTC of a PMSM drive. Stationary reference frame ($\alpha\beta$–axes) representations of the six non-zero voltage vectors with respect to dc-link voltage and switching states of the semiconductor devices are derived in Appendix C. The overall block diagram of the closed-loop DTC scheme of a BLDC motor drive in the constant torque region is represented in Fig. 2.3. The dotted area represents the stator flux linkage control part of the scheme used only for comparison purposes. When the two switches in Fig. 2.3 are changed from state 2 to state 1, flux control is considered in the overall system along with torque control. In the two-phase conduction mode the shape of stator flux linkage trajectory is ideally expected to be hexagonal, as illustrated with the straight dotted line in Fig. 2.1. However, the influence of the unexcited open-phase back-EMF causes each straight side of the ideal hexagonal shape of the stator flux linkage locus to be curved and the actual stator flux linkage trajectory tends to be more circular in shape, as shown in Fig. 2.1 with solid curved line [56]. In addition to the sharp changes, curved shape in the flux locus between two consecutive commutations complicates the control of the stator flux linkage amplitude because it depends on the size of the sharp dips, and the depth of the change may vary with sampling time, dc-link voltage, hysteresis bandwidth, motor parameters especially the phase inductance, motor speed, snubber circuit, and the amount of load torque. For example, if the phase inductance is low the current and torque ripples in the direct torque controlled motor drives will be much higher compared to the machines with higher phase inductance. Therefore, to obtain low current and

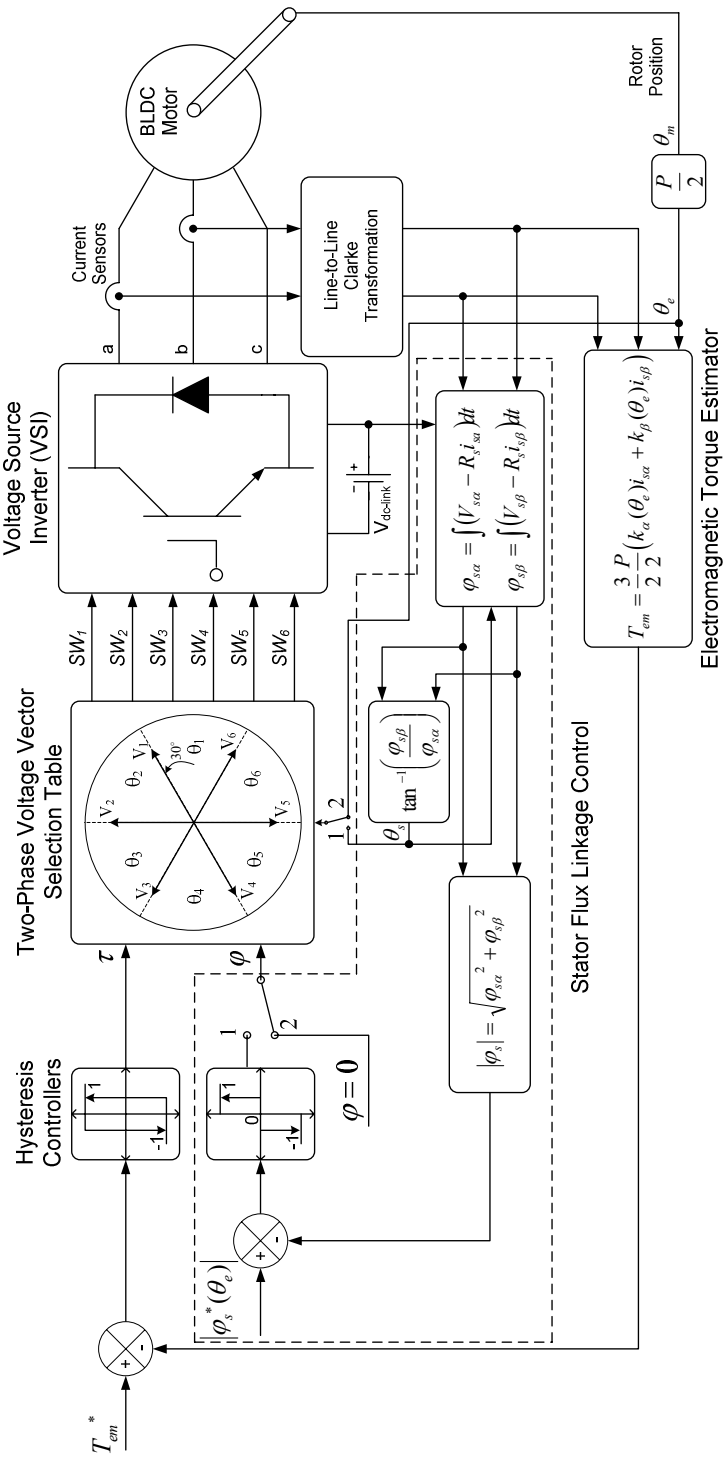

Fig. 2.3. Overall block diagram of the two-phase conduction DTC of a BLDC motor drive in the constant torque region.

torque ripples in direct torque controlled motor drives, machines with high inductance are preferred.

If a BLDC motor has an ideal trapezoidal back-EMF having a 120 electrical degree flat top, one current sensor on the dc-link can be used to estimate the torque. By knowing the sectors using hall-effect sensors the torque can be estimated with $T_{em} = 2k_e i_{dc}$, where k_e is the back-EMF constant and i_{dc} is the dc-link current. In reality, this might generate some low-frequency torque oscillations due to the approximation of the back-EMF as ideal trapezoid. To achieve a more accurate torque estimation, in general, for non-sinusoidal surface-mounted permanent magnet motors it is suggested that (2.16) should be used.

Usually the overall control system of a BLDC motor drive includes three hall-effect position sensors mounted on the stator 120 electrical degrees apart. These are used to provide low ripple torque control if the back-EMF is ideally trapezoidal because current commutation occurs only every 60 electrical degrees, as shown in Fig. 2.1. Nevertheless, using high resolution position sensors is quite useful if the back-EMF of BLDC motor is not ideally trapezoidal. The derivative of the rotor $\alpha\beta$–axes fluxes obtained from (2.18) over electrical position will cause problems mainly due to the sharp dips at every commutation point. The actual values of $\alpha\beta$–axes motor back-EMF constants k_α and k_β vs. electrical rotor position θ_e can be created in the look-up table, respectively with great precision depending on the resolution of the position sensor (for example incremental encoder with 2048 pulses/revolution), therefore a good torque estimation can be obtained in (2.16). Figures representing the actual line-to-line and $\alpha\beta$–

axes back-EMF constants $k_{ab}(\theta_e)$, $k_{bc}(\theta_e)$, $k_{ca}(\theta_e)$, $k_{\alpha}(\theta_e)$ and $k_{\beta}(\theta_e)$ are given in the Appendix A, respectively.

2.3. Simulation Results

The drive system shown in Fig. 2.3 has been simulated for various cases with and without stator flux control, switch states 1 and 2, respectively in order to demonstrate the validity of the proposed two-phase conduction DTC of a BLDC motor drive scheme.

To set the gating signals of the power switches easily and represent the real conditions in simulation as close as possible the electrical model of the actual BLDC motor with R-L elements and the inverter with power semiconductor switches considering the snubber circuit are designed in Matlab/Simulink® using the SimPower Systems toolbox.

The dead-time of the inverter and non ideal effects of the BLDC machine are neglected in the simulation model. The sampling interval is 25 μs. The switching table, which is given in Table II is employed for the proposed DTC of the BLDC motor drive. The magnitudes of the torque and flux hysteresis bands are 0.001 N·m, and 0.001 Wb, respectively. It may be noted that the zero voltage vector suggested in [56] is not used in the proposed scheme due to the reasons explained in Section 2.1.

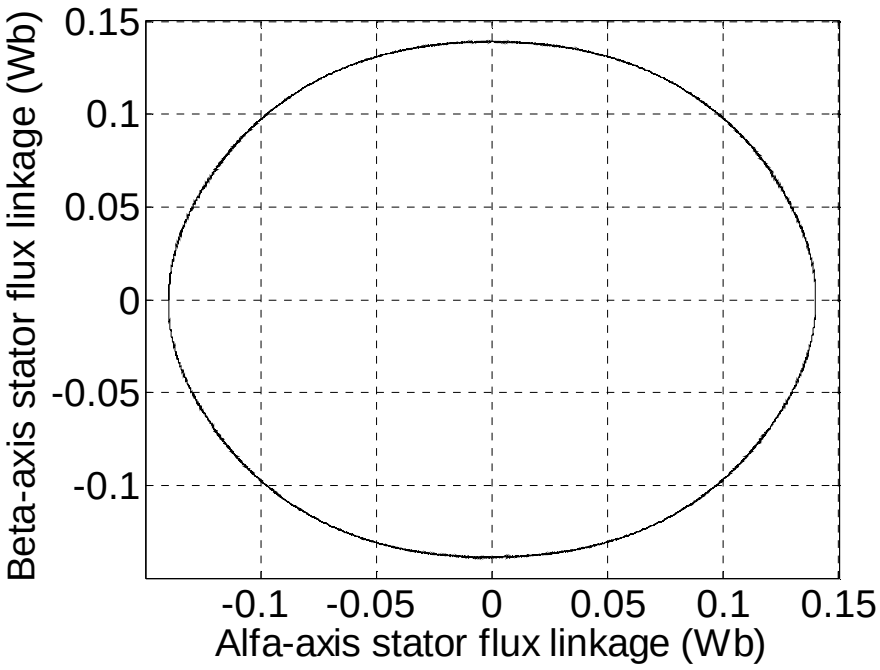

Fig. 2.4. Simulated open-loop stator flux linkage trajectory under the two-phase conduction DTC of a BLDC motor drive at no load torque (speed + torque control).

Figs. 2.4 and 2.5 show the simulation results of the uncontrolled open-loop stator flux linkage locus when 0 N·m and 1.2835 N·m load torque are applied to the BLDC motor with ideal trapezoidal back-EMF, respectively. Fig. 2.4 represents the removal of the free-wheeling diode effect on flux locus with unloaded condition. Steady-state speed control is performed with an inner-loop torque control without flux control. Stator flux linkage is estimated using (2.18) as an open-loop. As can be seen in Fig. 2.5 when the load torque level increases, more deep sharp changes are observed which increases the difficulty of the flux control if it is used in the control scheme. The steady-state speed is 30 mechanical rad/s and the dc-link voltage V_{dc} equals $40\sqrt{2}$ V. Since the speed is controlled a better open-loop circular flux trajectory is obtained.

Under only torque control, when the zero voltage vector V_0 is used to decrease the torque, as suggested in [56], larger, more frequent spikes on the phase voltages are observed in Fig. 2.6 compared to the ones used from the suggested voltage vector look-up table given in Table II.

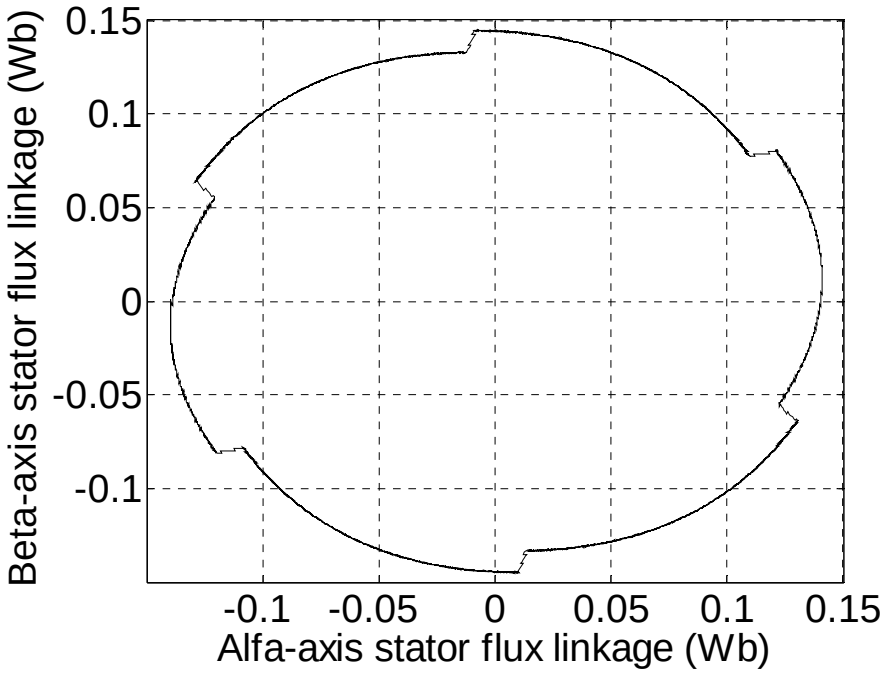

Fig. 2.5. Simulated open-loop stator flux linkage trajectory under the two-phase conduction DTC of a BLDC motor drive at 1.2835 N·m load torque (speed + torque control).

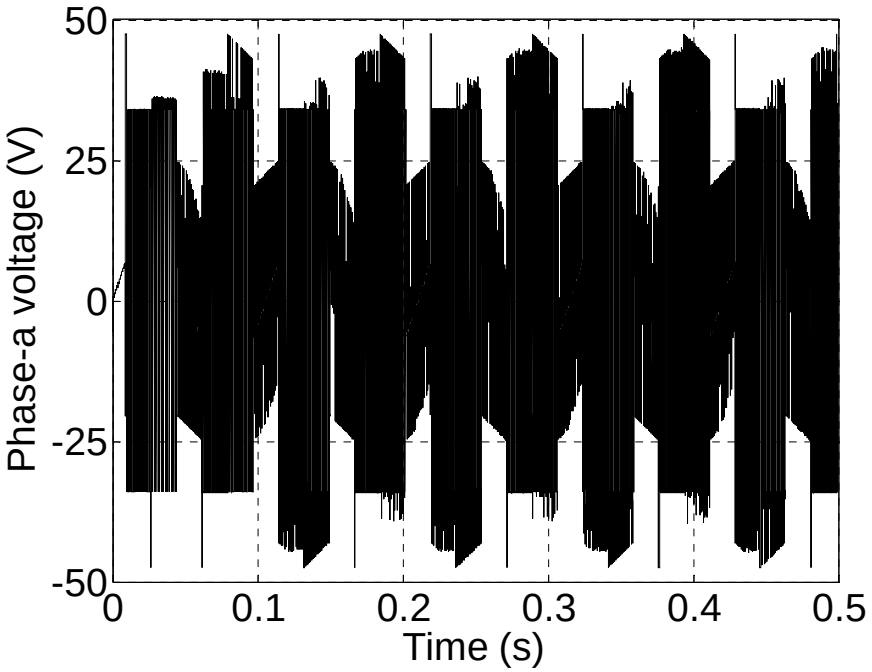

Fig. 2.6. Simulated phase–*a* voltage under 1.2 N·m load when zero voltage vector is used to decrease the torque (only torque control is performed).

Using the actual *αβ*–axes rotor flux linkages in (2.20) looks like the best solution for a good stator flux reference similar to the DTC of a PMSM drive. Unlike BLDC motor, in PMSM since both *α*– and *β*–axis motor back-EMFs are in sinusoidal shape, constant stator flux linkage amplitude is obtained. However, for BLDC motor, unexcited open-phase back-EMF effect on flux locus and more importantly the size of the sharp dips cannot easily be predicted to achieve a good stator flux reference in two-phase conduction mode. Fig. 2.7 represents the stator flux locus when back-EMF is not ideally a trapezoidal under full-load (1.2835 N·m). The simulation time is 3 seconds. As can be clearly seen in Fig. 2.7 that when flux is controlled the sharp changes in the flux locus, which are observed in Fig. 2.5, are reduced. Although the flux control is reasonable,

unwanted current amplitude is generated as seen in Fig. 2.8 to keep the torque and flux in the desired level.

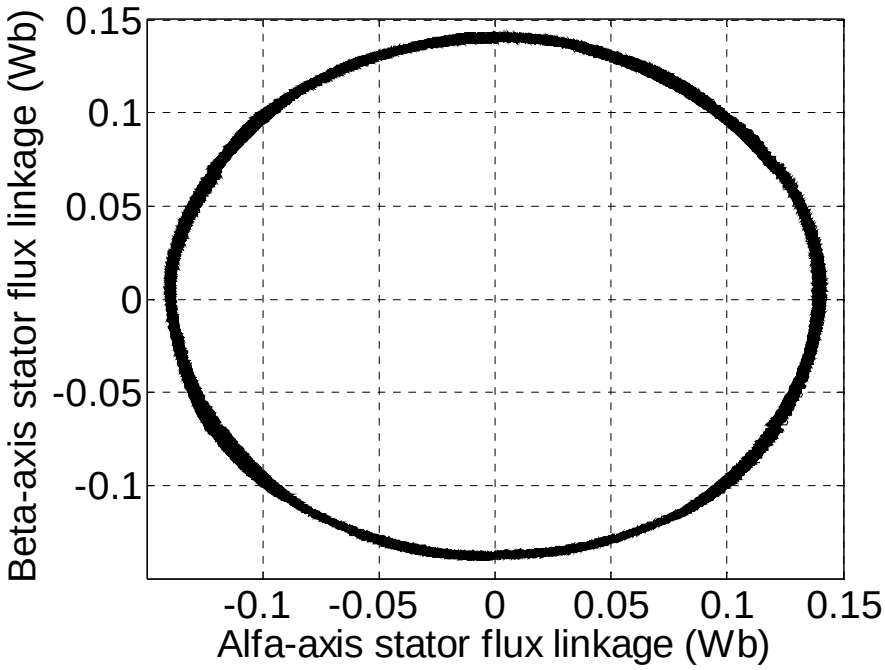

Fig. 2.7. Simulated stator flux linkage locus with non-ideal trapezoidal back-EMF under full load (speed + torque + flux control).

Even though the torque control still exists for some time with low-frequency oscillations, motor will be damaged because of high terminal current exceeding the peak current of 24 A, as shown in Fig. 2.8. Instability in the torque compared to the current does not occur except high ripples because hysteresis torque and flux controllers try to correct the errors in the torque and flux by applying unwanted voltage vectors. There is higher voltage than what is expected (~ 34 V) in the motor terminals compared to when just torque control is used without flux control. Because large and distorted terminal voltages exist, higher and distorted phase currents as seen in Fig. 2.8 are obvious. All

these problems are because of the flux control. There should be exact flux amplitude to be given as a reference flux value including sharp changes at every commutation points and curved shape between those commutation points, then appropriate flux control can be obtained without losing the torque control. However, to predict all these circumstances to generate a flux reference is cumbersome work which is unnecessary in the constant torque region.

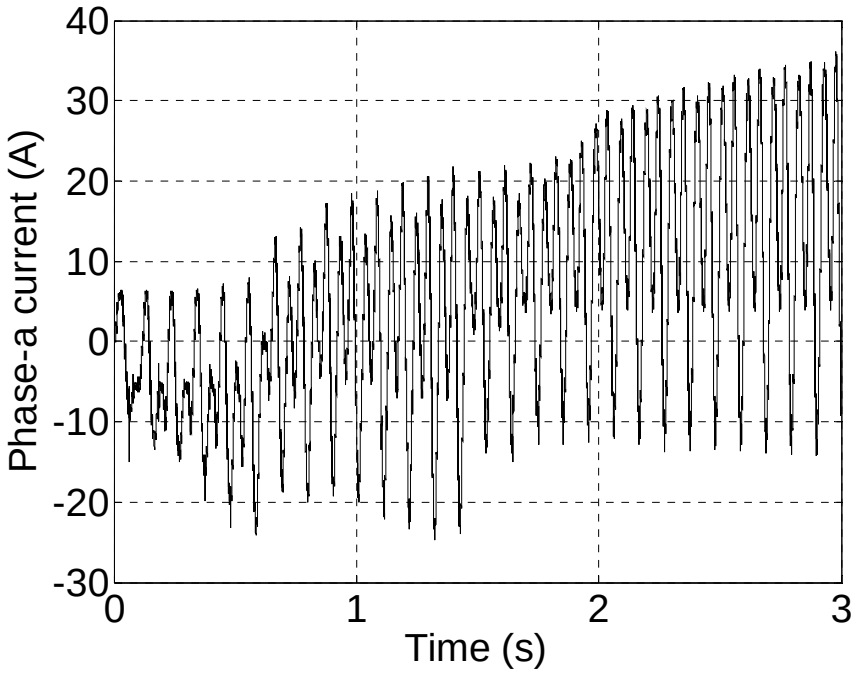

Fig. 2.8. Simulated phase–*a* current when flux control is obtained using (2.20) under full load (speed + torque + flux control).

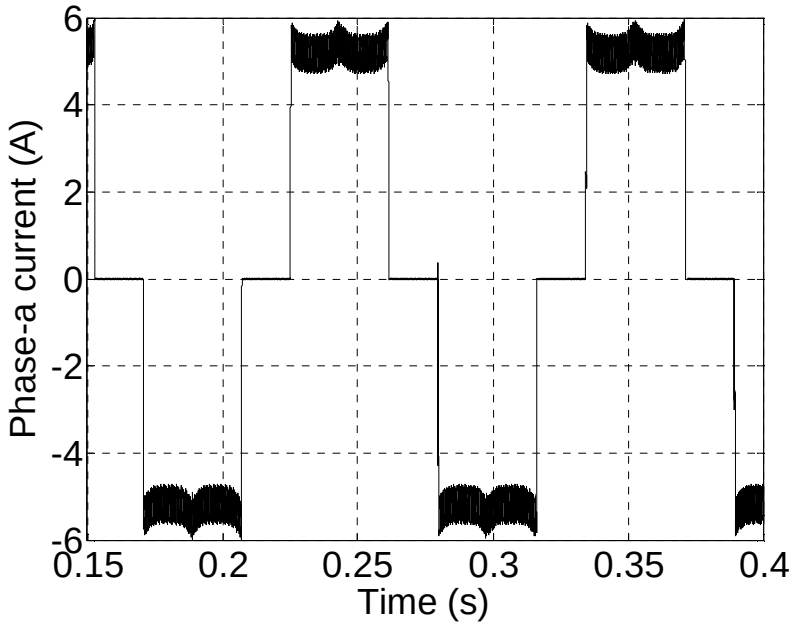

Fig. 2.9. Simulated phase–*a* current when just torque is controlled without flux control under 1.2 N·m load with non-ideal trapezoidal back-EMF (reference torque is 1.225 N·m).

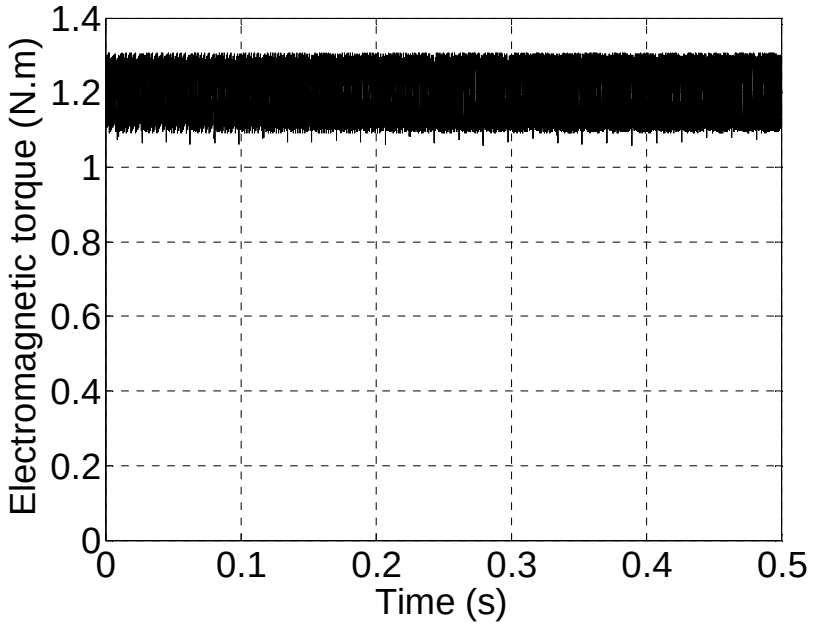

Fig. 2.10. Simulated electromagnetic torque when just torque is controlled without flux control under 1.2 N·m load with non-ideal trapezoidal back-EMF (reference torque is 1.225 N·m).

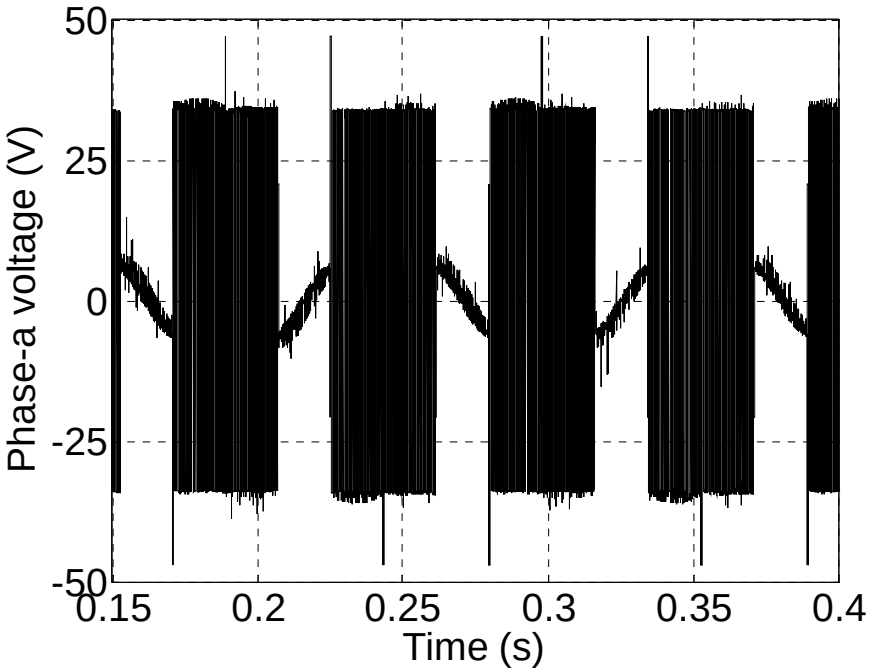

Fig. 2.11. Simulated phase–*a* voltage when just torque is controlled without flux control under 1.2 N·m load with non-ideal trapezoidal back-EMF (reference torque is 1.225 N·m).

Figs. 2.9–2.11 show phase–*a* current, electromagnetic torque and phase–*a* voltage, respectively under only torque control when the back-EMF is not ideally trapezoidal considering only the first, third and fifth harmonics of the fundamental ideal trapezoidal back-EMF. Reference torque is 1.225 N·m and the load torque is 1.2 N·m, thereby speed is kept at around 55 electrical rad/s for a better circular flux locus. If high resolution position sensor such as incremental encoder is used instead of the three hall-effect sensors, low-frequency torque oscillations can be minimized by using (2.16), as shown in Fig. 2.10. In (2.16), the product of the actual $\alpha\beta$–axes back-EMF constants by the corresponding $\alpha\beta$–axes currents and number of pole pairs provide the exact values of the α– and β–axis torque, respectively.

2.4. Experimental Results

The feasibility and practical features of the proposed DTC scheme of a BLDC motor drive have been evaluated using an experimental test-bed, as shown in Fig. 2.12. The proposed control algorithm is digitally implemented using the eZdsp^{TM} board from Spectrum Digital, Inc. based on TMS320F2812 DSP, as shown in Fig 2.12(a). In Fig. 2.12(b), the BLDC motor whose parameters are given in the Appendix A is coupled to the overall system.

In this section, transient and steady-state torque and current responses of the proposed two-phase conduction DTC scheme of a BLDC motor drive are demonstrated experimentally under 0.2 pu load torque condition. The experimental results are obtained from the datalog (data logging) module in the Texas Instruments Code Composer Studio^{TM} IDE software.

Fig. 2.13(a) and (b) illustrate the experimental results of the phase–*a* current and torque, respectively when only torque control is performed using (2.16), as shown in Fig. 2.3 with switch state 1. In Fig. 2.13(b), the reference torque is suddenly increased from 0.225 pu to 0.45 pu at 9.4 ms under 0.2 pu load torque. One per-unit is 1.146 N·m for torque, 5 A for current, and 1800 rpm for speed. The sampling time is chosen as 1/30000 second, hysteresis bandwidth is 0.001 N·m, dead-time compensation is included, and the dc-link voltage is set to $V_{dc} = 40\sqrt{2}$ V. As it can be seen in Fig. 2.13(a) and (b), when the torque is suddenly increased the current amplitude also increases and fast torque response is achieved. The high frequency ripples observed in the torque and current are related to the sampling time, hysteresis bandwidth, winding inductance, and dc-link

voltage. This is well in accordance with the simulation results in Figs. 2.9 and 2.10 where the sampling time is chosen as 25 μs.

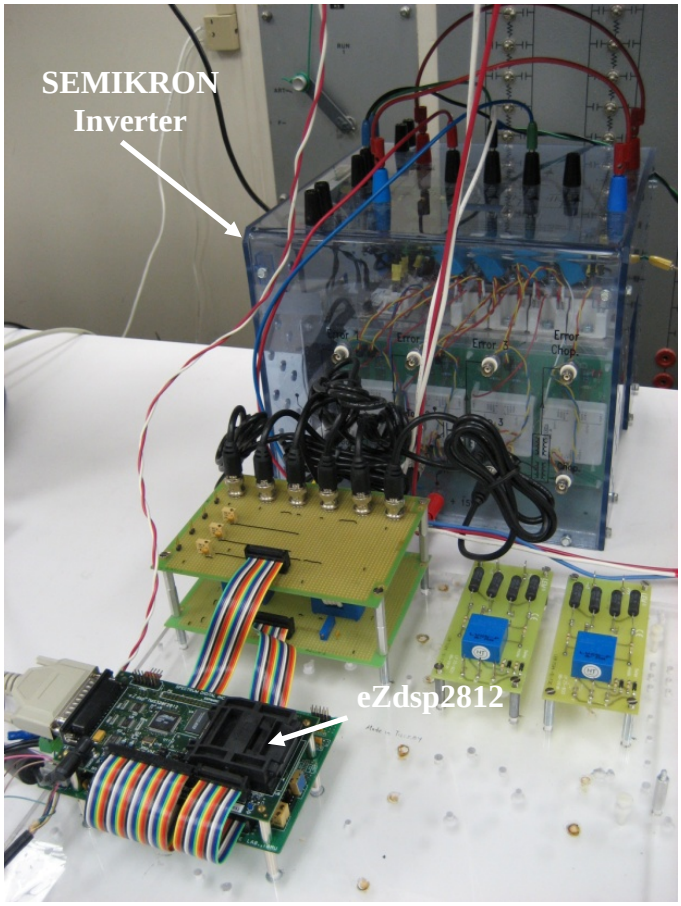

(a)

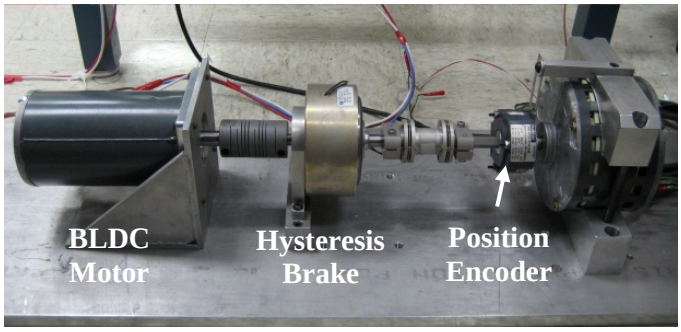

(b)

Fig. 2.12. Experimental test-bed. (a) Inverter and DSP control unit. (b) BLDC motor coupled to dynamometer and position encoder (2048 pulse/rev).

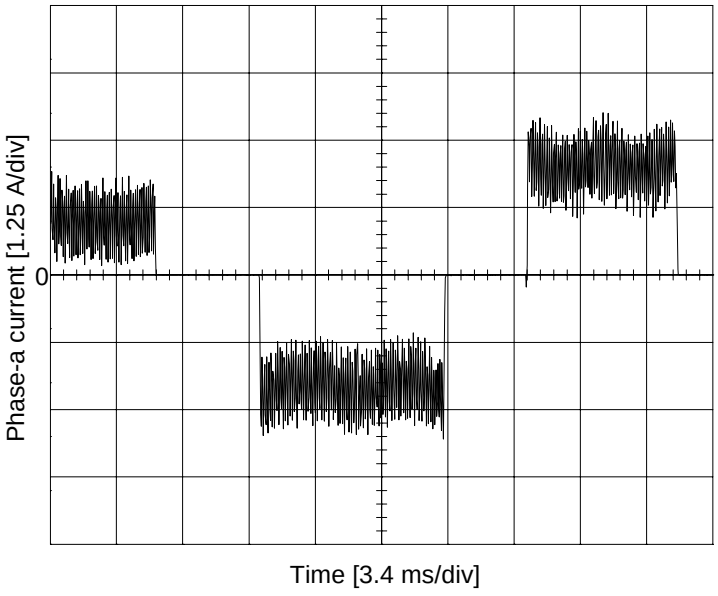

(a)

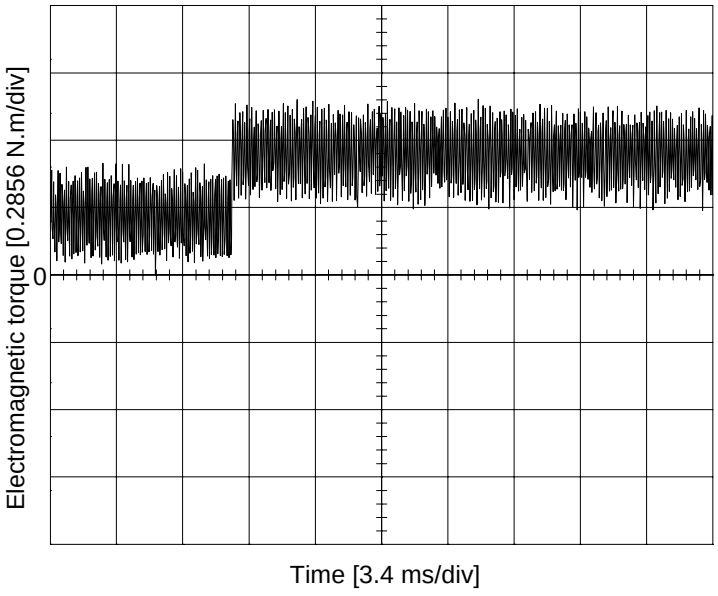

(b)

Fig. 2.13. (a) Experimental phase–*a* current and (b) electromagnetic torque under 0.2292 N·m (0.2 pu) load.

2.5. Conclusion

This study has successfully demonstrated application of the proposed two-phase conduction direct torque control (DTC) scheme for BLDC motor drives in the constant torque region. A look-up table for the two-phase voltage vector selection is designed to provide faster torque response both on rising and falling conditions. Compared to the three phase DTC technique, this approach eliminates the flux control and only torque is considered in the overall control system. Three reasons are given for eliminating the flux control. First, since the line-to-line back-EMF including the small voltage drops is less than the dc-link voltage in the constant torque region there is no need to control the flux amplitude. Second, with the two-phase conduction mode sudden sharp dips in the stator flux linkage locus occur that complicate the control scheme. The size of these sharp dips is unpredictable. Third, regardless of the stator flux linkage amplitude, the phase currents tend to match with the flat top portion of the corresponding trapezoidal back-EMF to generate constant torque.

CHAPTER III

POWER FACTOR CORRECTION OF DIRECT TORQUE CONTROLLED BRUSHLESS DC MOTOR WITH NON-SINUSOIDAL BACK-EMF USING TWO-PHASE CONDUCTION MODE

3.1. Introduction

In general, ac motor drives have very poor power factor due to the high number of harmonics in the line current. Power factor correction (PFC) method is a good candidate for ac-dc switched mode power supply in order to reduce the harmonics in the line current, increase the efficiency and capacity of motor drives, and reduce customers' utility bills. There are two general types of PFC methods to obtain a unity power factor: analog and digital PFC techniques. In the past, due to the absence of fast microprocessors and DSPs, analog PFC methods were the only choice for achieving the unity power factor. Many control strategies using analog circuits have been explored in the past, including average current control [59], peak current control [60], hysteresis control [61], nonlinear carrier control [62], etc. With the recent developments in the microprocessor and DSP technologies, there is a possibility of implementing the complicated PFC algorithms using these fast processors [63].

As compared to conventional analog controllers, digital regulators offer several advantages such as possibility of implementing nonlinear and sophisticated control

algorithms, reduction of the number of control components, high reliability, low sensitivity to component aging, better performance than that in analog implementation with the same cost, reduced susceptibility to environmental variations such as thermal drifts, and negligible offsets.

Digital control PFC implementations have been investigated by many researchers [64]–[66]. Majority of the work has been done on the implementation of the analog PFC techniques in the digital platform. There has been very little work done in the literature to implement the digital PFC methods on ac motor drives. The basic idea of the proposed PFC method in this paper is to update the required amount of duty cycle for boost converter in every sampling time of the DTC of BLDC motor drive.

In this section, first of all the principle of the average current control boost PFC with feed-forward voltage compensation technique is presented in Section 3.2. In Section 3.3, the hardware implementation and experimental results of the proposed DTC of BLDC motor drive in two-phase conduction mode using average current control with input voltage feed-forward compensation boost PFC including load disturbance are presented. The conclusion is presented in Section 3.4.

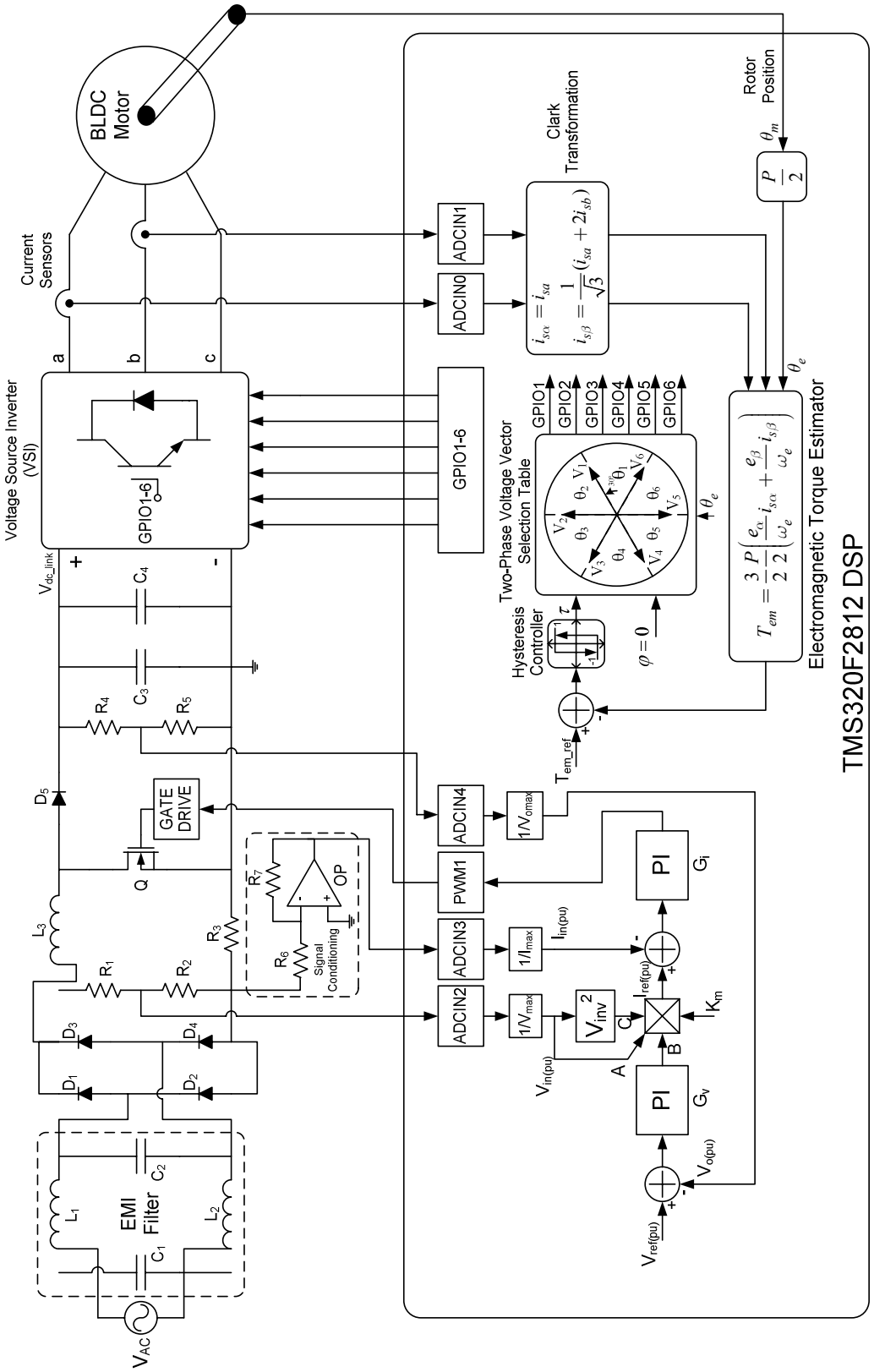

Fig. 3.1. Overall block diagram of the two-phase conduction DTC of a BLDC motor drive with boost PFC in the constant torque region.

3.2. The Average Current Control Boost PFC With Feed-Forward Voltage Compensation

The main topology of the power factor pre-regulator based on boost converter includes two parts: rectifier circuit and boost circuit. The block diagram and DSP control stage of the boost PFC using average current control with feed-forward voltage compensation is shown in Fig. 3.1. As can be seen in Fig. 3.1, in contrast to the conventional boost circuit, the large filter capacitor of the power factor pre-regulator is placed at the output of the system. As indicated in Fig. 3.1, three signals are required to implement the control algorithm. These are, the rectified input voltage V_{in}, the inductor current I_{in}, and the dc output voltage V_o. There are two feedback loops in the control system. The average output dc voltage V_o is regulated by a slow response (high bandwidth), whereas the inner loop that regulates the input current I_{in} is a much faster loop (low bandwidth).

For the purpose of digital control of a boost PFC converter, the instantaneous analog signals V_{in}, I_{in}, and V_o are all sensed and fed back to the DSP via three ADC channels ADCIN2, ADCIN3, and ADCIN4 at every sampling period, T_s respectively. Then they are converted to the per-unit equivalents using the gain blocks. The per-unit output voltage $V_{o(pu)}$ is compared to the desired per-unit reference voltage $V_{ref(pu)}$ and the difference signal ($V_{ref(pu)} - V_{o(pu)}$) is then fed into the voltage loop controller G_v. The output of the G_v, indicated as B, controls the amplitude of the per-unit reference current $I_{ref(pu)}$ such that for the applied load current and line voltage, the output voltage V_o is maintained at the reference level. Then, it is multiplied by the two other feed-forward

components, A and C, to generate the reference current command for the inner current loop. In Fig. 3.1, the component A represents the digitized instantaneous per-unit input sensed signal V_{in} and the component C is one over square of the per-unit averaged input voltage which equals $1/V_{dc(pu)}^2$. The derivation of the feed-forward voltage component C is given in Section 3.2.1. The per-unit reference current command $I_{ref(pu)}$ for the inner current loop has the shape of a rectified sinewave and its amplitude is such that it maintains the per-unit output dc voltage $V_{o(pu)}$ at per-unit reference voltage $V_{ref(pu)}$ level overcoming load and input voltage disturbances. The difference signal ($I_{ref(pu)} - I_{in(pu)}$) is then passed into the current loop controller G_i in which the PWM duty ratio command is generated for the boost converter switch to maintain the per-unit inductor current $I_{in(pu)}$ at the per-unit reference current $I_{ref(pu)}$ level. The multiplier gain K_m whose derivation is provided in Section 3.2.1 is also added to the control block which allows adjustments of the per-unit reference current $I_{ref(pu)}$ signal based on the converter input voltage operating range $V_{min} - V_{max}$ [67].

3.2.1. Calculation of Feed-Forward Voltage Component *C* and Multiplier Gain K_m

For simplicity per-unit system has been used to describe the components and all variables in the control system. Therefore, the voltage and current signals are automatically saved as per-unit (pu) numbers normalized with respect to their own maximum values.

The multiplier gain K_m is useful to adjust the reference current at its maximum when the PFC boost converter delivers the maximum load at the minimum input voltage

V_{in}. In Fig. 3.1, per-unit reference current $I_{ref(pu)}$ is expressed in terms of K_m, A, B, and C as follows:

$$I_{ref\,(pu)} = K_m ABC \tag{3.1}$$

where A is the per-unit value of the sensed input voltage V_{in}, B is the output of the voltage PI controller G_v, and C is the inverse square of the averaged input rectified voltage V_{dc}, respectively.

The average per-unit value $V_{dc(pu)}$ of the input per-unit voltage $V_{in(pu)}$ is given as

$$V_{dc\,(pu)} = \frac{1}{T}\int_0^T V_{in\,(pu)}\,dt \tag{3.2}$$

where T is the time period of the input voltage corresponding to the grid frequency which is 60 Hz in this case and $V_{in(pu)}$ is the per-unit value of the input rectified voltage normalized with respect to its maximum peak value V_{max}. In (3.2), the base value of the per-unit average rectified input voltage $V_{dc(pu)}$ is also chosen as V_{max}.

The maximum value of the average value V_{dc} of the sinewave input voltage is only $2V_{max}/\pi$. Therefore, the final per-unit representation of the average per-unit voltage $V_{dc(pu)}$ is given by

$$V_{dcx\,(pu)} = V_{dc\,(pu)}\,\frac{V_{max}}{(2V_{max}/\pi)} = \frac{\pi V_{dc\,(pu)}}{2} \tag{3.3}$$

The inverse per-unit voltage $V_{inv(pu)}$ of the average per-unit component $V_{dc(pu)}$ of the per-unit input voltage $V_{in(pu)}$ can be calculated as follows:

For per-unit representation of the average inverse voltage V_{inv}, maximum inverse voltage V_{inv_max} should be found which equals the inverse minimum of the average input

voltage $1/V_{dc\_min} = \pi/(2V_{min})$ where V_{min} is the minimum peak amplitude of the rectified input voltage selected based on the input operating voltage range of the PFC boost converter. Finally, the per-unit value of the inverse voltage $V_{inv(pu)}$ in terms of $V_{dc(pu)}$, V_{min}, and V_{max} is given as

$$V_{inv(pu)} = \frac{\left(\frac{1}{V_{dcx(pu)}V_{dc\_max}}\right)}{V_{inv\_max}} = \frac{2}{\pi V_{dc(pu)}}\frac{V_{min}}{V_{max}} \tag{3.4}$$

where V_{dc_max} is the maximum average input rectified voltage equals $1/V_{inv\_min} = 2V_{max}/\pi$. In (3.4), the numerator in parentheses represents the non per-unit value of the inverse average input voltage V_{inv}.

Once the inverse per-unit voltage $V_{inv(pu)}$ is calculated, the feed-forward voltage component C can be found as

$$C = V_{inv(pu)}{}^2 = \frac{4}{(\pi V_{dc(pu)})^2}\left(\frac{V_{\min}}{V_{\max}}\right)^2 = \frac{4}{(\pi V_{dc(pu)}K_m)^2} \tag{3.5}$$

where the multiplier gain K_m can be expressed using (3.1) such that the reference per-unit current $I_{ref(pu)}$ is at its maximum when the PFC boost converter delivers the maximum load at the minimum operating input voltage as

$$K_m = \frac{V_{\max}}{V_{\min}} \tag{3.6}$$

The overall block diagram of the closed-loop DTC scheme of a BLDC motor drive with average current control boost PFC in the constant torque region is represented in Fig. 3.1. In Fig. 3.1, since there is no PWM generation required in the proposed DTC

scheme, six GPIO pins for DTC scheme and only one PWM output pin for PFC algorithm are used to achieve the overall closed-loop control.

3.3. Experimental Results

The feasibility and practical features of the proposed DTC scheme of a BLDC motor drive with average current control boost PFC have been evaluated using an experimental test-bed, shown in Fig. 3.2. The proposed control algorithm is digitally implemented using the eZdsp^{TM} board from Spectrum Digital, Inc. based on a fixed-point TMS320F2812 DSP, as shown in Fig 3.2(a). In Fig. 3.2(b), the BLDC motor whose parameters are given in the Appendix A is coupled to the overall system.

The average current control boost PFC with feed-forward voltage compensation method has been implemented in a single sampling time of the proposed DTC of a BLDC motor drive under two-phase conduction mode in the constant torque region. The boost converter switch is FET47N60C3, and the diode is STTH8R06D. The passive components of the boost converter are the inductor L_3 = 1 mH and output filter capacitors $C_3 = C_4$ = 270 μF, as seen in Fig. 3.1. The boost converter switches at 80 kHz which is the sampling frequency of the overall control system and supplies 80 V_{dc} at the output. The input voltage range, V_{min} ─ V_{max}, is 28.28 V_{ac} ─ 70.71 V_{ac} peak. The EMI filter is used in order to reduce the high order switching harmonics in the line current which consists of the inductors $L_1 = L_2$ = 10 μH and the capacitors $C_1 = C_2$ = 1 μF.

Gain of the feed forward path K_m = 2.5 was selected in this implementation. In this paper, digital proportional-integral (PI) controllers are used in the voltage and

current loops. The coefficients of the PI voltage and current controllers are chosen as K_{pv} = 0.1736, K_{iv} = 0.01388, K_{pi} = 0.005, and K_{ii} = 0.03125, respectively. One per-unit is 1.146 N·m for torque, 5 A for current, and 1800 rpm for speed. Hysteresis bandwidth is 0.001 N·m, and the dead-time compensation is included as well.

In the implementation, over-current and voltage protections have been used for the inductor current and output voltage. Once the sensed inductor current and output dc voltage are higher than 8 A and 140 V, respectively a protection logic signal is generated and used to turn off the gate signal of the boost converter.

Steady-state current response of the proposed two-phase conduction DTC scheme of a BLDC motor drive with average current control boost PFC is demonstrated experimentally under 0.371 N·m load torque condition in Fig. 3.3 where the reference torque is 0.573 N·m. The experimental results are obtained from the datalog (data logging) module in the Texas Instruments Code Composer Studio™ IDE software. The high frequency ripples in the current observed in Fig. 3.3 depend on the hysteresis bandwidth of the torque control, sampling time, especially motor winding inductance, and the amount of dc-link voltage. Because the machine used in the tests has low winding inductance and the dc-link is selected quite high for better power factor, the current ripples are expected to be high as seen in Fig. 3.3.

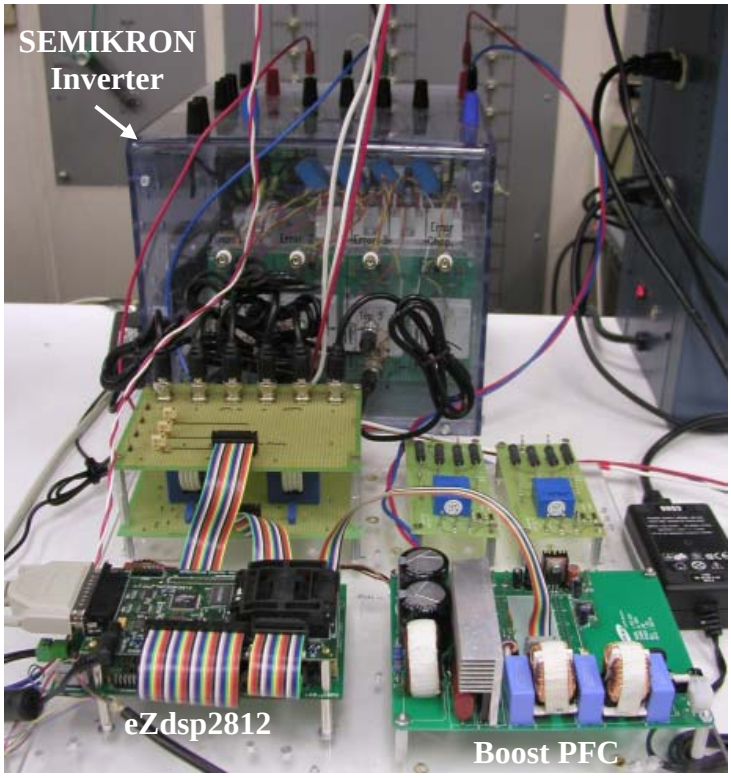

(a)

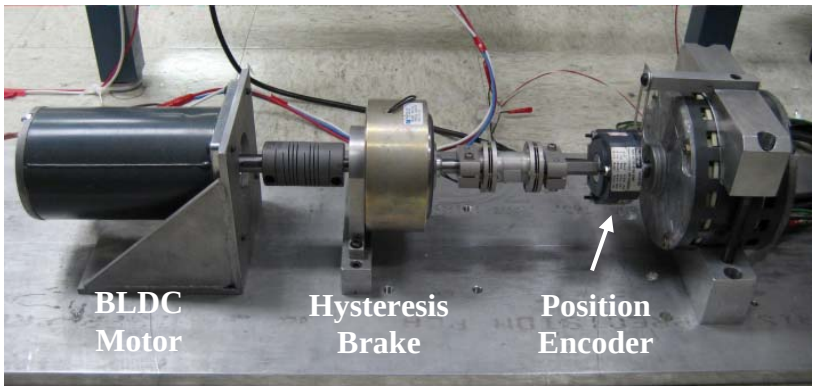

(b)

Fig. 3.2. Experimental test-bed. (a) Inverter, DSP control unit, and boost PFC board. (b) BLDC motor coupled to dynamometer and position encoder (2048 pulse/rev.).

Fig. 3.4 shows the measured output voltage, line voltage, and line current waveforms for the two-phase DTC of BLDC motor drive at no load and at the steady-state without PFC. The power factor under this operating condition is 0.7667. The

measured total harmonic distortion of the input line current and line voltage are 82.23% and 4.79%, respectively. The output active power is 55.3 W.

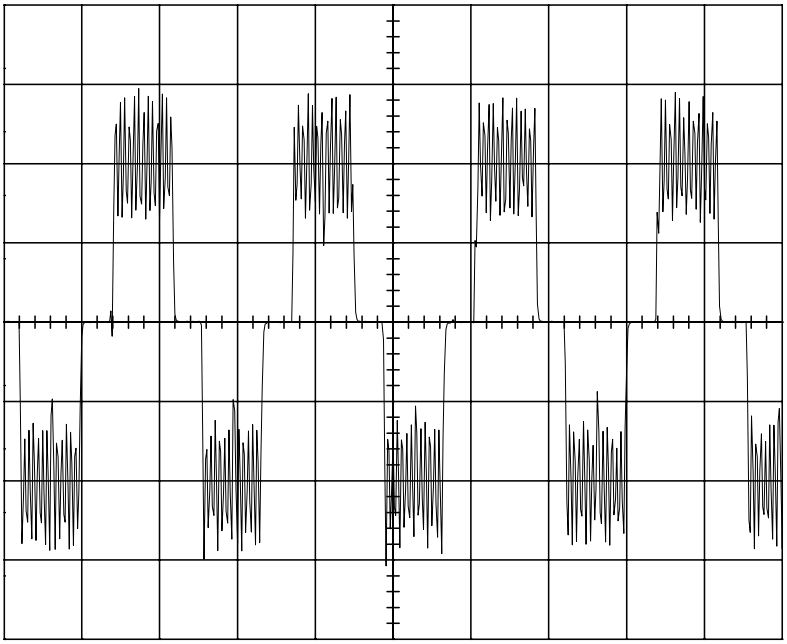

Fig. 3.3. Measured steady-state phase-a current of two-phase DTC of BLDC motor drive using boost PFC under 0.371 N·m load with 0.573 N·m reference torque. Current: 1.25 A/div. Time base: 0.7 ms/div.

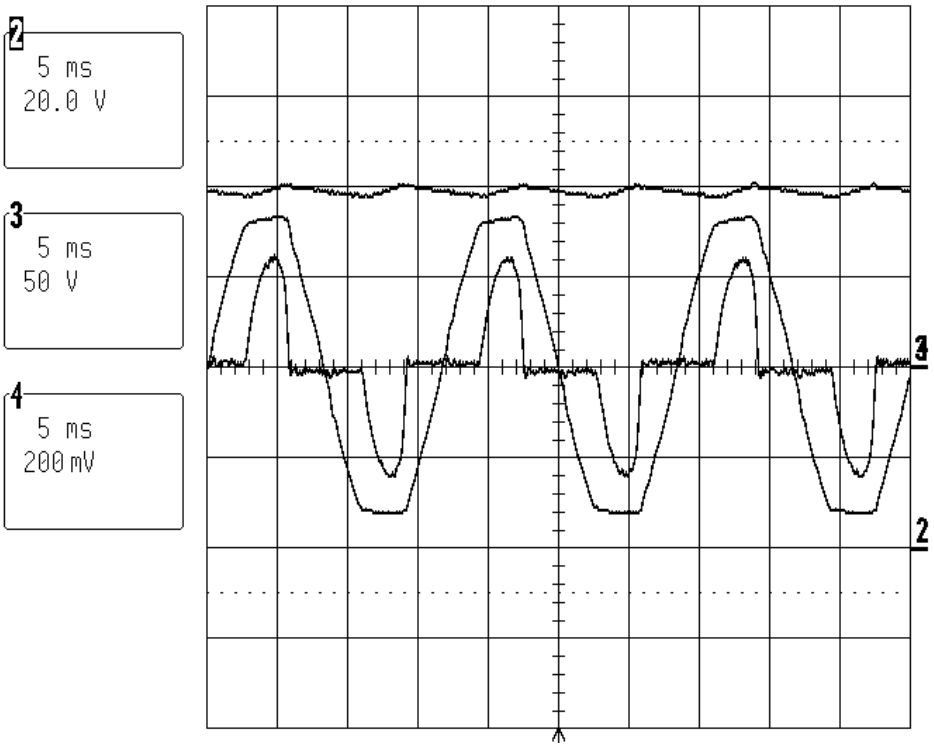

Fig. 3.4. Measured output dc voltage V_o, line voltage V_{line}, and line current I_{line} without PFC under no load with 0.4 N·m reference torque. (Top) Output dc voltage V_o = 80 V. (Middle) Line voltage V_{line} = 64.53 V_{rms}. (Bottom) Line current I_{line} = 1.122 A. V_o: 20 V/div; I_{line}: 2 A/div; V_{line}: 50 V/div. Time base: 5 ms/div.

Since no PFC control has been applied to the two-phase conduction DTC of BLDC motor drive, the power factor is poor and the line current has harmonics in it as can be seen in Fig. 3.4. Moreover, the output dc voltage also has some fluctuations due to the absence of the PFC control. These problems can be eliminated by using a PFC control algorithm during a single sampling period of the DTC of BLDC motor drive system.

The output dc voltage, input line current, and line voltage waveforms for the two-phase DTC of BLDC motor control at no load and at the steady-state with average

current control boost PFC are shown in Fig. 3.5. The measured total harmonic distortion of the input line current and line voltage are 5.45% and 3.45%, respectively and the measured power factor is 0.9997. The output active power of the total system is 69.3 W. Since the PFC algorithm is adapted to the overall DTC of BLDC motor drive system, low-frequency oscillations on dc-link voltage is reduced and the line current is more sinusoidal, thereby eliminating harmonics as seen in Fig. 3.5 compared to the ones shown in Fig. 3.4. Thus, the power factor and the efficiency of the total system are improved considerably.

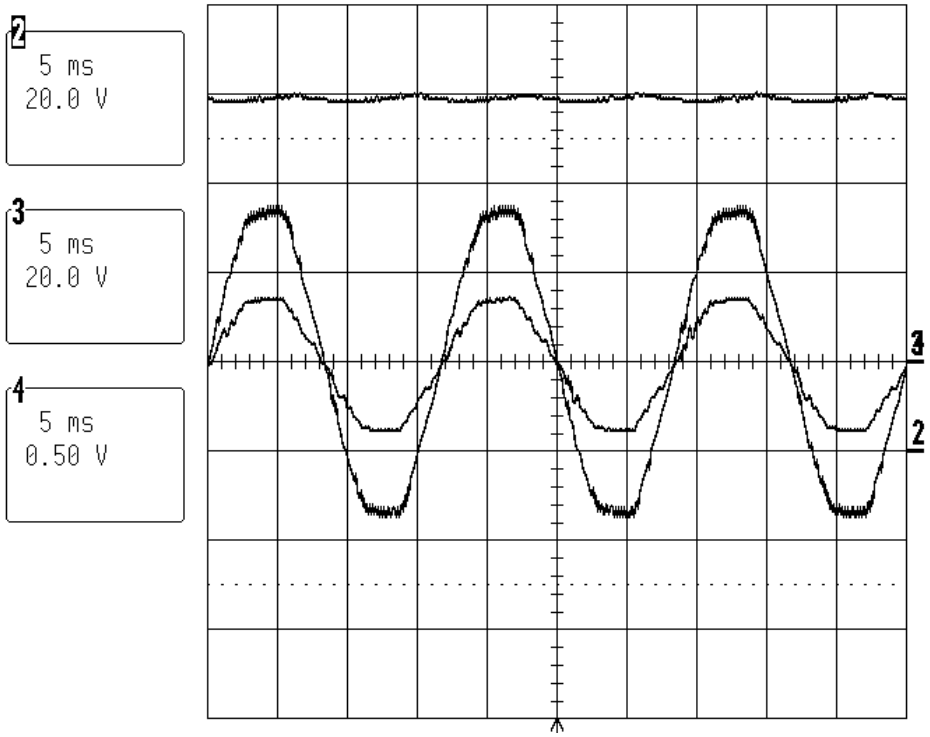

Fig. 3.5. Measured steady-state output dc voltage V_o, line voltage V_{line}, and line current I_{line} with PFC under no load with 0.4 N·m reference torque. (Top) Output dc voltage V_o = 80 V. (Middle) Line voltage V_{line} = 25.43 V_{rms}. (Bottom) Line current I_{line} = 2.725 A. V_o: 20 V/div; I_{line}: 5 A/div; V_{line}: 50 V/div. Time base: 5 ms/div.

Fig. 3.6 shows the measured output voltage, line voltage, and line current waveforms for the two-phase DTC of BLDC motor control under 0.371 N·m load at the steady-state with PFC. The power factor under this operating condition is 0.9997. The measured total harmonic distortion of the input line current and line voltage are 5.05% and 3.43%, respectively. The output active power of the total system in this case is 108.6 W.

Due to the existence of the load torque, output dc voltage in Fig. 3.6 has some distortion as compared to the dc output voltage shown in Fig. 3.5. There has not been a significant difference observed in the line currents and line voltages between Fig. 3.5 and Fig. 3.6.

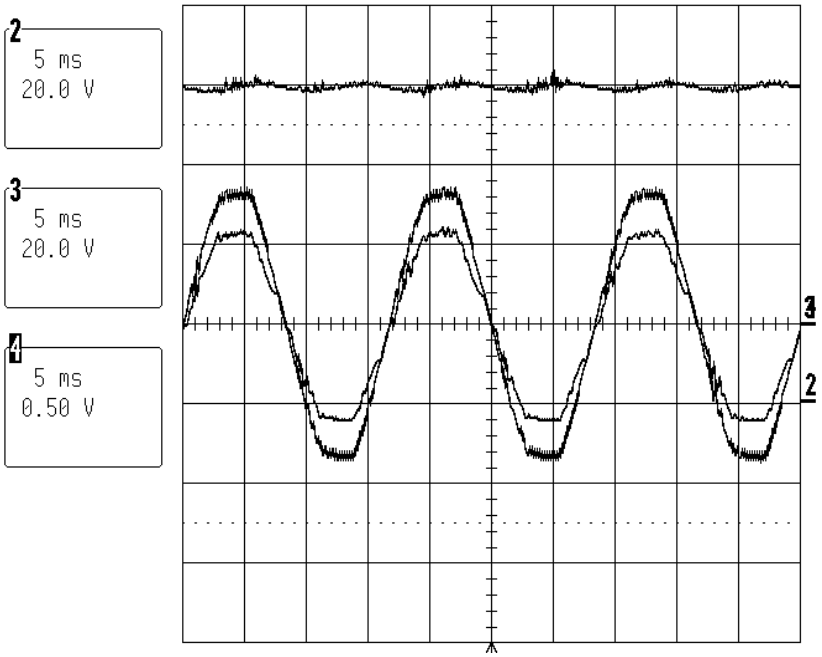

Fig. 3.6. Measured steady-state output dc voltage V_o, line voltage V_{line}, and line current I_{line} with PFC under 0.371 N·m load with 0.573 N·m reference torque. (Top) Output dc voltage V_o = 80 V. (Middle) Line voltage V_{line} = 25.2 V_{rms}. (Bottom) Line current I_{line} = 4.311 A. V_o: 20 V/div; I_{line}: 5 A/div; V_{line}: 50 V/div. Time base: 5 ms/div.

3.4. Conclusion

The digital implementation of the DTC for BLDC motor drive using two-phase conduction mode with average current control boost PFC during a single sampling period of the motor drive system has been successfully demonstrated on an eZdsp^{TM} board featuring a TMS320F2812 DSP. A prototype boost PFC controlled by a DSP evaluation board was built to verify the proposed digital control PFC strategy along with the DTC of BLDC motor drive system. Experimental results show that, based on the proposed average current control boost PFC with input voltage compensation algorithm, the power factor of 0.9997 is achieved at the steady-state under 20 to 50 V_{rms} input voltage range conditions. Moreover, the proposed PFC control strategy can achieve smooth output dc voltage which is applied to the BLDC motor drive and sinusoidal line current waveform with THD as low as 5%. Therefore, the power factor and the overall efficiency of the DTC of BLDC motor drive are increased considerably.

CHAPTER IV

DIRECT TORQUE CONTROL OF FOUR-SWITCH BRUSHLESS DC MOTOR WITH NON-SINUSOIDAL BACK-EMF USING TWO-PHASE CONDUCTION MODE

4.1. Introduction

Brushless dc motors have been used in variable speed drives for many years due to their high efficiency, high power factor, high torque, simple control, and lower maintenance [41]. Low cost and high efficiency variable speed motor drives have had growing interest over the years. Minimizing the switch counts has been proposed to replace the traditional six-switch three-phase inverter. Van Der Broeck has demonstrated the possibility to implement a three phase ac motor drive system employing the four-switch three phase inverter [68]. In [68], although the topology of the four-switch inverter for the induction motor is identical to the BLDC motor, conventional four-switch PWM schemes used for induction motor drives cannot be directly applied to BLDC motor drive. Three phase conduction scheme is presented which is inherently difficult to use in brushless dc motor drive systems incorporating only 120 electrical degree current conduction. This is due to the limited voltage space vectors of the conventional four-switch scheme. Therefore, in order to use the four-switch inverter topology for the three-phase BLDC motor drive, only two phase conduction voltage space vectors (line-to-line voltage vectors) should be obtained from the four-switch

inverter. This theory is presented in [69] where special current control method is performed for the two modes of operation (mode 2 and 5) such that when two phases which are not connected to the center of the dc-link capacitors conduct, they are individually controlled by the hysteresis PWM current controllers. By doing so, current distortions on each phase caused by the back-EMF of the inactive third phase, which is connected to the center part of the split dc-link capacitors, are reduced.

One of the other solutions to the limited voltage space vector problem is to modify the conventional voltage controlled PWM strategies, such as space vector PWM technique presented in [70, 71]. However, in [70, 71] several proportional and integral controllers are needed along with *abc* to $\alpha\beta$ (stationary reference frame) and $\alpha\beta$ to *abc* transformations for both currents and voltages. Moreover, reference current generation scheme is proposed which requires commutation interval times. Those interval times are dependant on several motor parameters such as winding inductance, dc-link voltage and back-EMF. Therefore, more complicated and parameter sensitive drive system is inevitable.

The most popular way to control BLDC motors using four- or six-switch inverter is by PWM current control in which a two-phase feeding scheme is considered with variety of PWM modes such as soft switching, hard-switching, and etc. In this work, unlike the methods discussed in [68, 70, 71], a novel direct torque control scheme including the actual pre-stored back-EMF constants vs. electrical rotor position look-up table is proposed for BLDC motor drive with two-phase conduction scheme using four-switch inverter. Therefore, low-frequency torque ripples and torque response time are

minimized compared to conventional four-switch PWM current and voltage controlled BLDC motor drives. This is achieved by properly selecting the inverter voltage space vectors of the two-phase conduction mode from a simple look-up table at a predefined sampling time.

It is believed that the direct torque controlled BLDC motor drive compared to a PWM voltage controlled one has higher dynamic speed/torque response and does not rely on some tedious calculations. Instead, the DTC of a BLDC motor drive depends on a keen and detailed observation of the overall operation, so that it dramatically reduces equations from the conventional control scheme, such as space vector PWM and etc. and is simple to implement from the hardware and software points of view [69].

The four-switch DTC of a BLDC motor drive operating in two-phase conduction mode which is similar to [72] is simplified to just a torque controlled drive by intentionally keeping the stator flux linkage amplitude almost constant by eliminating the flux control in the constant torque region. It is shown that in the constant torque region under the two-phase conduction DTC scheme using four-switch (or six-switch) inverter, the amplitude of the stator flux linkage cannot easily be controlled due to the sharp changes and the curved shape of the flux vector between two consecutive commutation points in the stator flux linkage locus. Since the flux control along with PWM generation is removed, fewer algorithms are required for the proposed control scheme.

Specifically, it is shown that rather than attempting to control the stator flux amplitude in two-phase conduction DTC of BLDC motor drive, only the electromagnetic

torque is controlled. It will be shown that due to the sharp changes, which occur every 60 electrical degrees, flux amplitude control is quite difficult. Moreover, it will be explained in detail that there is no need to control the stator flux linkage amplitude of a BLDC motor in the constant torque region. The stator flux linkage position in the trajectory is helpful to find the right sector for the torque control in sensorless applications of BLDC motor drives. Therefore, the torque is controlled while the stator flux linkage amplitude is kept almost constant on purpose [72]. In the proposed method, a simple two-phase four-switch inverter voltage space vector look-up table is developed to control the electromagnetic torque. Moreover, to obtain smooth torque characteristics a new switching logic is designed and incorporated with the two-phase four-switch voltage space vector look-up table. Simulated and experimental results are presented to illustrate the validity and effectiveness of the two-phase four-switch DTC of a BLDC motor drive in the constant torque region.

4.2. Topology of the Conventional Four-Switch Three-Phase AC Motor Drive

4.2.1. Principles of the Conventional Four-Switch Inverter Scheme

In four-switch three-phase inverter system, there are four possible switching patterns to generate three-phase currents, as shown in Fig. 4.1 with ideal switches; these four switching patterns are (0, 0), (0, 1), (1, 0), and (1, 1) where “0” means the lower switch is turned on and “1” the upper switch is turned on in each leg of the inverter. In the same figure, the free-wheeling diodes as well as phase back-EMFs are ignored. As it can be seen in Fig. 4.1 that in three-phase four-switch system the two switches on the same leg never turn on and off at the same time. However, in six-switch inverter, two

zero voltage space vectors, (0, 0, 0) and (1, 1, 1), cannot supply the dc-link to the load, therefore no current flows through the load. The main difference of the four-switch inverter compared to its counterpart six-switch one is that one phase is always connected to the center tap of the split capacitors, so that there will always be current flowing through that phase even with voltage vectors (0, 0) and (1, 1), as shown in Fig. 4.1. Under balanced load condition with four-switch topology, there will be no current flow through the phase which is connected to the midpoint of the split capacitors using two possible non-zero voltage vectors, (1, 0) and (0, 1), as seen in Fig. 4.1. When voltage vectors (1, 0) and (0, 1) are used and the load is not completely balanced, only the resultant current of the other two phases flow through the phase connected to the midpoint of the split capacitors.

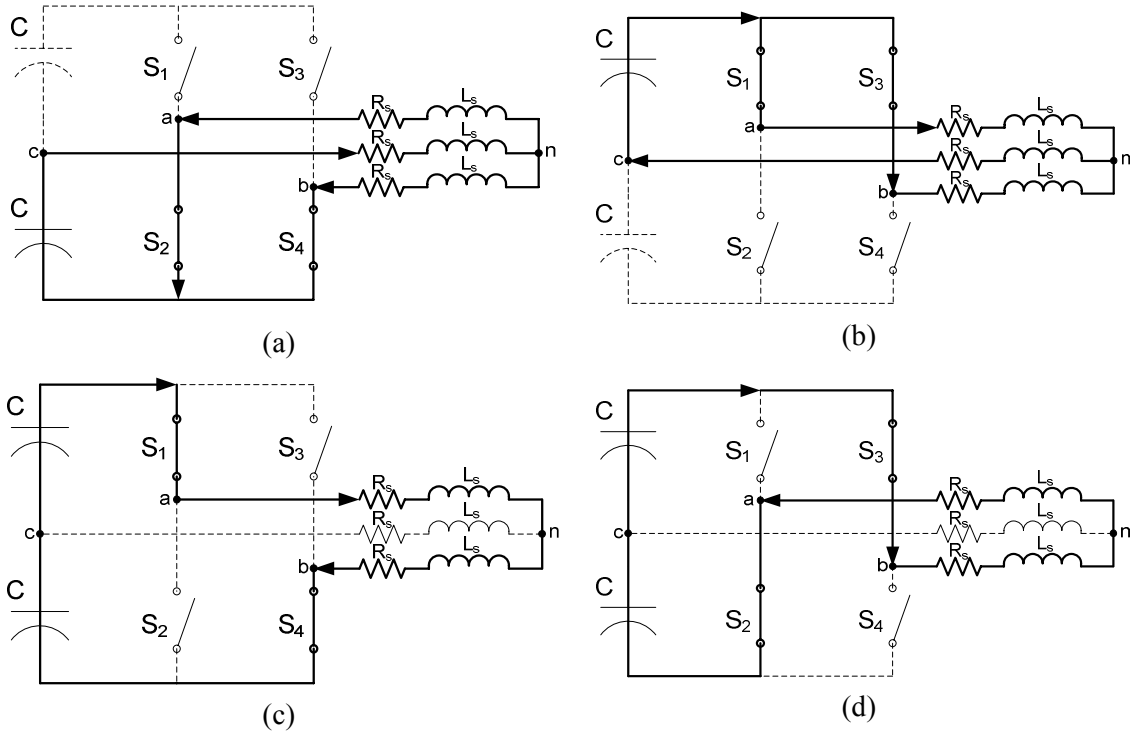

Fig. 4.1. Conventional four-switch voltage vector topology. (a) (0,0) vector, (b) (1,1) vector, (c) (1,0) vector, and (d) (0,1) vector [69].

4.2.2. Applicability of the Conventional Method to the BLDC Motor Drive

Generating a 120 electrical degree current conduction is inherently difficult with the conventional four-switch topology because a BLDC motor with non-sinusoidal back-EMF (i.e. trapezoidal) requires a quasi-square wave current profile to generate constant output torque compared to that of a permanent magnet synchronous motor with sinusoidal back-EMF requiring sinewave current. These currents which have 120 electrical degrees conduction period are synchronized with the flat portion of the corresponding phase back-EMFs, therefore a smooth electromagnetic torque can be obtained. As a result, at every instant of time only two phases conduct and the other phase is supposed to be inactive. Although four voltage vectors in conventional four-switch inverter system are sufficient enough to control the three-phase ac motors using PWM techniques, additional voltage vectors are required for BLDC motor with two-phase conduction mode in order to control the midpoint current of the split capacitors at a desired value. Since the conventional method cannot provide a two-phase conduction method completely, a new control scheme with new switching patterns should be developed such that only two of the three motor phases conduct. This will be explained in detail in Section 4.3. Since for three phase ac induction motor and PMSM drives at any instant of time there are always three-phase currents flowing through the machine, summation of the three-phase currents under balanced condition is always zero. Also, at any time none of the phase currents become zero. This scenario is not true for BLDC motor with two-phase conduction where 120 electrical degrees of one complete cycle (360 degree) of each phase currents will be zero. There will be cases where only phase–*a*

and –*b* currents are supposed to be conducting and phase–*c* current is zero as shown in Mode II and V of Fig. 4.2. However, because of the phase back-EMF (phase–*c*) there will be a current flowing in or out of phase–*c* through the dc-link. Therefore, special attention should be given to the phase which is connected to the center of the split capacitors in four-switch BLDC motor drive scheme.

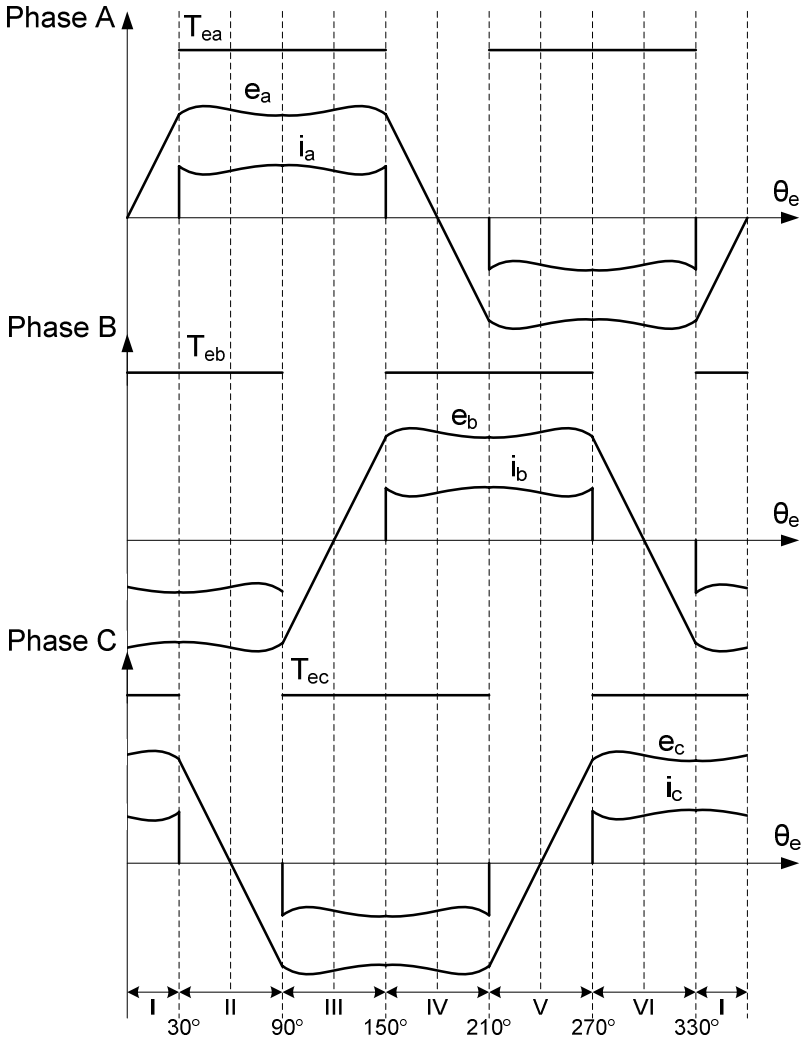

Fig. 4.2. Actual (realistic) phase back-EMF, current, and phase torque profiles of the three-phase BLDC motor drive with four-switch inverter.

4.3. The Proposed Four-Switch Direct Torque Control of BLDC Motor Drive

4.3.1. Principles of the Proposed Four-Switch Inverter Scheme

The key issue in the proposed four-switch DTC of a BLDC motor drive in the constant torque region is to estimate the electromagnetic torque correctly similar to the six-switch version given in [72]. For a surface-mounted BLDC motor the back-EMF waveform is non-sinusoidal (trapezoidal), irrelevant of conducting mode (two or three-phase), therefore (4.1) which is given in the stationary reference frame should be used for the electromagnetic torque calculation [50, 56, 72].

$$T_{em} = \frac{3}{2}\frac{P}{2}\left[\frac{e_\alpha}{\omega_e} i_{s\alpha} + \frac{e_\beta}{\omega_e} i_{s\beta}\right] = \frac{3}{2}\frac{P}{2}\left[k_\alpha(\theta_e) i_{s\alpha} + k_\beta(\theta_e) i_{s\beta}\right] \tag{4.1}$$

where P is the number of poles, θ_e is the electrical rotor angle, ω_e is the electrical rotor speed, and $k_\alpha(\theta_e)$, $k_\beta(\theta_e)$, e_α, e_β, $i_{s\alpha}$, $i_{s\beta}$ are the stationary reference frame ($\alpha\beta$–axes) back-EMF constants, motor back-EMFs, and stator currents, respectively. Since the second equation in (4.1) does not involve the rotor speed in the denominator there will be no problem estimating the torque at zero and near zero speeds. Therefore, it is used in the proposed control system instead of the one on the left in (4.1).

The $\alpha\beta$–axes rotor flux linkages $\varphi_{r\alpha}$ and $\varphi_{r\beta}$ are obtained as

$$\begin{aligned} \varphi_{r\alpha} &= \varphi_{s\alpha} - L_s i_{s\alpha} \\ \varphi_{r\beta} &= \varphi_{s\beta} - L_s i_{s\beta} \end{aligned} \tag{4.2}$$

where $\varphi_{s\alpha}$ and $\varphi_{s\beta}$ are the α– and β–axis stator flux linkages, respectively. By using (4.2), reference stator flux linkage command $|\varphi_s(\theta_e)|^*$ for DTC of BLDC motor drive in the constant torque region can be obtained similar to the DTC of a PMSM drive as

$$\left|\varphi_s(\theta_e)\right|^* = \left|\varphi_r(\theta_e)\right| = \sqrt{\varphi_{r\alpha}(\theta_e)^2 + \varphi_{r\beta}(\theta_e)^2} \tag{4.3}$$

Since the electromagnetic torque is proportional to the product of back-EMF and its corresponding current, the phase currents are automatically shaped to obtain the desired electromagnetic torque characteristics using (4.1). When the actual stationary reference frame back-EMF constant waveforms from the pre-stored look-up table are used in (4.1), much smoother electromagnetic torque is obtained as shown in Fig. 4.2.

From the detail investigation of the back-EMF, current, and phase torque profile of the three-phase BLDC motor as shown in Fig. 4.2, one can obtain a solution to the problems that occur in the conventional four-switch topology explained in Section 4.2.2. As can be observed in Fig. 4.2 that to generate constant electromagnetic torque due to the characteristics of the BLDC motor, such as two-phase conduction, only two of the three phase torque are involved in the total torque equation during every 60 electrical degrees and the remaining phase torque equals zero as shown in Table III. The total electromagnetic torque of PMAC motors equals the summation of each phase torque which is given by

$$T_{em} = T_{ea} + T_{eb} + T_{ec} \tag{4.4}$$

where $T_{ea} = e_a i_a / \omega_m$, $T_{eb} = e_b i_b / \omega_m$, and $T_{ec} = e_c i_c / \omega_m$.

In the constant torque region (below base speed) when the line-to-line back-EMF voltage is smaller than the dc bus voltage there is no reason to change the amplitude of stator flux linkage. Above base speed, however, the motor performance will significantly deteriorate because the back-EMF exceeds the dc bus voltage, and the stator inductance X_s will not allow the phase current to develop quick enough to catch up to the flat top of

the trapezoidal back-EMF. Beyond the base speed the desired torque cannot be achieved unless other techniques such as phase advancing, 180 degree conduction, etc are used [58]. Operation of the DTC of a BLDC motor above the base speed is not in the scope of this work.

TABLE III
ELECTROMAGNETIC TORQUE EQUATIONS FOR THE OPERATING REGIONS

Mode I ($0°<\theta<30°$)	$T_{em} = T_{eb} + T_{ec}$ and $T_{ea} = 0$
Mode II ($30°<\theta<90°$)	$T_{em} = T_{ea} + T_{eb}$ and $T_{ec} = 0$
Mode III ($90°<\theta<150°$)	$T_{em} = T_{ea} + T_{ec}$ and $T_{eb} = 0$
Mode IV ($150°<\theta<210°$)	$T_{em} = T_{eb} + T_{ec}$ and $T_{ea} = 0$
Mode V ($210°<\theta<270°$)	$T_{em} = T_{ea} + T_{eb}$ and $T_{ec} = 0$
Mode VI ($270°<\theta<330°$)	$T_{em} = T_{ea} + T_{ec}$ and $T_{eb} = 0$

It has been observed from the stator flux linkage trajectory that when conventional two-phase four-switch PWM current control is used sharp dips occur every 60 electrical degrees. This is due to the operation of the freewheeling diodes. The same phenomenon has been noticed when the DTC scheme for a BLDC motor is used, as shown in Fig. 4.3. Due to the sharp dips in the stator flux linkage space vector at every commutation (60 electrical degrees) and the tendency of the currents to match with the flat top portion of the phase back-EMF for smooth torque generation, there is no easy way to control the stator flux linkage amplitude. On the other hand, rotational speed of the stator flux linkage can be easily controlled, therefore fast torque response is obtained. The size of the sharp dips is quite unpredictable and depends on several factors which will be explained in the later part of this section and the related simulations are provided

in the Section 4.4. The best way to control the stator flux linkage amplitude is to know the exact shape of it, but it is considered too cumbersome in the constant torque region. If the effect of unexcited open phase back-EMF and the free-wheeling diodes are neglected more hexagonal shape of stator flux locus can be obtained as shown in Fig. 4.3 with straight dotted lines. However, the stator flux locus obtained in the actual implementation is shown in Fig. 4.3 with solid curved lines. Therefore, in the four-switch DTC of a BLDC motor drive with two-phase conduction scheme, the flux error φ in the voltage vector selection look-up table is always selected as zero and only the torque error τ is used depending on the error level of the actual torque from the reference torque. If the reference torque is bigger than the actual torque, within the hysteresis bandwidth, the torque error τ is defined as "1," otherwise it is "-1", as shown in Table III. The BLDC motor model and representation of two-phase switching states of the four-switch inverter are illustrated in Fig. 4.4.

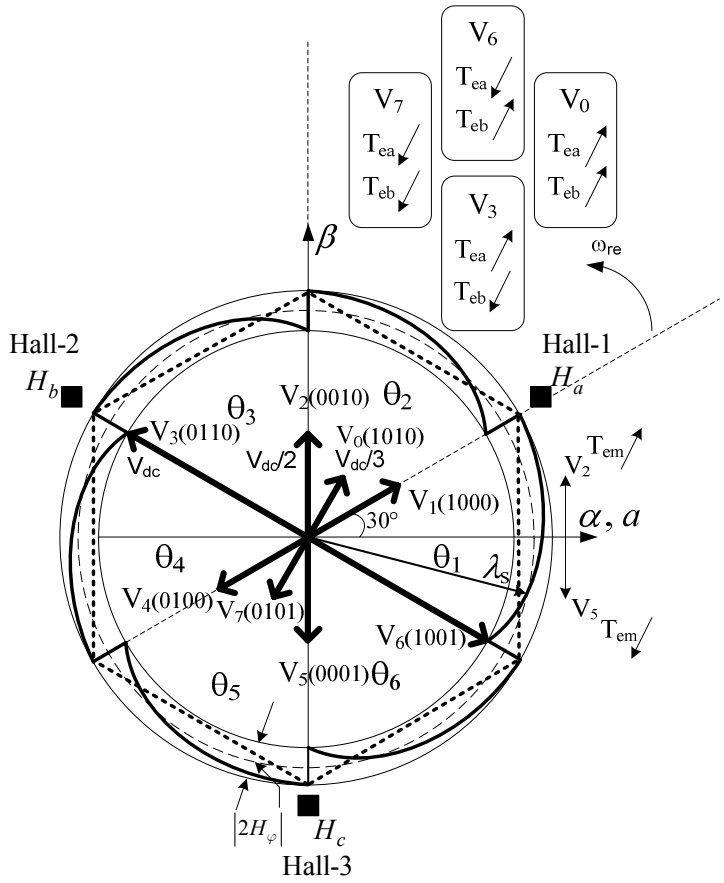

Fig. 4.3. Actual (solid curved lines) and ideal (straight dotted lines) stator flux linkage trajectories, representation of the four-switch two-phase voltage space vectors, and placement of the three hall-effect sensors in the stationary $\alpha\beta$–axes reference frame ($V_{dc\_link} = V_{dc}$).

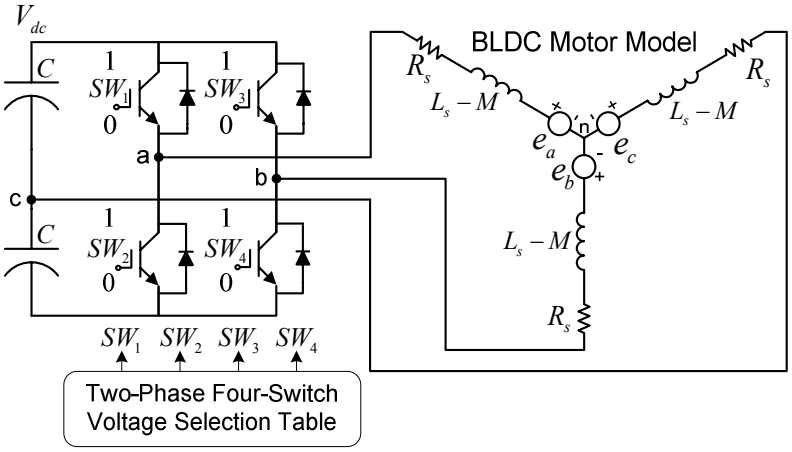

Fig. 4.4. Representation of two-phase switching states of the four-switch inverter voltage space vectors for a BLDC motor.

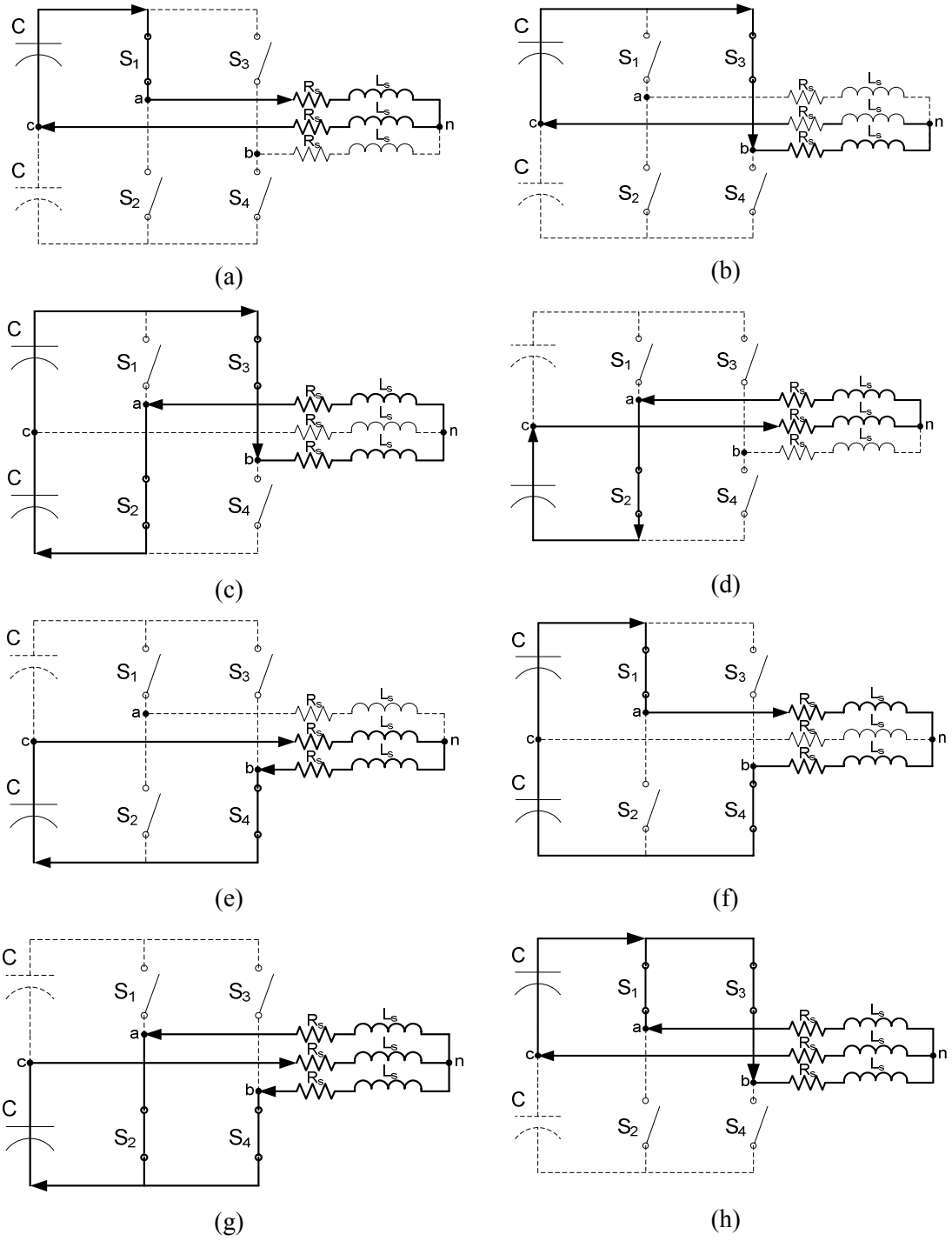

Fig. 4.5. Proposed four-switch voltage vector topology for two-phase conduction DTC of BLDC motor drives. (a) $V_1(1000)$ vector, (b) $V_2(0010)$ vector, (c) $V_3(0110)$ vector, (d) $V_4(0100)$ vector, (e) $V_5(0001)$ vector, (f) $V_6(1001)$, (g) $V_7(0101)$, and (h) $V_0(1010)$.

4.3.2. Control of Electromagnetic Torque by Selecting the Proper Stator Voltage Space Vectors

A change in the torque can be achieved by keeping the amplitude of the stator flux linkage constant and increasing the rotational speed of the stator flux linkage as fast as possible. This allows a fast torque response to be achieved. It is shown in this section that the rotational speed of the stator flux linkage can be controlled by selecting the proper voltage vectors while keeping the flux amplitude almost constant, in other words eliminating the flux control in the constant torque region.

To obtain the six modes of operation in four-switch DTC of BLDC motor drive, a simple voltage vector selection look-up table is designed as shown in Table IV. Normally, six-possible voltage space vectors of four-switch topology are supposed to be used in Table IV as shown in Fig. 4.5(a)–(f) similar to the six-switch version, however two of the voltage vectors V_3 and V_6 as shown in Fig. 4.5 create problems in the torque control. When they are directly used in the voltage vector selection table (Table IV), back-EMF of the uncontrolled phase (phase–*c*) generates undesired current therefore distortions occur in each phase torque. As a result, undesired electromagnetic torque is inevitable. Therefore, when the rotor position is in the Sector II and V, special switching pattern should be adapted, as shown in Table V (CCW). At Sectors II and V, phase–*a* and –*b* torque are independently controlled by the hysteresis torque controllers. Additional two voltage vectors V_0 and V_7 which are used in conventional four-switch PWM scheme are included in the voltage selection look-up table to obtain smooth torque production in two-phase conduction four-switch DTC of BLDC motor drive.

TABLE IV

TWO-PHASE FOUR-SWITCH VOLTAGE VECTOR SELECTION FOR DTC OF BLDC MOTOR DRIVE (CCW)

φ	τ	θ					
		θ_1	θ_2	θ_3	θ_4	θ_5	θ_6
1	*1*	*V_1(1000)*	*V_2(0010)*	*V_3(0110)*	*V_4(0100)*	*V_5(0001)*	*V_6(1001)*
	-1	*V_6(1001)*	*V_1(1000)*	*V_2(0010)*	*V_3(0110)*	*V_4(0100)*	*V_5(0001)*
0	**1**	**V_2(0010)**	~~**V_3(0110)**~~	**V_4(0100)**	**V_5(0001)**	~~**V_6(1001)**~~	**V_1(1000)**
	-1	**V_5(0001)**	~~**V_6(1001)**~~	**V_1(1000)**	**V_2(0010)**	~~**V_3(0110)**~~	**V_4(0100)**
-1	*1*	*V_3(0110)*	*V_4(0100)*	*V_5(0001)*	*V_6(1001)*	*V_1(1000)*	*V_2(0010)*
	-1	*V_4(0100)*	*V_5(0001)*	*V_6(1001)*	*V_1(1000)*	*V_2(0010)*	*V_3(0110)*

Note: The italic grey area and vectors in the "X" area are not used in the proposed four-switch DTC of a BLDC motor drive.

TABLE V

VOLTAGE VECTOR SELECTION IN SECTORS II AND V FOR FOUR-SWITCH DTC OF BLDC MOTOR DRIVE (CCW)

φ	τ_{ea}	τ_{eb}	θ_2	θ_5
0	1	1	V_0(1010)	V_7(0101)
		-1	V_6(1001)	V_3(0110)
	-1	1	V_7(0101)	V_6(1001)
		-1	V_3(0110)	V_0(1010)

Since the upper and lower switches in a phase leg may both be simultaneously off, irrespective of the state of the associated freewheeling diodes in two-phase conduction mode, four digits are required for the four-switch inverter operation, one digit for each switch [56]. Therefore, there is a total of eight useful voltage vectors for the two-phase conduction mode in the proposed DTC of BLDC motor drive which can be represented as $V_{0,1,2,\ldots,6,7}$ (SW_1, SW_2, SW_3, SW_4), as shown in Fig. 4.3. The eight

possible two-phase four-switch voltage vectors and current flow are depicted in Fig. 4.5. Stationary reference frame ($\alpha\beta$–axes) representations of the eight voltage vectors with respect to dc-link voltage and switching states of the semiconductor devices are derived in Appendix D. The purpose of the hysteresis torque regulation is to shape the quasisquare wave current within acceptable ripple band as the inverse top portion of the actual back-EMF as shown in Fig. 4.2, therefore smoother torque can be obtained. In Fig. 4.5, the solid lines represent current direction and the dotted lines show inactive sections. The detailed switching sequence and torque regulation are showed in Fig. 4.6 for four-switch DTC of BLDC motor drive. The overall block diagram of the closed-loop four-switch DTC scheme of a BLDC motor drive in the constant torque region is represented in Fig. 4.7. The dotted area represents the stator flux linkage control part of the scheme used only for comparison purpose. When the two switches in Fig. 4.7 are changed from state 2 to state 1, flux control is considered in the overall system along with torque control. In the two-phase conduction mode the shape of stator flux linkage trajectory is ideally expected to be hexagonal, as illustrated with the straight dotted lines in Fig. 4.3. However, the influence of the unexcited open-phase back-EMF causes each straight side of the ideal hexagonal shape of the stator flux linkage locus to be curved and the actual stator flux linkage trajectory tends to be more circular in shape, as shown in Fig. 4.3 with solid curved lines [56]. In addition to the sharp changes, the curved shape in the flux locus between two consecutive commutations complicates the control of the stator flux linkage amplitude because it depends on the size of the sharp dips, and the depth of the change may vary with sampling time, dc-link voltage, hysteresis

bandwidth, motor parameters especially the winding inductance, motor speed, snubber circuit, and the amount of load torque.

Usually the overall control system of a BLDC motor drive includes three hall-effect position sensors mounted on the stator 120 electrical degrees apart, as shown in Fig. 4.3. These are used to provide good torque control if the back-EMF is ideally trapezoidal because current commutation occurs only every 60 electrical degrees. Nevertheless, using high resolution position sensors is quite useful if the back-EMF of BLDC motor is not ideally trapezoidal. To achieve a more accurate torque estimation, in general, for non-sinusoidal surface-mounted permanent magnet motors it is suggested that (4.1) should be used. The derivative of the rotor $\alpha\beta$–axes fluxes obtained from (4.2) over electrical position, which is described in (4.1), will cause problems mainly due to the sharp dips at every commutation point. The actual values of $\alpha\beta$–axes back-EMF constants k_α and k_β vs. electrical rotor position θ_e can be created in the look-up table, respectively with great precision depending on the resolution of the position sensor (for example incremental encoder with 2048 pulses/revolution), therefore a good torque estimation can be obtained in (4.1).

4.3.3. Torque Control Strategies of the Uncontrolled Phase-*c*

For direct torque control, Fig. 4.5(a) and (b) are not applicable due to the three-phase conduction mode instead of a desired two-phase conduction. Modification in PWM scheme presented in [70, 71] could be a solution if not for its tedious computation. If torque or current is going to be controlled using hysteresis controllers, then those voltage space vectors cannot be used in two-phase BLDC motor drive. On the other

hand, even though voltage vectors shown in Fig. 4.5(c) and (d) are two-phase conductions through phase–*a* and –*b*, there will be always current trying to flow in phase–*c* due to its back-EMF and the absence of switches controlling its current. As a result, there will be a distorted current in phase–*c* as well as in phase–*a* and –*b*. Therefore, voltage space vectors of phase–*a* and –*b* conduction can be difficult to implement for BLDC motor drive unless some modifications are applied to overcome the back-EMF effect of the phase–*c* in these conditions. Selecting the right switching pattern to control the torque on phase–*a* and –*b* independently will reduce the distorted currents on those phases and result in a smoother overall electromagnetic torque production, which is shown in the simulations. Solution to the above phenomenon is explained in detail below:

For BLDC motor with two-phase conduction, one of the phase torque should be zero as shown in Table III. This can be achieved in Sectors 1, 3, 4 and 6 whereas in Sectors 2 and 5 phase–*c* torque T_{ec} is uncontrollable due to the split capacitors. In Sectors 2 and 5, voltage vectors V_3 and V_6 cannot be directly used, instead phase torque T_{ea} and T_{eb} should be individually controlled by properly selecting the S1, S2, S3, and S4 switches, such as if the rotor position resides in Sector 2 and the rotor rotates in CCW direction then to increase the phase–*a* torque T_{ea} S1 should be "0" and S2 is "1" and vice versa to decrease the T_{ea}. To increase the phase–*b* torque T_{eb} S3 should be "0" and S4 should be "1" and vice versa to decrease the T_{eb}. Reference torque value for those phase torque should be half of the desired total reference torque $T_{earef} = T_{ebref} = T_{ref}/2$. This special torque control phenomenon can be explained with the aid of the simplified

equivalent circuit in Fig. 4.6. Consequently, in Mode II and V only phase–*a* and –*b* torque are controlled independently and therefore the T_{ec} is tried to be kept at zero value. This will eliminate the distorted torque problem on each phase in two-phase conduction four-switch DTC of a BLDC motor drive.

The direction of the rotor is important to define the specific switching pattern. If the rotor direction is CW, then the above claims are reversed, such as in Sector 2 to increase the phase–*a* torque T_{ea} S1 is "1" and S2 is "0" and vice versa for decrementing the T_{ea}. The same is true for the phase–*b* torque T_{eb}.

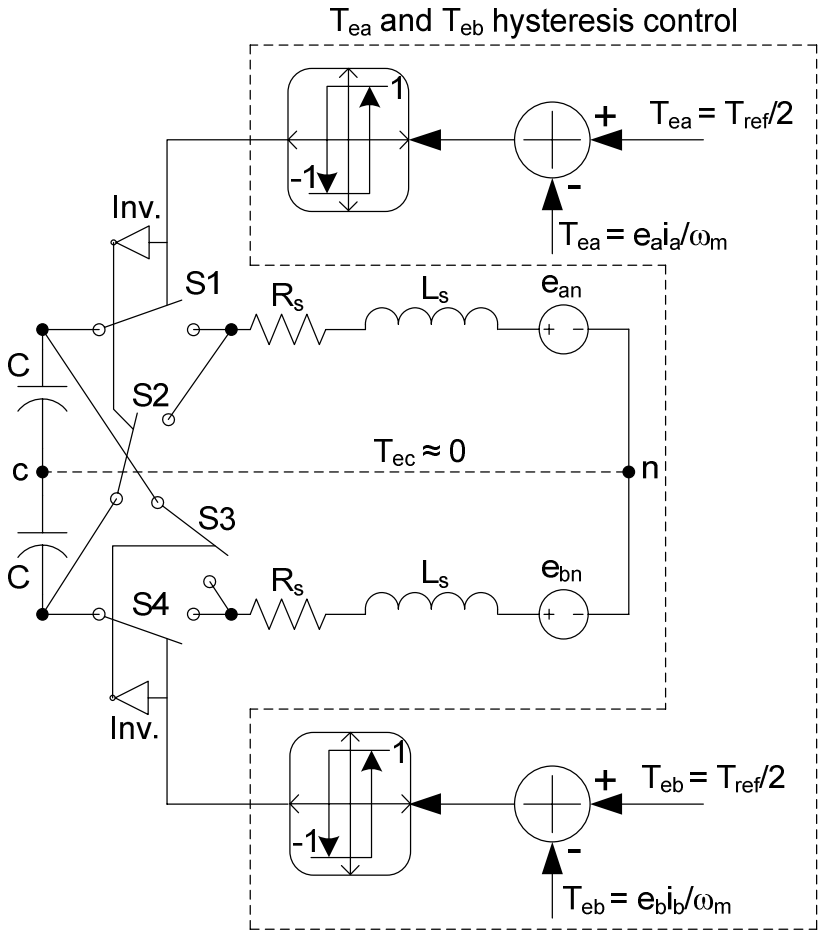

Fig. 4.6. Individual phase–*a* and –*b* torque control, T_{ea} and T_{eb} , in Sectors 2 and 5.

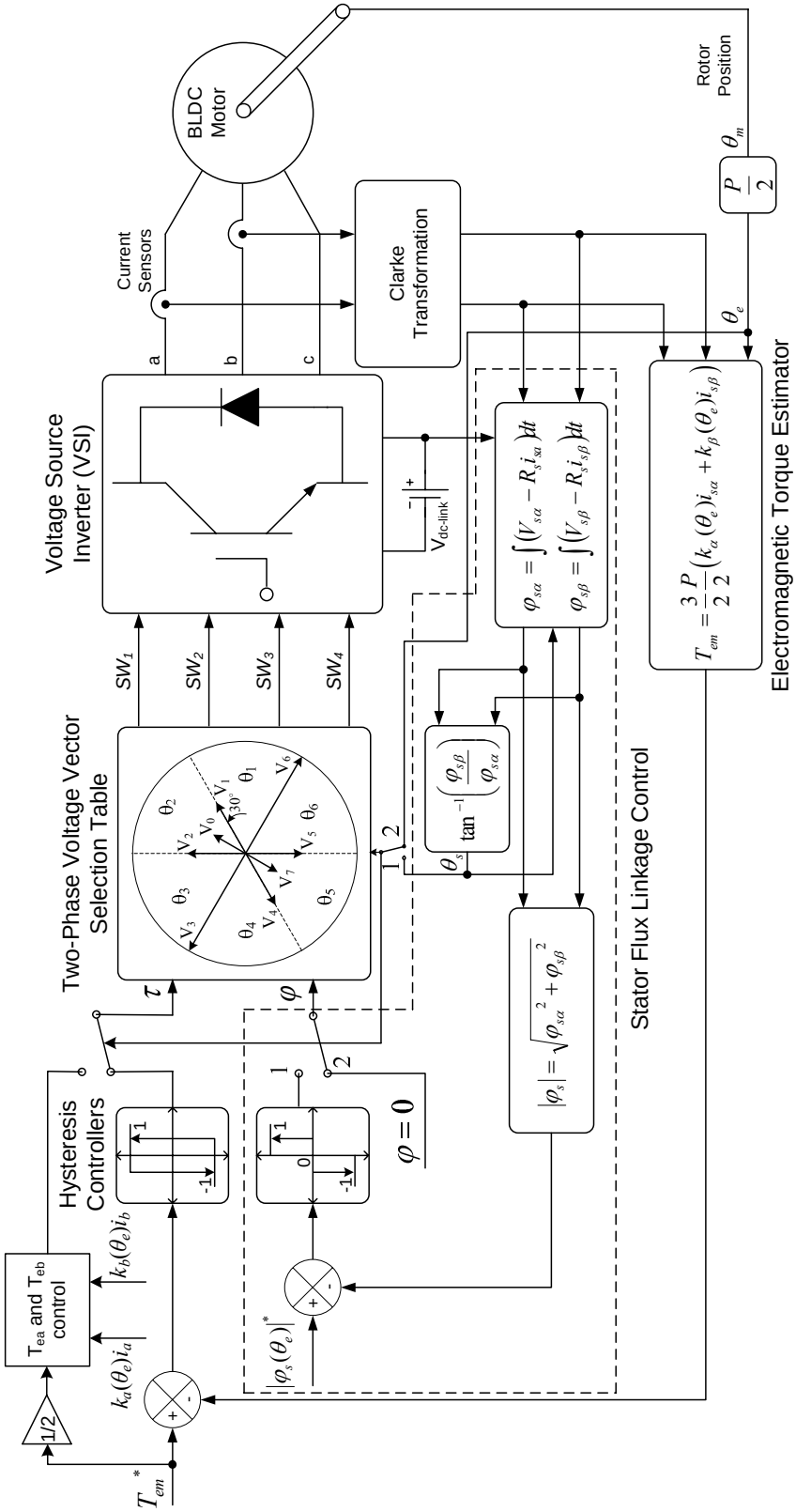

Fig. 4.7. Overall block diagram of the four-switch two-phase conduction DTC of a BLDC motor drive in the constant torque region.

Another problem to overcome is eliminating the high torque ripples in Mode 2 and 5 where full dc-link is applied to the motor terminals compared to the other sectors where only half and one third of the dc-link voltage is used. During Sectors 2 and 5 where the individual torque control is performed, bandwidth of the hysteresis torque controllers are chosen about 1000 times less than the normal case which is used in Sectors 1, 3, 4, and 6. Therefore, ripples in the current and eventually in the torque are equalized during the entire electrical cycle.

Normally with four-switch inverter only half of the dc-link voltage is applied to the motor terminals compared to the six-switch inverter. This problem can be overcome by using voltage doubler half-bridge diode rectifier which can also be used for power factor correction if two diodes are replaced with active power semiconductors such as IGBTs and MOSFETs.

From the equivalent circuit given in Fig. 4.6, if phase–*a* and –*b* torque are individually controlled as explained above, the influence of the back-EMF of the phase–*c* can be blocked, there is no current flow in phase–*c*, therefore its torque (T_{ec}) will be almost zero. As a result, in Sectors 2 and 5, phase–*a* and –*b* torque should be controlled independently, in other words switching signals at S1 (or S2) and S4 (or S3) should be created individually making additional voltage vectors V_0 and V_7 which act as a zero voltage vector at Sectors 2 and 5 in four-switch DTC of a BLDC motor drive scheme using two phase conduction mode. Additional voltage vectors and their logic depending on the errors of phase–*a* and –*b* torque are depicted in Table V.

At Sectors 2 and 5, complementary switches in both phase–*a* and –*b* legs cannot be turned off at the same time as in V_4 and V_5, therefore inverse logic is applied in Fig. 4.6.

4.4. Simulation Results

The drive system shown in Fig. 4.7 has been simulated for various cases with and without stator flux control, switch states 1 and 2, respectively in order to demonstrate the validity of the proposed four-switch DTC of a BLDC motor drive scheme with two-phase conduction.

To set the gating signals of the power switches easily and represent the real conditions in simulation as close as possible the electrical model of the actual BLDC motor with R-L elements and the inverter with power semiconductor switches considering the snubber circuit are designed in Matlab/Simulink® using the SimPower Systems toolbox.

The dead-time of the inverter and non ideal effects of the BLDC machine are neglected in the simulation model. The sampling interval is 25 μs. The switching tables, which are given in Table IV and V, are employed for the proposed DTC of the BLDC motor drive. The magnitudes of the torque hysteresis band used in Sectors 1, 3, 4, and 6 $\tau_{1,3,4,6}$, and flux hysteresis band are 0.08 N·m and 0.001 Wb, respectively. Torque hysteresis bandwidth in Sectors 2 and 5 $\tau_{2,5}$ is chosen as 0.08/1000 N·m to equal the high frequency ripple width of both current and torque in one complete electrical cycle.

Figs. 4.8 and 4.9 show the simulation results of the uncontrolled open-loop stator flux linkage locus when 0 N·m and 1.2835 N·m load torque are applied to the BLDC

motor with actual back-EMF waveforms, respectively. Steady-state speed control is performed with an inner-loop torque control without flux control. Stator flux linkage is estimated as an open-loop which is illustrated with dotted area in Fig. 4.7 without connection of switch state 1 to the overall control scheme. As can be seen in Fig. 4.9 when the load torque level increases, more deep sharp changes are observed which increase the difficulty of the flux control if it is used in the control scheme. The steady-state speed is 30 mechanical rad/s and the dc-link voltage V_{dc} equals $80\sqrt{2}$ V. Since the speed is controlled a better open-loop circular flux trajectory is obtained. The overall time for this simulation is 0.25 second.

Using the actual $\alpha\beta$–axes rotor flux linkages in (4.3) looks like the best solution for a good stator flux reference similar to the DTC of a PMSM drive. Unlike BLDC motor, in PMSM since both α– and β–axis motor back-EMFs are in sinusoidal shape, constant stator flux linkage amplitude is obtained. However, for BLDC motor, unexcited open-phase back-EMF effect on the flux locus and more importantly the size of the sharp dips cannot easily be predicted to achieve a good stator flux reference in two-phase conduction mode. Fig. 4.10 represents the steady-state estimated stator flux locus whose reference obtained in (4.3) when back-EMF is not ideally a trapezoidal under full-load (1.2835 N·m). The simulation time for this case is 3 seconds. The motor speed is 30 mechanical rad/s. Due to the distorted voltage and current, the estimation of stator flux locus goes unstable as can be seen in Fig. 4.10.

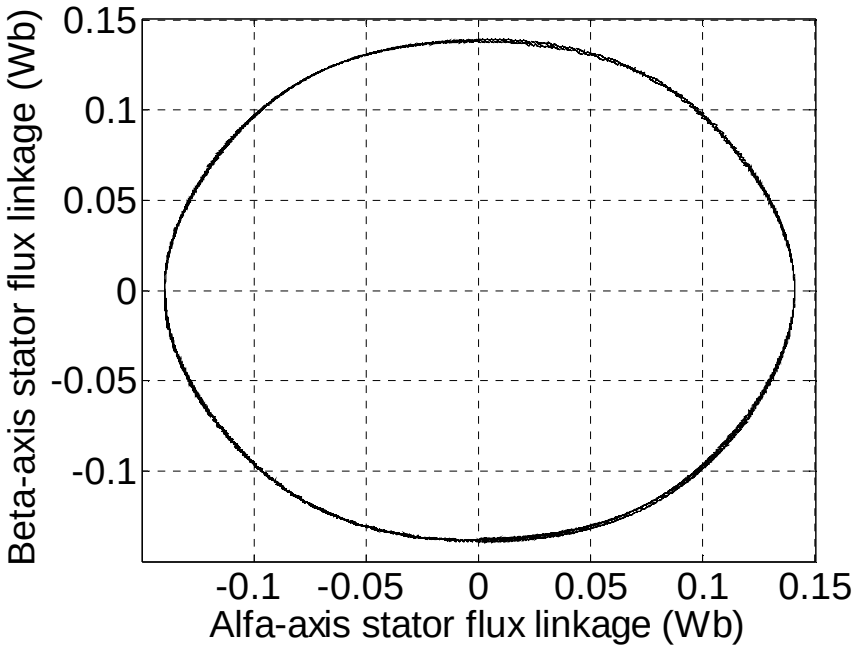

Fig. 4.8. Simulated open-loop stator flux linkage trajectory under the four-switch two-phase conduction DTC of a BLDC motor drive at no load torque (speed + torque control).

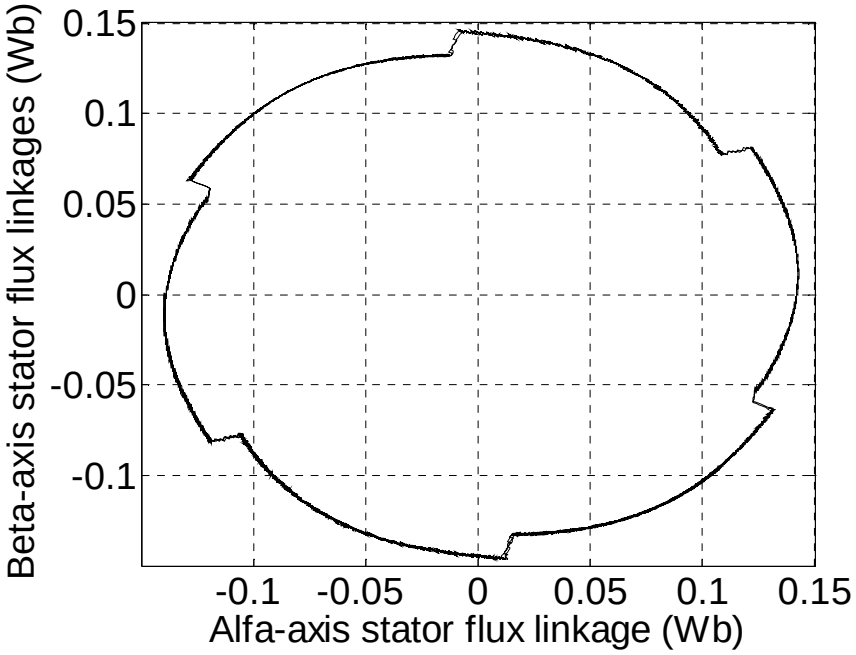

Fig. 4.9. Simulated open-loop stator flux linkage trajectory under the four-switch two-phase conduction DTC of a BLDC motor drive at 1.2835 N·m load torque (speed + torque control).

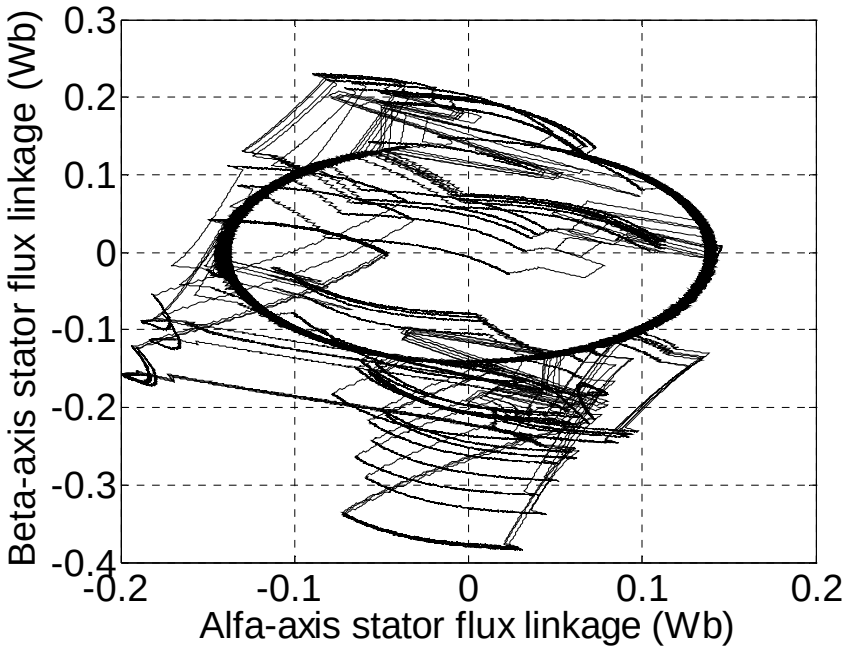

Fig. 4.10. Simulated stator flux linkage locus whose reference is chosen from (4.3) under full load (speed + torque + flux control).

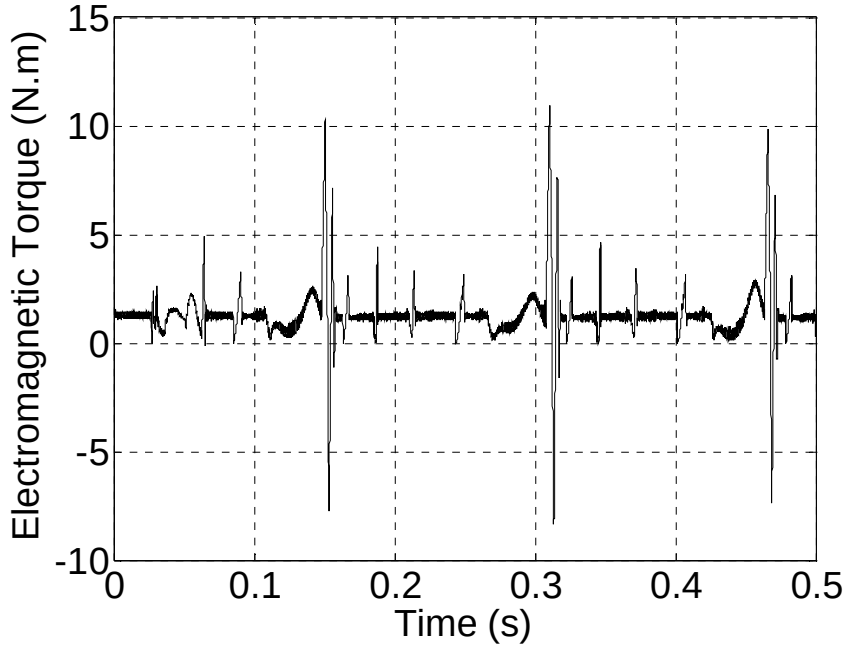

Fig. 4.11. Simulated electromagnetic torque using actual $\alpha\beta$–axes motor back-EMFs under full load (speed + torque + flux control).

Instability in the torque is observed in Fig. 4.11 where huge torque transients occur mainly at the commutation points. During Sectors 2 and 5 the torque estimation results in even larger transients which are unacceptable in real conditions. The reason of instability in the torque estimation is because of considering the flux control with a large reference flux to estimated flux ratio or vice versa during especially commutation periods in two-phase controlled four-switch DTC of a BLDC motor drive. There should be exact flux amplitude to be given as a reference flux value including sharp changes at every commutation point and curved shape between those commutation points, then appropriate flux control can be obtained without losing the torque control. However, to predict all these circumstances to generate a flux reference is a cumbersome work which is unnecessary in the constant torque region.

Although the phase currents illustrated in Fig. 4.12 seem to be stable only until the second commutation point so as the electromagnetic torque as shown in Fig. 4.11. Then, the currents become unstable exceeding the peak current of 24 A due to the huge mismatch of the reference flux versus estimated flux in the two-phase conduction DTC of BLDC motor drive scheme. Once the currents go unstable the current dependant torque estimation is also affected enormously as can be seen in Fig. 4.11.

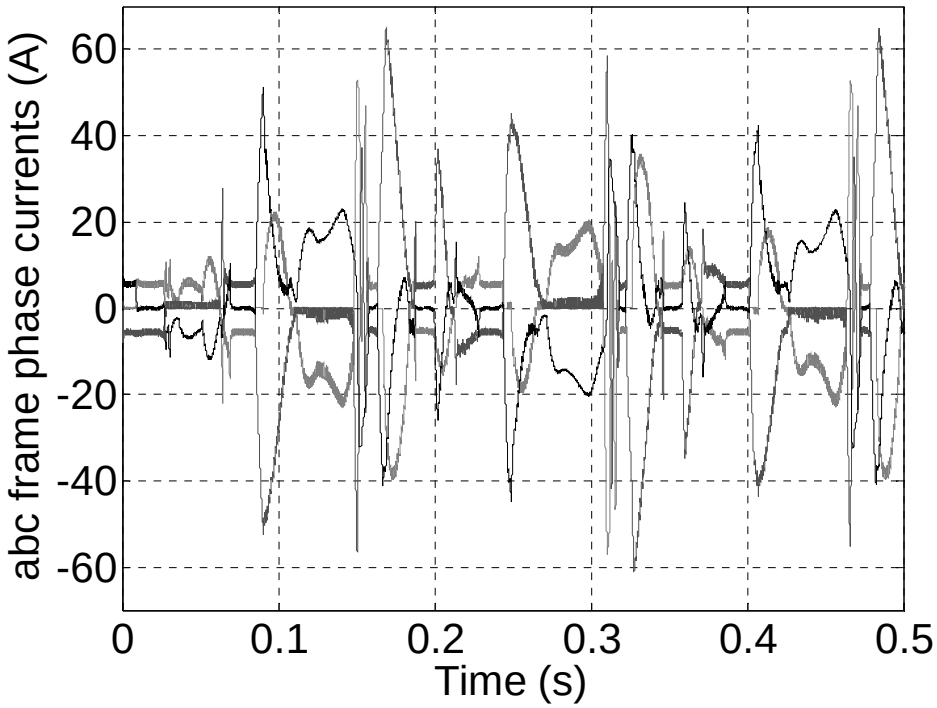

Fig. 4.12. Simulated *abc* frame phase currents when stator flux reference is obtained from (4.3) under full load (speed + torque + flux control).

Figs. 4.13 and 4.14 show *abc* frame phase currents and electromagnetic torque, respectively under only torque control when the actual phase back-EMFs are considered in the simulation. Due to the individual torque control at Sectors 2 and 5 ripples on phase–*c* current during zero-crossing points are clearly visible in Fig. 4.13. The torque ripples of phase–*c* as a consequence of individual torque control scheme are not large enough to distort the torque estimation as illustrated with grey circle in Fig. 4.14. High-frequency current and torque ripples observed in Figs. 4.13 and 4.14 are due to the high dc-link voltage, high sampling time, low winding inductance, high torque hysteresis bandwidth, etc. Those ripples can be minimized by selecting the proper values of dc-link voltage and hysteresis band size. Once the dc-link voltage is reduced to obtain less high-

frequency ripples the hysteresis band size $\tau_{1,3,4,6}$ of Sectors 1, 3, 4, and 6 should also be decreased accordingly to get an equal ripple size in one complete electrical cycle for both currents and torque. The size of the torque hysteresis bandwidth at Sectors 2 and 5 $\tau_{2,5}$ is still kept as $\tau_{1,3,4,6}$ /1000 N·m. In Fig. 14, reference torque is 0.51 N·m and the load torque is 0.5 N·m, thereby steady-state speed is kept around 30 electrical rad/s for a better circular flux locus. If high resolution position sensor such as incremental encoder is used instead of the three hall-effect sensors, low-frequency torque oscillations can be minimized by using (4.1), as shown in Fig. 4.14. In (4.1), the exact shapes of phase back-EMF constants are obtained offline and transformed to $\alpha\beta$–axes. Thus, the product of the real back-EMF constant values by the corresponding $\alpha\beta$–axes currents, and number of pole pairs provide the exact values of the α– and β–axis torque, respectively.

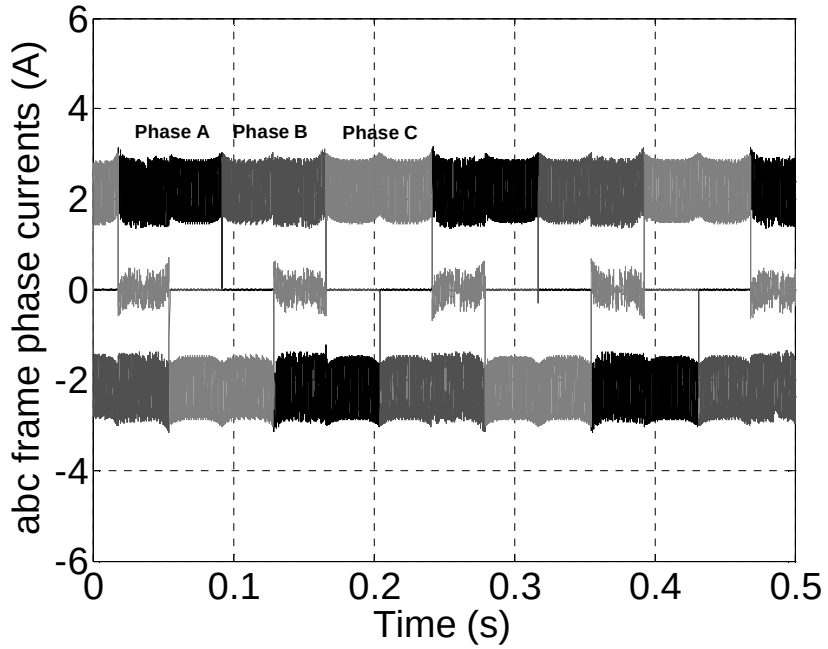

Fig. 4.13. Simulated *abc* frame phase currents when just torque is controlled without flux control under 0.5 N·m load using actual back-EMFs (reference torque is 0.51 N·m).

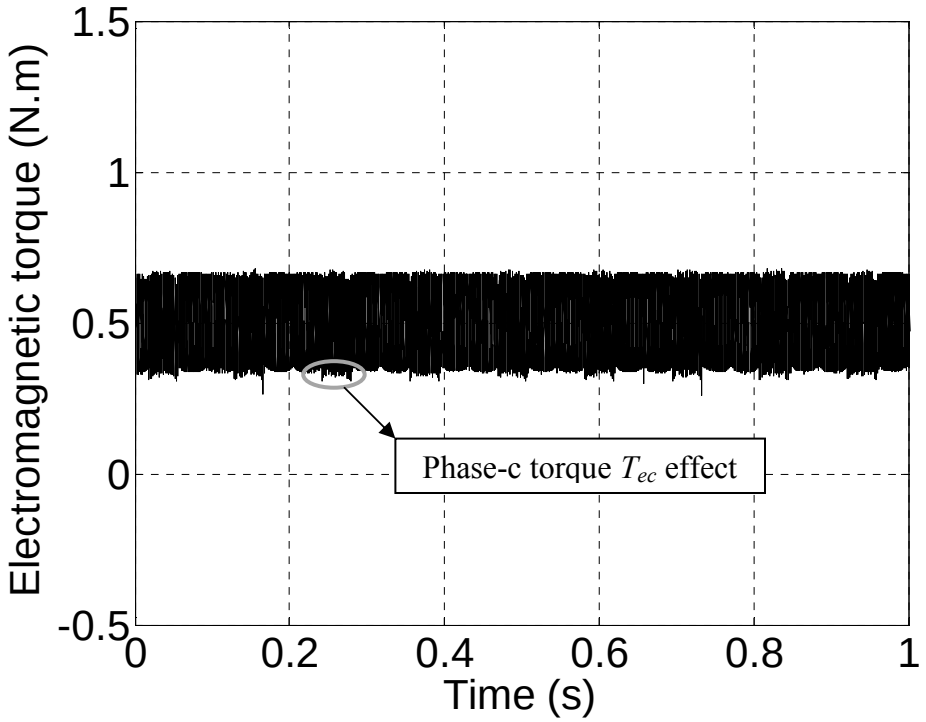

Fig. 4.14. Simulated electromagnetic torque when just torque is controlled without flux control under 0.5 N·m load using actual back-EMFs (reference torque is 0.51 N·m).

4.5. Experimental Results

The feasibility and practical features of the proposed four-switch DTC of a BLDC motor drive scheme have been evaluated using an experimental test-bed, shown in Fig. 4.15. The proposed control algorithm is digitally implemented using the eZdsp^{TM} board from Spectrum Digital, Inc. based on TMS320F2812 DSP, as shown in Fig 4.15(a). In Fig. 4.15(b), the BLDC motor whose parameters are given in the Appendix A is coupled to the overall system.

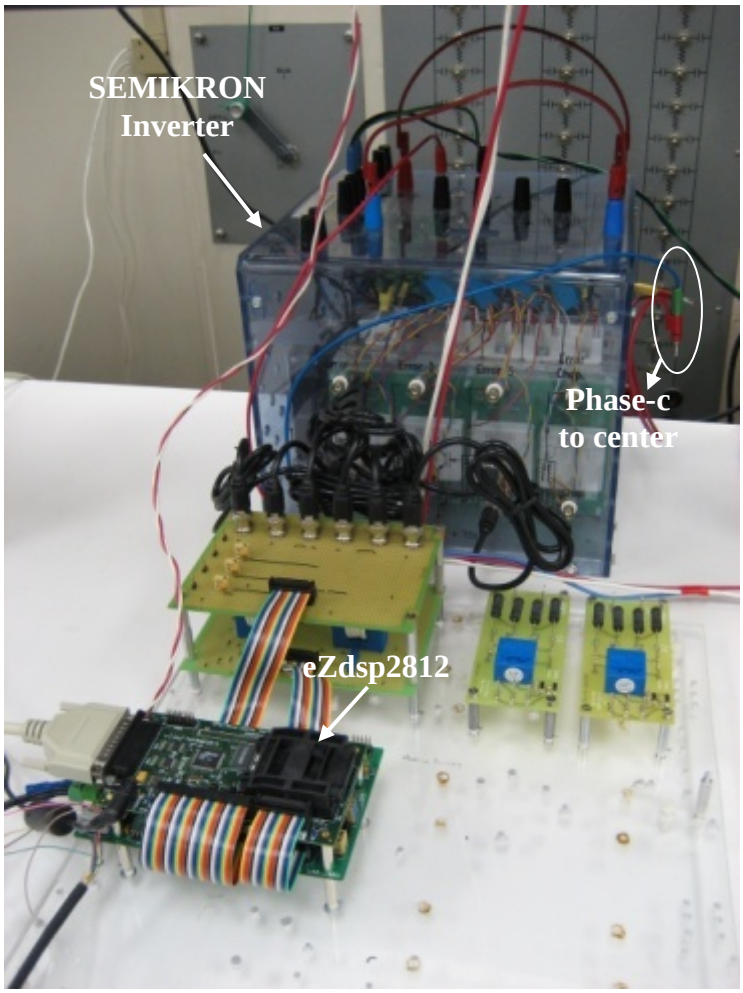

(a)

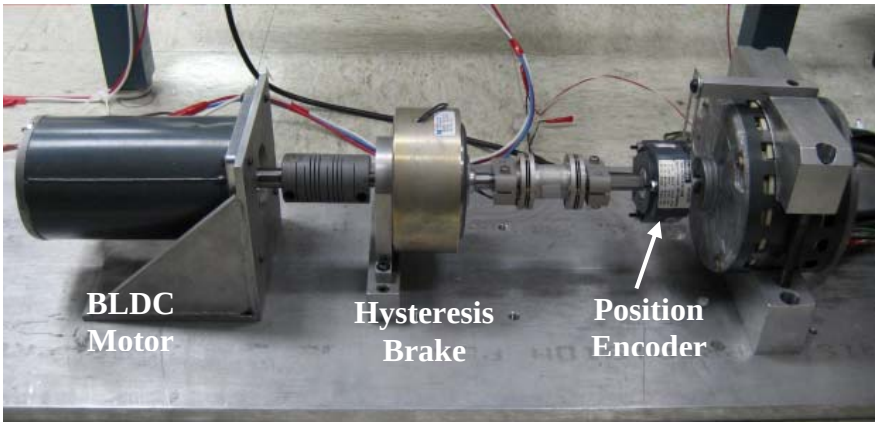

(b)

Fig. 4.15. Experimental test-bed. (a) Four-switch inverter and DSP control unit. (b) BLDC motor coupled to dynamometer and position encoder (2048 pulse/rev).

In this section, transient and steady-state torque and current responses of the proposed four-switch two-phase conduction DTC scheme of a BLDC motor drive are demonstrated experimentally under 0.5 N·m load torque condition. The experimental results are obtained from the datalog (data logging) module in the Texas Instruments Code Composer Studio™ IDE software.

Fig. 4.16 illustrates the experimental results of the torque and *abc* frame phase currents when only torque control is performed using (4.1).. In Fig. 4.16, the reference torque is suddenly increased 25 percent from 0.51 N·m to 0.6375 N·m at 0.05 s under 0.5 N·m load torque. The sampling time is chosen as 25 μs, hysteresis bandwidth is 0.05 N·m for Sectors 1, 3, 4, and 6, for Sectors 2 and 5 it is selected as 0.0005 N·m to equalize the high-frequency ripple widths with the ones in the other sectors, the dead-time compensation is included, and the dc-link voltage is set to $V_{dc} = 80\sqrt{2}$ V. As it can be seen in Fig. 4.16, when the torque is suddenly increased the current amplitudes also increase and fast torque response is achieved. The high frequency ripples observed in the torque and current are related to the sampling time, hysteresis bandwidth, winding inductance, and dc-link voltage. Those ripples can be minimized by properly selecting the dc-link voltage and torque hysteresis band size. The steady-state experimental results are well in accordance with the simulation results obtained in Figs. 4.13 and 4.14. Since only the torque is controlled without speed control, the time range of control system under transient state is selected short. The motor speeds up to a very large value if the motor is run longer under only torque control.

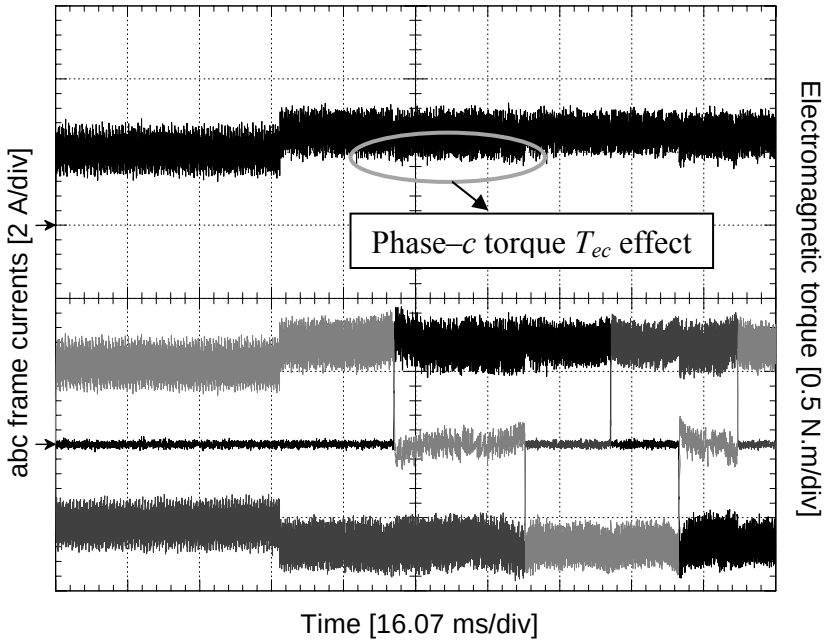

Fig. 4.16. Top: Steady-state and transient experimental electromagnetic torque in per-unit under 0.5 N·m load torque (0.5 N·m/div). Bottom: Steady-state and transient experimental *abc* frame phase currents (2 A/div) and time base: 16.07 ms/div.

4.6. Conclusion

This study has successfully demonstrated application of the proposed four-switch two-phase conduction direct torque control (DTC) scheme for BLDC motor drives in the constant torque region. A look-up table for the two-phase voltage selection is designed to provide faster torque response. In addition, for effective torque control, a novel switching pattern incorporating with the voltage vector look-up table is developed and implemented for the two-phase four-switch DTC of a BLDC motor drive to produce the desired torque characteristics. Furthermore, to eliminate the low-frequency torque oscillations caused by the non-ideal trapezoidal shape of the actual back-EMF waveform

of the BLDC motor, a pre-stored back-EMF versus electrical rotor position look-up table is designed and used in the torque estimation.

Compared to the three phase DTC technique, this approach eliminates the flux control and only torque is considered in the overall control system. Three reasons are given for eliminating the flux control. First, since the line-to-line back-EMF including the small voltage drops is less than the dc-link voltage in the constant torque region there is no need to control the flux amplitude. Second, with the two-phase conduction mode sudden sharp dips in the stator flux linkage locus occur that complicate the control scheme. The size of these sharp dips is unpredictable. Third, regardless of the stator flux linkage amplitude, the phase currents tend to match with the flat top portion of the corresponding trapezoidal back-EMF to generate constant torque. The simulation and experimental results show that it is possible to achieve two-phase conduction DTC of a BLDC motor drive using four-switch inverter.

CHAPTER V

SENSORLESS DIRECT TORQUE AND INDIRECT FLUX CONTROL OF BRUSHLESS DC MOTOR WITH NON-SINUSOIDAL BACK-EMF

5.1. Introduction

The permanent magnet synchronous motor (PMSM) and brushless dc (BLDC) motor drives are used extensively in several high-performance applications, ranging from servos to traction drives, due to several distinct advantages such as high power density, high efficiency, large torque to inertia ratio, and simplicity in their control.

In many applications, obtaining a low-frequency ripple-free torque and instantaneous torque and even flux control are of primary concern for BLDC motors with non-sinusoidal back-EMF. If the actual back-EMF of a BLDC motor is not ideal trapezoidal having a 120 degrees flat top, control scheme with discrete position sensing will generate low-frequency torque pulsations depending on the shape of the back-EMF.

A great deal of study has been devoted to the current and torque control methods employed for BLDC motor drives to minimize the torque pulsations mainly caused by commutation and non-ideal shape of back-EMF. One of the most popular approaches is a generalized harmonic injection approach by numerical optimization solutions to find out optimal current waveforms based on back-EMF harmonics to minimize mutual and cogging torque [73]–[78], [47]–[49]. In [47], it is shown that torque ripple can be minimized by appropriately selecting the current harmonics to eliminate both excitation

and cogging torque ripple components. The complex exponential Fourier series decomposition is used in [48] to find a closed-form solution for the current harmonics that eliminate torque ripple and maximize efficiency simultaneously. In [49], the prior works are extended to include the case of finite supply voltage and verified by *di/dt* capability. Those approaches limit Fourier coefficients up to an arbitrary high harmonic order due to calculation complexity [79].

In [45], electromagnetic torque is calculated from the product of the instantaneous back-EMF and current both in two-phase and in the commutation period. Then, the pre-stored phase back-EMF values are obtained using mid-precision position sensor. As a result, torque pulsations due to the commutation are considerably reduced compared to the conventional PI current controller even for BLDC motor with non-ideal trapezoidal back-EMF. However, phase resistance is neglected and the torque estimation depends on parameters such as dc-link voltage and phase inductance. Moreover, instead of a simple voltage selection look-up table technique more sophisticated PWM method is used to drive the BLDC motor. Also, two phase conduction method instead of a three-phase one is used which is problematic in the high speed applications.

In [47], the instantaneous torque is directly controlled by variable structure strategy (VSS) in *dq*–axes synchronous reference frame in which the torque pulsations mainly caused by a conventional sinusoidal current control are minimized. Torque estimation algorithm operates well down to zero speed, but depends on pre-knowledge of the harmonic torque coefficients of the machine, which are subject to motor parameter variations and difficult to obtain.

Torque coefficients in [47] are updated using an on-line recursive least square estimator in [48], however it is computationally intensive and difficult to implement because it requires differentiation of the motor current. Real-time harmonics flux estimator to calculate the sixth-harmonic current that must be injected to cancel the sixth- and twelfth-harmonic pulsating torque components rather than depending on stored coefficients is reported in [49]. However, obtaining those harmonics is a quite complicated task. Moreover, instead of a simple voltage vector selection method more complicated SVPWM technique is used to drive the motor. Since the torque is not controlled directly, fast torque response cannot be achieved. Also, rotor speed is measured by an expensive resolver and back-EMF harmonics higher than sixth order are neglected for simplification resulting in a reduction of the accuracy in the estimation algorithms in which the knowledge of the fundamental peak magnet flux is required.

In [46], the disadvantages observed in [47]–[49] are claimed to be improved by proposing a new instantaneous torque control. It is based on the model reference adaptive system (MRAS) technique and the torque is calculated by using the estimated flux and measured current. Then, the torque is instantaneously controlled by the torque controller using the integral variable structure control (IVSC) and the space-vector pulse-width modulation (SVPWM). Thus, good steady-state performance and switching characteristics are obtained. Compared to LSM, this technique does not require the differentiation of the motor current and the estimating performance is less sensitive to the measurement noise. Torque and speed pulsations are effectively reduced. Nevertheless, this technique increases the complexity of the control system.

In [50], predetermination of optimal current wave shapes using Park like *dq*–axes reference frame is obtained by adding some harmonics to the fundamental current to cancel specific torque harmonic components. However, these optimal current references are not constant and require very fast controllers especially when the motor operates at high speed. Moreover, the bandwidth of the classical proportional plus integral (PI) controllers does not allow tracking all of the reference current harmonics.

Problems in [50] are claimed to be solved in [51] such that a new torque control strategy using the *ba–ca* reference frame is proposed in which easily accessible line-to-line back-EMFs are measured and stored in a look-up table. Smooth and maximum torque is obtained, however this technique presents a steady-state torque error compared to the *dq*–axes reference frame scheme in [50] and the motor is driven by digital scalar modulation technique which operates like a SVPWM, therefore a more complicated control is inevitable.

Since the Park Transformation and its extensions proposed in [50] do not linearize completely the non-linear model of the machine, state feedback linearization technique is applied in order to obtain the desired high performance torque control in [52]. Additionally, more tedious computations are needed to be performed compared to [50], which complicates the real-time implementation of the control strategy.

The optimum current excitation methods, considering the unbalanced three-phase stator windings as well as non-identical and half-wave asymmetric back-EMF waveforms in BLDC motor, are reported in [43], [79]. These methods avoid the complicated harmonic coefficient calculation based on the optimization approach. In

[43], each phase back-EMF versus rotor position data is stored in a look-up table. Then, they are transformed to the *dq*–axes synchronous reference frame. The *d*–axis current is assumed to be zero and the *q*–axis current is obtained from the desired reference torque, motor speed, and the *q*–axis back-EMF. Consequently, inverse park transformation is applied to the *dq*–axes currents to obtain the *abc* frame optimum reference current waveforms. Minimum torque ripple and maximum efficiency are achieved at low speeds for a BLDC motor. However, three hysteresis current controllers with PWM generation, which increases the complexity of the drive, are used to drive the BLDC motor. Several transformations are required in order to get the *abc* frame optimum reference current waveforms. These transformations complicate the control algorithm and the scheme could not directly control the torque, therefore fast torque response cannot be achieved. Three offline measured back-EMF waveforms are needed for the torque estimation. Moreover, stator flux is not controlled, therefore high speed applications are not possible. In [79], an alternative simple and straightforward solution to eliminate torque ripple in BLDC machines is presented. This method is not *dq* based approach as in [43] and hence do not require the *dq* transformation which increases the complexity of the control system. The copper loss minimization strategy is also utilized. However, the pre-measured three line-to-neutral back-EMF waveforms are needed and three phase currents are controlled instead of *dq*–axes currents. Therefore, field-weakening operation cannot easily be performed.

In [41, 80], the method of multiple reference frames is employed in the development of a state variable model for BLDC drives with non-sinusoidal back-EMF

waveforms. This model has the desirable features of being valid for transient and steady-state analysis as well as having state variables that are constant in the steady-state. This method results in the same torque capability during constant torque region as in the six-step current control technique. Also, the same level of controllability as in the case of sinusoidal PMSM over the flux weakening region and regeneration operation compared to the conventional six-step BLDC drive system is achieved [41]. However, the method involves tedious algorithms which increase the complexity of the control system. Moreover, in [41], to determine the right *d*–axis current in flux-weakening region the high order *d*–axis harmonic current values are required which are quite difficult to obtain. Also, the back-EMF is assumed to be ideal trapezoidal and its harmonics higher than seventh order are neglected which results in a reduction of the accuracy in the overall system.

Direct torque control (DTC) scheme was first proposed by Takahashi [53] and Depenbrock [54] for induction motor drives in the mid 1980s. More than a decade later, in the late 1990s, DTC techniques for both interior and surface-mounted synchronous motors (PMSM) were analyzed [55]. More recently, application of DTC scheme is extended to BLDC motor drives to minimize the low-frequency torque ripples and torque response time as compared to conventional PWM current controlled BLDC motor drives [56, 72]. In [56] and [72], the voltage space vectors in a two-phase conduction mode are defined and a stationary reference frame electromagnetic torque equation is derived for surface-mounted permanent magnet synchronous machines with non-sinusoidal back-EMF (BLDC, and etc.). It is shown in [72] that only electromagnetic

torque in the DTC of BLDC motor drive under two-phase conduction mode can be controlled. Flux control is not trivial due to the sharp changes whose amplitudes are unpredictable depending on several factors such as load torque, dc-link voltage, winding inductance, etc.

In this chapter, the torque control method presented in [56] and [72] is adapted to the position sensorless direct torque control scheme for three-phase conduction BLDC motor by using the new Line-to-Line Park Transformation which forms a 2x2 matrix instead of the conventional 2x3 matrix. Therefore, rather than three line-to-neutral back-EMF waveforms which are not directly available in the motor easily accessible two line-to-line back-EMF waveforms (e_{ba} and e_{ca}) are obtained offline and converted to the electrical rotor position dependant line-to-line back-EMF constants ($k_{ba}(\theta_e)$ and $k_{ca}(\theta_e)$). Then, they are converted to dq–axes equivalents ($k_d(\theta_e)$ and $k_q(\theta_e)$) using Line-to-Line Park Transformation. dq–axes back-EMF constants versus electrical rotor position data ($k_d(\theta_e)$ and $k_q(\theta_e)$) are stored in a look-up table for the torque estimation. As opposed to the prior two-phase conduction methods, this DTC technique can control both torque and stator flux of the BLDC motor simultaneously, therefore field-weakening operation is possible. The electrical rotor position is estimated using winding inductance and stationary reference frame stator flux linkages and currents. The proposed sensorless DTC method controls the torque directly and stator flux amplitude indirectly using d–axis current. Since the stator flux is estimated, position sensorless DTC of BLDC motor drive scheme can be achieved. Unlike those for motor with sinusoidal back-EMFs, optimal current references for a non-sinusoidal back-EMF motor (BLDC) in the

synchronous reference frame are not constant, therefore current wave shapes require very fast controllers in particular at high speed. Classical bandwidth of the controller (such as proportional-integral–PI) does not allow tracking all of the reference current harmonics [51]. Since the hysteresis controllers used in the proposed DTC scheme are not fast controllers like PI, they can easily regulate not only constant but also the varying references (torque and flux). Simulation and experimental results are presented to illustrate the validity and effectiveness of the sensorless three-phase conduction DTC of a BLDC motor drive.

5.2. The Proposed Line-to-Line Clarke and Park Transformations in 2x2 Matrix Form

5.2.1. Conventional Park Transformation for Balanced Systems

In 1929, R. H. Park [81] introduced a new approach to electric machine analysis. In [81], Park Transformation is developed such that stator quantities of a synchronous machine are transformed onto a *dq* reference frame that is fixed to the rotor, with the positive *d*–axis aligned with the magnetic axis of the field winding and the positive *q*–axis is defined as leading the positive *d*–axis by $\pi/2$ [82]. Therefore, from the rotor point of view, all the variables can be observed as constant values. As a result, this transformation has created a revolutionary idea that all the time varying quantities in a polyphase machine are converted to orthogonal two-phase equivalents which are controllable constant values. For the balanced *n*–phase to two-phase case, Park Transformation can be expressed excluding the zero-sequence term as

$$\left[X_{dq}\right] = \left[T(\theta)\right]\left[X_{123\ldots n}\right] \tag{5.1}$$

where

$$\left[T(\theta)\right] = \frac{2}{3}\begin{bmatrix} \cos\left(\frac{P}{2}\theta\right) & \cos\left(\frac{P}{2}\theta - \xi\right) & \ldots \cos\left(\frac{P}{2}\theta - (n-1)\xi\right) \\ \sin\left(\frac{P}{2}\theta\right) & \sin\left(\frac{P}{2}\theta - \xi\right) & \ldots \sin\left(\frac{P}{2}\theta - (n-1)\xi\right) \end{bmatrix} \tag{5.2}$$

The coefficient 2/3 in (5.2) is used to make the transformation power invariant and θ is the electrical angle between adjacent magnetic axes of the uniformly distributed n–phase windings. The transformation angle θ is the angular displacement of the rotor reference frame.

The more general balanced three-phase to two-phase Park Transformation without a zero-sequence term X_0 can be expressed as

$$\begin{bmatrix} X_d \\ X_q \end{bmatrix} = \left[T(\theta)\right]\begin{bmatrix} X_a \\ X_b \\ X_c \end{bmatrix} \tag{5.3}$$

where the dq transformation matrix $\left[T(\theta)\right]$ is defined as

$$\left[T(\theta)\right] = \frac{2}{3}\begin{bmatrix} \cos\theta & \cos\left(\theta - 2\pi/3\right) & \cos\left(\theta + 2\pi/3\right) \\ \sin\theta & \sin\left(\theta - 2\pi/3\right) & \sin\left(\theta + 2\pi/3\right) \end{bmatrix} \tag{5.4}$$

In (5.4), q–axis is lagging the d–axis by π/2. Another method uses a qd transformation in which the q–axis leads the d–axis and the transformation angle θ is between the q–axis and the a–axis instead of d–axis and a–axis as in (5.4) [82]. However, both methods will produce the same results.

5.2.2. The Proposed Line-to-Line Clarke and Park Transformations for Balanced Systems

Since the balanced systems in *dq*–axes reference frame do not require a zero sequence term, first the Line-to-Line Clarke Transformation from the balanced three-phase quantities is derived and, then the Line-to-Line Park Transformation forming a 2x2 matrix instead of a 2x3 matrix as in (5.4) for three-phase systems can be obtained in the followings:

Line-to-Line Clarke Transformation which requires only two input variables (*bc* and *ca* frame) can be obtained from conventional *abc* frame version as follows:

First, classical Clarke Transformation, *abc* to *αβ* frame, is derived by replacing zero with the transformation angle θ in (5.4) and the matrix form is obtained as

$$\begin{bmatrix} X_\alpha \\ X_\beta \end{bmatrix} = \left[T_{\alpha\beta} \right] \begin{bmatrix} X_a \\ X_b \\ X_c \end{bmatrix} \tag{5.5}$$

where

$$\left[T_{\alpha\beta} \right] = \frac{2}{3} \begin{bmatrix} 1 & -\frac{1}{2} & -\frac{1}{2} \\ 0 & \frac{\sqrt{3}}{2} & -\frac{\sqrt{3}}{2} \end{bmatrix} \tag{5.6}$$

X_α and X_β are the stationary reference frame components, and X_a, X_b, and X_c are the *abc* frame components. In (5.5), X represents machine variables such as currents, voltages, flux linkages, back-EMFs, and etc.

If X_α and X_β are expanded and algebraically manipulated, the line-to-line representations of X_α and X_β in *ba–ca* reference frame are attained respectively as

$$X_\alpha = \frac{2X_a - X_b - X_c}{3} = \frac{X_a - X_b + X_a - X_c}{3} = \frac{-X_{ba} - X_{ca}}{3} \tag{5.7}$$

and

$$X_\beta = \frac{\sqrt{3}}{3}\left(X_b - X_c\right) = \frac{\sqrt{3}}{3}\left(X_b - X_a + X_a - X_c\right) = \frac{\sqrt{3}}{3}\left(X_{ba} - X_{ca}\right) \tag{5.8}$$

where $X_{ba} = X_b - X_a$ and $X_{ca} = X_c - X_a$.

Using the results obtained in (5.7) and (5.8), X_α and X_β can be rewritten in matrix form as

$$\begin{bmatrix} X_\alpha \\ X_\beta \end{bmatrix} = \left[T_{LL}\right]\begin{bmatrix} X_{ba} \\ X_{ca} \end{bmatrix} \tag{5.9}$$

where

$$\left[T_{LL}\right] = \begin{bmatrix} -\frac{1}{3} & -\frac{1}{3} \\ \frac{\sqrt{3}}{3} & -\frac{\sqrt{3}}{3} \end{bmatrix} \tag{5.10}$$

As it can be seen in (5.10) that original Clarke Transformation forming a 2x3 matrix given in (5.8) excluding the zero-sequence term can be simplified to a 2x2 matrix which requires only two input variables.

Second, to obtain *abc* to *ba–ca* frame transformation the inverse of the Clarke Transformation matrix $\left[T_{\alpha\beta}\right]$ given in (5.6) is required. Since the zero-sequence term is removed, $\left[T_{\alpha\beta}\right]$ is not square anymore, but it is still singular and therefore pseudo-inverse can be found in the followings:

$$\left[T_{\alpha\beta}\right]^+ = \left[T_{\alpha\beta}\right]^T \left(\left[T_{\alpha\beta}\right]\left[T_{\alpha\beta}\right]^T\right)^{-1} \tag{5.11}$$

where $\left[T_{\alpha\beta}\right]^{+}$ and $\left[T_{\alpha\beta}\right]^{T}$ are the pseudo-inverse and transpose of the original Clarke Transformation matrix $\left[T_{\alpha\beta}\right]$, respectively.

Abc to *ba–ca* transformation matrix can be derived using the pseudo-inverse matrix $\left[T_{\alpha\beta}\right]^{+}$, original Clarke Transformation matrix $\left[T_{\alpha\beta}\right]$ and Line-to-Line Clarke Transformation matrix $\left[T_{LL}\right]$ as follows:

$$\left[T_{\alpha\beta}\right]^{+}\left[T_{\alpha\beta}\right]\begin{bmatrix} X_a \\ X_b \\ X_b \end{bmatrix} = \left[T_{\alpha\beta}\right]^{+}\left[T_{LL}\right]\begin{bmatrix} X_{ba} \\ X_{ca} \end{bmatrix} \tag{5.12}$$

hence

$$\begin{bmatrix} X_a \\ X_b \\ X_b \end{bmatrix} = \begin{bmatrix} -\frac{1}{3} & -\frac{1}{3} \\ \frac{2}{3} & -\frac{1}{3} \\ -\frac{1}{3} & \frac{2}{3} \end{bmatrix}\begin{bmatrix} X_{ba} \\ X_{ca} \end{bmatrix} \tag{5.13}$$

Then, the *ba–ca* to *dq* frame Line-to-Line Park Transformation can be written using (5.4) in (5.13) as

$$\begin{bmatrix} X_d \\ X_q \end{bmatrix} = \left[T(\theta)\right]\begin{bmatrix} -\frac{1}{3} & -\frac{1}{3} \\ \frac{2}{3} & -\frac{1}{3} \\ -\frac{1}{3} & \frac{2}{3} \end{bmatrix}\begin{bmatrix} X_{ba} \\ X_{ca} \end{bmatrix} \tag{5.14}$$

After (5.14) is expanded and simplified using some trigonometric equivalence, the following 2x2 Line-to-Line Park Transformation matrix form is obtained:

$$\begin{bmatrix} X_d \\ X_q \end{bmatrix} = \frac{2}{3}\begin{bmatrix} \sin(\theta - \pi/6) & -\sin(\theta + \pi/6) \\ -\cos(\theta - \pi/6) & \cos(\theta + \pi/6) \end{bmatrix}\begin{bmatrix} X_{ba} \\ X_{ca} \end{bmatrix} \tag{5.15}$$

5.3. The Proposed Sensorless DTC of BLDC Drive Using Three-Phase Conduction

5.3.1. Principles of the Proposed Method

In this work, indirect torque control method of BLDC motor explained in [43] is extended to a direct torque and indirect flux control technique which is suitable for sensorless and field-weakening operations. The proposed method transforms *abc* frame quantities to *dq* frame ones using the new 2x2 Line-to-Line Park Transformation matrix. Rather than three measured phase back-EMFs which are used in [43], in the proposed balanced system only two electrical rotor position dependant back-EMF constants ($k_d(\theta_e)$ and $k_q(\theta_e)$) are required in the torque estimation algorithm. Since the numbers of input variables (current and back-EMF) are reduced from three to two, much simpler Park Transformation can be used as given in (5.15). Therefore, the amount of multiplications and sine/cosine functions are minimized.

Unlike previous two-phase conduction DTC of BLDC motor drive techniques which are proposed in [56, 72], this method uses DTC technique with three-phase conduction, therefore field-weakening operation as well as a much simpler position sensorless technique can easily be achieved. Compared to the two-phase conduction DTC scheme, this DTC method differs by its torque estimation and voltage vector selection table which is similar to the one used for DTC of PMSM drives explained in [10]. Although stator flux estimation algorithm in both methods (two-phase and three-phase conduction) is the same due to the similar machine model in which the back-EMF

shape separates the two from each other, in two-phase conduction scheme the stator flux amplitude is uncontrollable. Since the proposed technique adopts three-phase conduction, there is a possibility to control the stator flux amplitude without commutation issue, therefore field-weakening and sensorless operations which involve back-EMF estimation can easily be performed. Moreover, this DTC method controls the voltage vectors directly from a simple look-up table depending on the outcome of hysteresis torque and indirect flux controllers, thus the overall control is much simpler and faster torque response can be achieved compared to the conventional PWM control techniques.

Unless the harmonic components of field distribution and inductance variation are considered, the synchronously rotating *dq* reference frame analysis is no longer valid for BLDC motors with non-sinusoidal back-EMF because the stator to rotor mutual inductance does not vary sinusoidally [43]. Since the proposed DTC of BLDC motor drive method does not consider performing a modeling and simulation of the motor itself as in the Fourier analysis and multiple reference frame operations, the *dq* reference frame approach can easily be adopted to the DTC scheme to obtain a low-frequency ripple free torque based on the minimum input power.

Most of the previous work to eliminate low-frequency torque ripples for BLDC motors assumed that the neutral point of the motor is available. Measurement of the three-phase back-EMFs requires access to the neutral point connection of the stator. In most cases, this represents extra cost and inconvenience to the motor installation.

Especially, in Y-connected systems, the neutral point is generally not available. Therefore, it is not practical and cumbersome to extract the neutral point [43].

For PMSM with non-sinusoidal back-EMF constituting odd harmonics, stator flux linkages $\varphi_{ds}^{\ r}$ and $\varphi_{qs}^{\ r}$ in the *dq*–axes rotor reference frame can be obtained, respectively as [47]

$$\varphi_{ds}^{\ r} = L_{ds} i_{ds}^{\ r} + L_{dqs} i_{qs}^{\ r} + L_{dsf} i_f \tag{5.16}$$

$$\varphi_{qs}^{\ r} = L_{qs} i_{qs}^{\ r} + L_{qds} i_{ds}^{\ r} + L_{qsf} i_f \tag{5.17}$$

where L_{dqs} and L_{qds} are the mutual inductances between *d*– and *q*–axis, respectively. $i_{ds}^{\ r}$ and $i_{qs}^{\ r}$, L_{ds} and L_{qs} are the *d*– and *q*–axis currents and inductances, respectively. L_{dsf} and L_{qsf} are the mutual inductances between *dq*–axes and permanent magnet, respectively. i_f is the equivalent current generated by PM.

All the machine inductances given in (5.16) and (5.17) can be written considering the flux harmonics which are multiple of six as [43]

$$L_{ds} = L_{ds0} + L_{ds6}\cos 6\theta_r + L_{ds12}\cos 12\theta_r + \cdots \tag{5.18}$$

$$L_{dqs} = L_{dqs6}\sin 6\theta_r + L_{dqs12}\cos 12\theta_r + \cdots \tag{5.19}$$

$$L_{dsf} = L_{dsf} + L_{dsf6}\sin 6\theta_r + L_{dsf12}\cos 12\theta_r + \cdots \tag{5.20}$$

$$L_{qs} = L_{qs0} + L_{qsf6}\cos 6\theta_r + L_{qsf12}\cos 12\theta_r + \cdots \tag{5.21}$$

$$L_{qds} = L_{qds6}\sin 6\theta_r + L_{qds12}\sin 12\theta_r + \cdots \tag{5.22}$$

$$L_{qsf} = L_{qsf} + L_{qsf6}\cos 6\theta_r + L_{qsf12}\cos 12\theta_r + \cdots \tag{5.23}$$

As it can be seen in (5.18)–(5.23) that the inductances in the rotor reference frame are not constant as in pure sinewave machines and represented by the fundamental term and/or multiple of six because the third harmonic and its multiples are internally cancelled out in the Y-connected three-phase systems and from the remaining harmonics, 5th and 7th harmonics transform into 6th harmonics, 11th and 13th harmonics transform into 12th harmonics, and so on.

The motors with high-coercive PM material, the effects of the inductance harmonics in the stator winding can be negligible for the torque pulsation which is mainly produced by the flux harmonics in the PM. Therefore, for machines with surface-mount magnet rotor (BLDC) it can be assumed that L_{ds} and L_{qs} are constant, i.e., $L_{ds} = L_{qs} = L_{ds0} = L_{qs0} = L_s$, and $L_{dqs} = L_{qds} = 0$ Thus, stator flux linkages in rotor *dq* reference frame given in (5.16) and (5.17) can be rewritten as

$$\varphi_{ds}{}^{r} = L_{ds} i_{ds}{}^{r} + L_{dsf} i_f \tag{5.24}$$

$$\varphi_{qs}{}^{r} = L_{qs} i_{qs}{}^{r} + L_{qsf} i_f \tag{5.25}$$

If the second term on the right hand side in (5.24) and (5.25) is expanded into the time-varying equivalence, the following equations are obtained:

$$\varphi_{ds}{}^{r} = L_s i_{ds}{}^{r} + \varphi_r{}' \sum_{n=1}^{\infty} \left(K_{6n-1} - K_{6n+1} \right) \cos\left(6n\theta_r \right) + \varphi_r{}' \tag{5.26}$$

$$\varphi_{qs}{}^{r} = L_s i_{qs}{}^{r} + \varphi_r{}' \sum_{n=1}^{\infty} \left(K_{6n-1} + K_{6n+1} \right) \sin\left(6n\theta_r \right) \tag{5.27}$$

where φ_r' is the peak value of the fundamental rotor magnetic flux linkage, the coefficients K_{6n-1} and K_{6n+1} represent the odd harmonics of the phase back-EMF other than the third and its multiples. K_{6n-1} equals $\left[\sin(6n-1)\alpha\right]/\left[(6n-1)^3\sin\alpha\right]$, and K_{6n+1} is $\left[\sin(6n+1)\alpha\right]/\left[(6n+1)^3\sin\alpha\right]$. α is the angle between zero-crossing and phase back-EMF where it becomes flat at the top. Fundamental peak value of the rotor magnet flux linkage φ_r' equals $(4k_e/\alpha\pi)\sin\alpha$ where k_e is the line-to-neutral back-EMF constant.

Although the equations to obtain coefficients K_{6n-1} and K_{6n+1} are approximations considering the back-EMF of BLDC motor consists of odd harmonics, they can also be obtained by Fourier analysis with more precise results, however it is a cumbersome work. Furthermore, the amounts of harmonics are limited due to the complication. In this work, the exact shape of only two line-to-line back-EMFs (e_{ba} and e_{ca}) are used without Fourier decomposition, therefore more realistic results can be achieved.

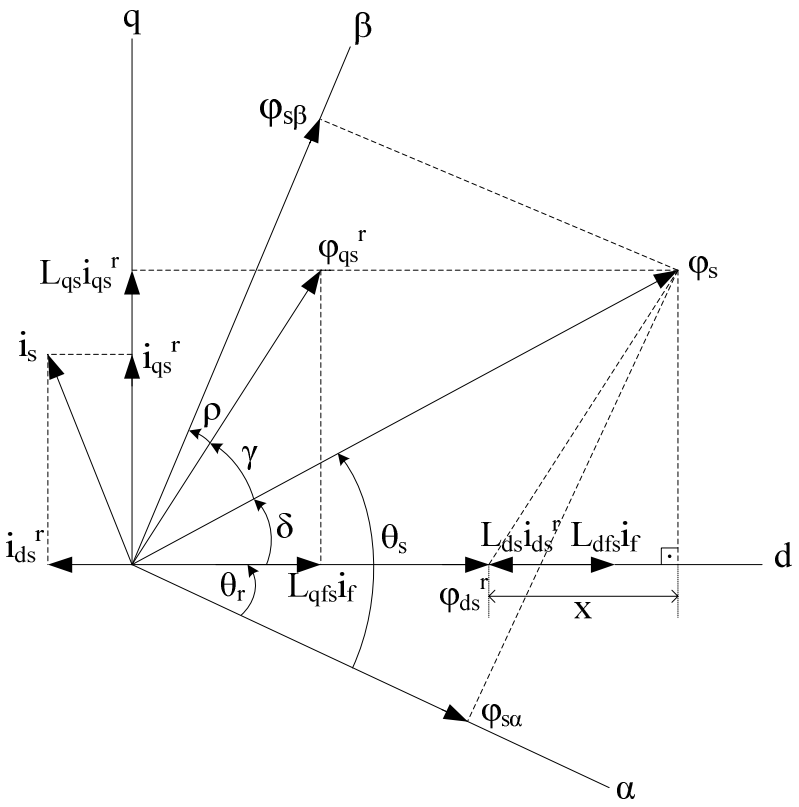

Fig. 5.1. Rotor and stator flux linkages of a BLDC motor in the stationary *αβ*–plane and synchronous *dq*–plane.

Equations (5.26) and (5.27) are very close approximations of stator flux linkages in *dq* reference frame for the PMSM with non-sinusoidal back-EMF. It can be seen that they are not constant as in pure sinusoidal ac machines. Inductances and stator flux linkages vary by the six times of the fundamental frequency. One of the reasons to derive the equivalent inductance and then the *dq* frame stator flux linkages in BLDC motor is that it can be easily observable which parameters affect the amplitude of the stator flux linkages. Stator flux linkage amplitude $|\varphi_s| = \sqrt{\left(\varphi_{ds}{}^r\right)^2 + \left(\varphi_{qs}{}^r\right)^2}$ can be changed by varying the *d*–axis current $i_{ds}{}^r$ in (5.26) assuming the torque is constant and

it is proportional to $i_{qs}^{\ r}$, therefore an indirect flux control can be achieved in the proposed DTC of BLDC motor drive. Although $i_{qs}^{\ r}$ is assumed constant meaning that it has an offset to generate an average torque, to obtain a smooth electromagnetic torque it varies by six times the fundamental frequency because flux harmonics given in (5.26) and (5.27) generate torque pulsations on the order of six and multiples of six. Since flux-weakening operation is not in the scope of this paper, *d*–axis current reference is selected zero. The phasor diagram for stator flux linkage vectors in BLDC motor can be drawn in the rotor *dq* and stationary (*αβ*) reference frames as shown in Fig. 5.1 where $L_{dqs} = L_{qds} = 0$. In Fig. 5.1, unlike PMSM with sinusoidal back-EMF synchronous reference frame flux linkages $\varphi_{ds}^{\ r}$ and $\varphi_{qs}^{\ r}$ vary with time, therefore stator flux amplitude $|\varphi_s|$ is not constant anymore in the trajectory. γ, ρ, and δ in Fig. 5.1 can be obtained respectively as

$$\gamma = \sin^{-1}\left(L_{qs} i_{qs}^{\ r} / \varphi_{qs}^{\ r}\right) + \cos^{-1}\left(L_{qs} i_{qs}^{\ r} / \varphi_s\right) - \pi / 2 \tag{5.28}$$

$$\rho = -\left(\theta_s + \gamma - \pi / 2\right) \tag{5.29}$$

and

$$\delta = \pi / 2 - \cos^{-1}\left(L_{qs} i_{qs}^{\ r} / \varphi_s\right) \tag{5.30}$$

Moreover, *x* in Fig. 5.1 can be expressed as

$$x = \varphi_{qs}^{\ r} \cos\left[\sin^{-1}\left(L_{qs} i_{qs}^{\ r} / \varphi_s\right)\right] \tag{5.31}$$

5.3.2. Electromagnetic Torque Estimation in *dq* and *ba–ca* Reference Frames

Because of the rotor position dependant terms in the *dq* frame stator flux linkages in (5.26) and (5.27) and inductances in (5.18)–(5.23), conventional torque estimation in stator reference frame used for DTC of sinusoidal ac motors is no longer valid for BLDC motor, therefore a new torque estimation algorithm is derived in *dq* frame consisting of actual *dq*–axes back-EMF constants and currents. Instead of the actual back-EMF waveforms, Fourier approximation of the back-EMFs could have been adopted in the torque estimation, but the results would not truly represent the reality and more complex computations are required.

The torque estimation is the key factor in the proposed DTC scheme. First, two line-to-line back-EMF waveforms $e_{ba}(\theta_e)$ and $e_{ca}(\theta_e)$ are obtained offline and converted to the *ba–ca* frame back-EMF constants $k_{ba}(\theta_e)$ and $k_{ca}(\theta_e)$. The Line-to-Line Park Transformation matrix in (5.15) is used to obtain the *dq* reference frame back-EMF constants $k_d(\theta_e)$ and $k_q(\theta_e)$, where θ_e is the electrical rotor angular position. Then, they are stored in a look-up table for electromagnetic torque estimation.

The electromagnetic torque T_{em} estimation algorithm can be derived for a balanced system in *dq* reference frame by equating the electrical power absorbed by the motor to the mechanical power produced ($P_i = P_m = T_{em}\omega_m$) as follows:

$$T_{em} = \frac{3P}{4\omega_{re}}\left(e_q(\theta_e)i_{qs}{}^r + e_d(\theta_e)i_{ds}{}^r\right) = \frac{3P}{4}\left(k_q(\theta_e)i_{qs}{}^r + k_d(\theta_e)i_{ds}{}^r\right) \qquad (5.32)$$

where P is the number of poles, ω_e is the electrical rotor speed, $e_q(\theta_e)$ and $e_d(\theta_e)$, $i_{qs}^{\ r}$ and $i_{ds}^{\ r}$, $k_q(\theta_e)$ and $k_d(\theta_e)$ are the dq–axes back-EMFs, currents, and back-EMF constants according to the electrical rotor position, respectively. As it can be noticed that the right hand-side equation in (5.32) eliminates the speed term in the denominator which causes problem at zero and near zero speeds.

Instead of dq frame torque equation in (5.32), much more computation intensive ba–ca frame torque estimation could have been used. Ba–ca frame electromagnetic torque equation whose derivation provided in Appendix B can be expressed as

$$T_{em} = \frac{P}{6}\left[\left(2k_{ba}(\theta_e) - k_{ca}(\theta_e)\right)i_{ba} + \left(2k_{ca}(\theta_e) - k_{ba}(\theta_e)\right)i_{ca}\right] \tag{5.33}$$

where $k_{ba}(\theta_e) = k_b(\theta_e) - k_a(\theta_e)$, and $k_{ca}(\theta_e) = k_c(\theta_e) - k_a(\theta_e)$, i_{ba} and i_{ca} are the line-to-line back-EMF constants according to the electrical rotor position, and line-to-line currents, respectively.

However, because ba–ca frame torque equation in (5.33) involves more calculations, the dq frame torque equation in (5.32) instead of (5.33) is used in the proposed DTC scheme.

5.3.3. Control of Stator Flux Linkage Amplitude

The stator voltage equations of a BLDC motor can be obtained in the stationary reference frame similar to PMSM as follows:

$$V_{s\alpha} = R_s i_{s\alpha} + \frac{d\varphi_{s\alpha}}{dt}$$
$$V_{s\beta} = R_s i_{s\beta} + \frac{d\varphi_{s\beta}}{dt} \tag{5.34}$$

where

$$\varphi_{s\alpha} = L_s i_{s\alpha} + \varphi_{r\alpha}$$
$$\varphi_{s\beta} = L_s i_{s\beta} + \varphi_{r\beta} \tag{5.35}$$

In (5.35), $\varphi_{r\alpha}$ and $\varphi_{r\beta}$ are the rotor flux linkages. It is obvious that they do not vary sinusoidally as opposed to PMSM due to the non-sinusoidal back-EMF.

Since BLDC motor does not have sinusoidal back-EMF, the stator flux trajectory is not pure circular as in PMSM. It is more like a decagonal shape as shown in Fig. 5.2. Thus, direct stator flux amplitude control in a BLDC motor is not trivial as in PMSM such that rotor position varying flux command should be considered. However, this is a complicated way to control the stator flux linkage amplitude. Therefore, in this work instead of $|\varphi_s|$ itself its amplitude is indirectly controlled by *d*–axis current. In the constant torque region i_{ds} is controlled as zero and in the flux-weakening region it is decreased for a certain amount depending on the operational speed to achieve maximum torque. As a result, in this work stator flux linkage amplitude is indirectly kept at its optimum level while the motor speed is less than the base speed.

Since stationary reference frame voltage equations in BLDC motor are same as the ones for PMSM, stator flux linkages in stationary reference frame can be depicted in a similar fashion as

$$\begin{aligned}\varphi_{s\alpha} &= \int \left(V_{s\alpha} - R_s i_{s\alpha}\right) dt \\ \varphi_{s\beta} &= \int \left(V_{s\beta} - R_s i_{s\beta}\right) dt\end{aligned} \tag{5.36}$$

where $V_{s\alpha}$ and $V_{s\beta}$ can be found from a dc-link voltage sensor depending on the sector where stator flux linkage is located.

During the sampling interval time, one out of the six voltage vectors is applied, and each voltage vector applied during the pre-defined sampling interval is constant, then (5.36) can be rewritten as:

$$\begin{aligned}\varphi_{s\alpha} &= V_{s\alpha} t - R_s \int i_{s\alpha} dt + \varphi_{s\alpha}(0) \\ \varphi_{s\beta} &= V_{s\beta} t - R_s \int i_{s\beta} dt + \varphi_{s\beta}(0)\end{aligned} \tag{5.37}$$

where $\varphi_{s\alpha}(0)$ and $\varphi_{s\beta}(0)$ are the initial stator flux linkages at the instant of switching. If the line-to-line back-EMF constant k_{LL} is roughly known, and let say the rotor is brought to zero position (phase–*a*), initial stator flux linkages at start-up can be obtained by integrating the back-EMF in which the ideal trapezoidal is assumed as given in Appendix E. Therefore, approximate initial starting flux values at zero position can be obtained as $\varphi_{s\alpha}(0) = 2k_{LL}\pi / \left(3\sqrt{3}\right)$ and $\varphi_{s\beta}(0) = 0$.

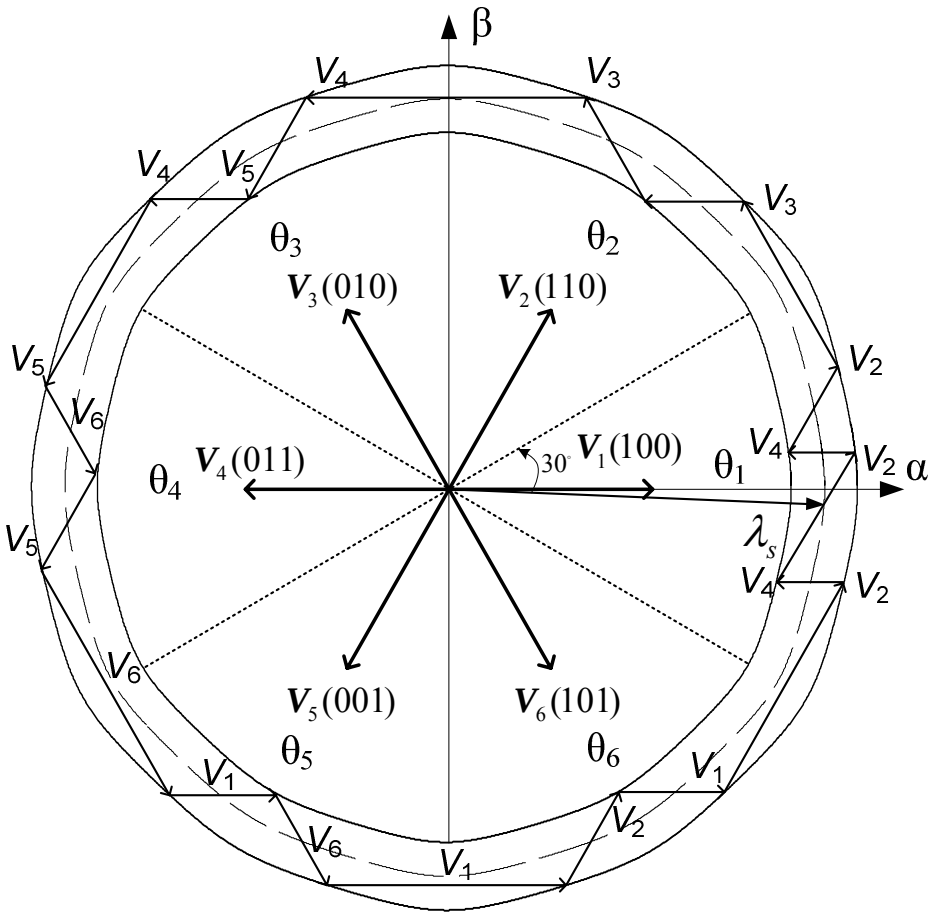

Fig. 5.2. Decagon trajectory of stator flux linkage in the stationary *αβ*–plane.

5.3.4. Control of Stator Flux Linkage Rotation and Voltage Vector Selection for DTC of BLDC Motor Drive

In BLDC motor, if the load angle δ in Fig. 5.1 is increased then the torque variation is increased. To increase the load angle δ the stator flux vector should turn faster than rotor flux vector. The rotor flux rotation depends on the mechanical speed of the rotor, so to decrease load angle δ the stator flux should turn slower than rotor flux.

Therefore, the electromagnetic torque can be controlled effectively by controlling the amplitude and rotational speed of stator flux vector φ_s .

The switching table for controlling both the amplitude and rotating direction of the stator flux linkage is given in Table VI.

TABLE VI

SWITCHING TABLE FOR DTC OF BLDC MOTOR USING THREE-PHASE CONDUCTION

φ	τ	θ					
		θ(1)	θ(2)	θ(3)	θ(4)	θ(5)	θ(6)
$\varphi = 1$	$\tau = 1$	$\mathbf{V}_2(110)$	$\mathbf{V}_3(010)$	$\mathbf{V}_4(001)$	$\mathbf{V}_5(101)$	$\mathbf{V}_6(110)$	$\mathbf{V}_1(110)$
	$\tau = -1$	$\mathbf{V}_6(101)$	$\mathbf{V}_1(100)$	$\mathbf{V}_2(010)$	$\mathbf{V}_3(011)$	$\mathbf{V}_4(110)$	$\mathbf{V}_5(110)$
$\varphi = -1$	$\tau = 1$	$\mathbf{V}_3(010)$	$\mathbf{V}_4(011)$	$\mathbf{V}_5(101)$	$\mathbf{V}_6(100)$	$\mathbf{V}_1(110)$	$\mathbf{V}_2(110)$
	$\tau = -1$	$\mathbf{V}_5(001)$	$\mathbf{V}_6(101)$	$\mathbf{V}_1(110)$	$\mathbf{V}_2(010)$	$\mathbf{V}_3(110)$	$\mathbf{V}_4(110)$

The output of the torque hysteresis comparator is denoted as τ, the output of the flux hysteresis comparator as φ and the flux linkage sector is denoted as θ. The torque hysteresis comparator is a two valued comparator; τ = -1 means that the actual value of the torque is above the reference and out of the hysteresis limit and τ = 1 means that the actual value is below the reference and out of the hysteresis limit. The same is applied to the flux hysteresis comparator.

5.3.5. Estimation of Electrical Rotor Position

Electrical rotor position θ_e which is required in the Line-to-Line Park Transformation and torque estimation algorithm can be found using (5.35) and (5.36) as

$$\theta_e = \tan^{-1}\left(\frac{\varphi_{s\beta} - L_s i_{s\beta}}{\varphi_{s\alpha} - L_s i_{s\alpha}}\right) \tag{5.38}$$

Practical implementation of an integrator for stator flux linkage estimation in (5.37) is not an easy task. Using a pure integrator causes a dc drift and initial value problems. A small dc offset in the measured voltage and current signals due to noise or measurement error can cause the pure integrator to saturate.

Many attempts have been made to modify the pure integrator by implementing it using a low pass filter. However, low pass filter produces errors in magnitude and phase angle, especially when the motor runs at a frequency lower than the filter cutoff frequency [83].

To solve the above common problems for integrators, a special integration algorithm for estimating the stator flux linkage proposed in [83] is used in this work. Although the method in [83] is designed for sinewave systems, the algorithm is still applicable to a BLDC motor with varying stator flux linkage amplitude as shown in Fig. 5.2 in which ω_c is the cut-off frequency and θ_s is the stator flux linkage position. Second algorithm in [83] which is the modified integrator with an amplitude limiter illustrated in Fig. 5.3 is used for the stator flux linkage estimation in the proposed position sensorless three-phase conduction DTC of BLDC motor drive scheme. The maximum amplitude of the stator flux linkage reference approximated as $2k_{LL}\pi/\left(3\sqrt{3}\right)$ is set for the limiter in Fig. 5.3 when the motor speed is less than the base speed. If the motor operates in the field weakening region, the limiter value should be selected properly, but this is not in the scope of this work.

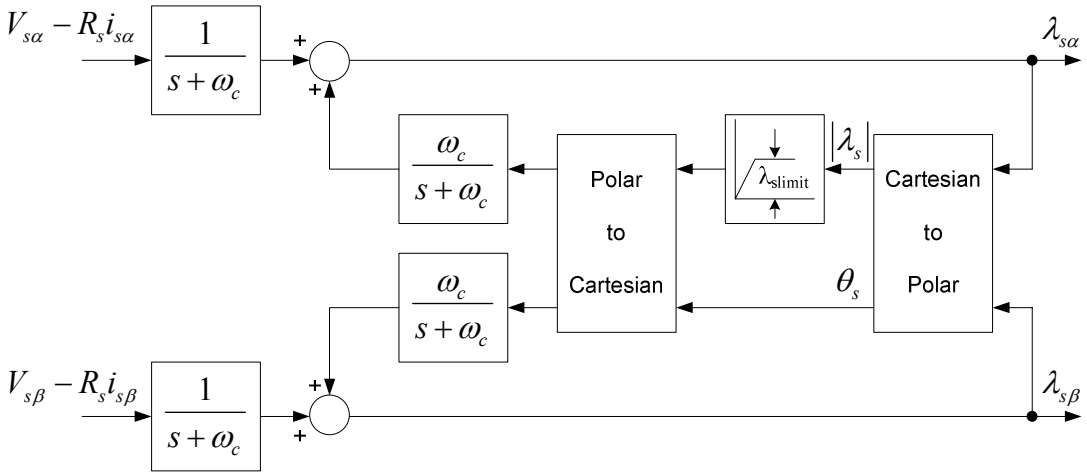

Fig. 5.3. BLDC motor stator flux linkage estimation with an amplitude limiter [83].

5.4. Simulation Results

The drive system shown in Fig. 5.4 has been simulated in order to demonstrate the validity of the proposed position sensorless three-phase conduction DTC of a BLDC motor drive scheme using line-to-line machine model.

To set the gating signals of the power switches easily and represent the real conditions in simulation as close as possible the electrical model of the actual BLDC motor with R-L elements and the inverter with power semiconductor switches considering the snubber circuit are designed in Matlab/Simulink® using the SimPower Systems toolbox.

The dead-time of the inverter and non ideal effects of the BLDC machine are neglected in the simulation model. The sampling interval is 15 μs. The switching table, which is given in Table VI is employed for the proposed DTC of the BLDC motor drive. The magnitudes of the torque and flux hysteresis bands are 0.001 N·m, and 0.001 Wb, respectively.

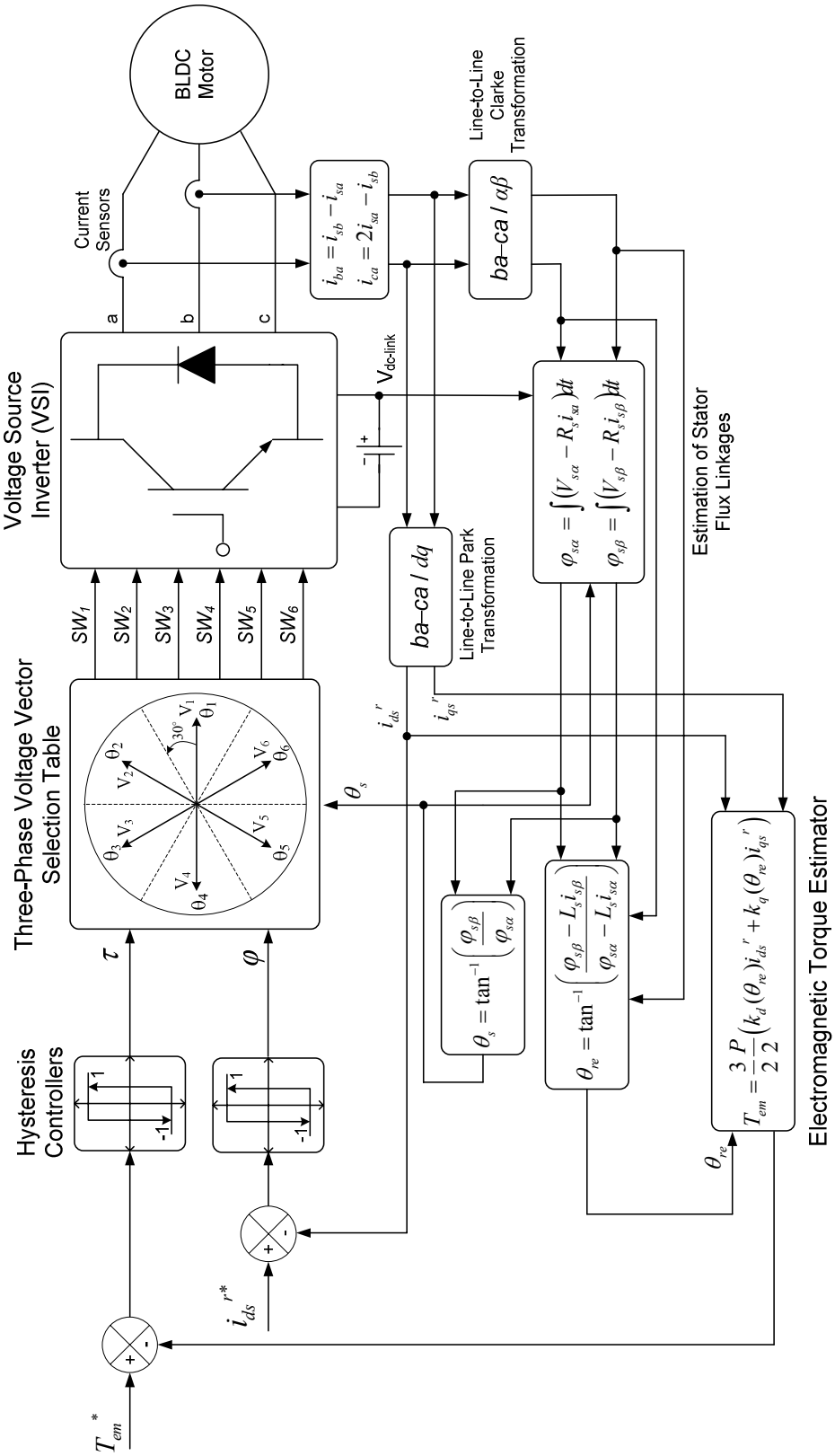

Fig.5. 4. Overall block diagram of the position sensorless direct torque and indirect flux control (DTIFC) of BLDC motor drive using three-phase conduction mode.

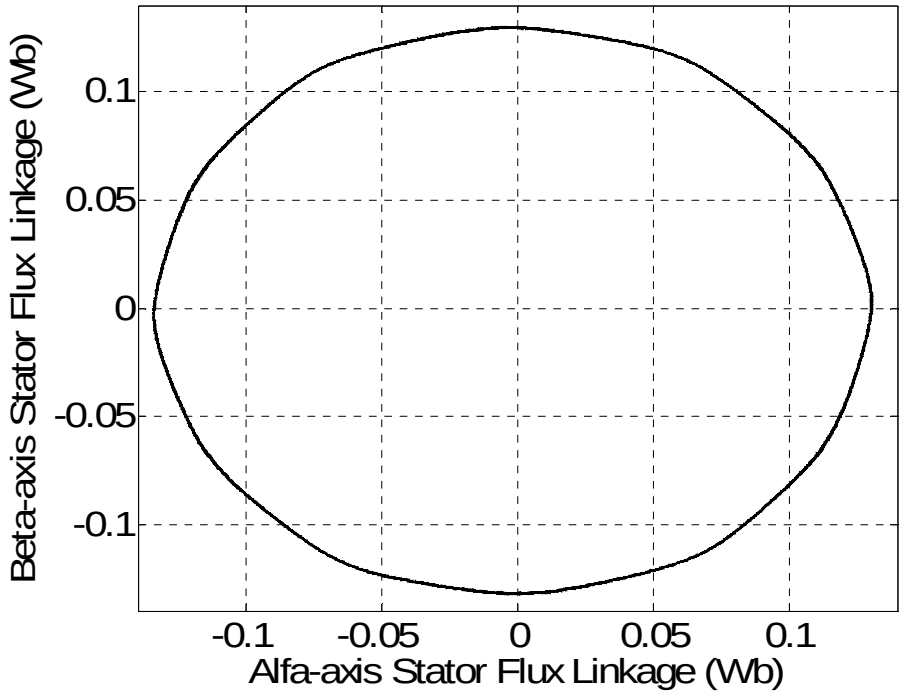

Fig. 5.5. Simulated indirectly controlled stator flux linkage trajectory under the sensorless three-phase conduction DTC of a BLDC motor drive at 0.5 N·m load torque ($i_{ds}^{r*} = 0$).

Fig. 5.5 shows the simulation results of the indirectly controlled stator flux linkage locus by controlling the *d*–axis rotor ref. frame current ($i_{ds}^{r*} = 0$) when 0.5 N·m load torque is applied to the BLDC motor. Actual line-to-line back-EMF waveforms are used in the BLDC motor model. Due to the non-sinusoidal waveform of the actual back-EMFs the dodecagon shape in the flux locus is observed in Fig. 5.5. The simulation system is run 0.7 second. It is seen from Fig. 5.5 that the amplitude of the stator flux linkage is indirectly controlled quite well at its required value, which is the amplitude of the magnet flux linkage, in the constant torque region. It is noted that the amplitude of the magnet flux varies non-sinusoidally as expected. Actual values of the stationary reference frame rotor flux linkages $\varphi_{r\alpha}(\theta_e)$ and $\varphi_{r\beta}(\theta_e)$ can be obtained by integrating

the corresponding actual stationary reference frame back-EMFs $e_\alpha(\theta_e)$ and $e_\beta(\theta_e)$ over time. Torque reference is selected as 0.51 N·m to obtain a steady-state condition under 0.5 N·m load torque. Since $i_{ds}^{r*} = 0$, motor runs in the constant torque region ($\omega_e < \omega_{base}$). The steady-state speed is 30 mechanical rad/s and the dc-link voltage V_{dc} equals $40\sqrt{2}$ V. In the simulation, it is assumed that the rotor starts at its initial position $\theta_e = 0$ [region θ(1)].

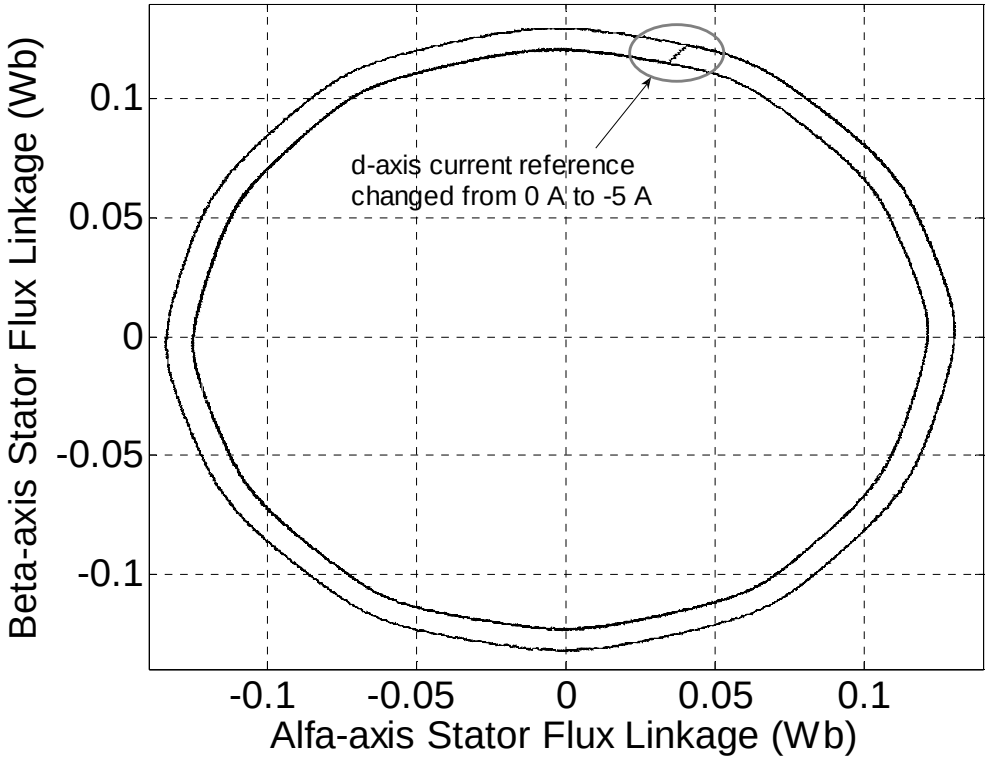

Fig. 5.6. Simulated indirectly controlled stator flux linkage trajectory under the sensorless three-phase conduction DTC of a BLDC motor drive when i_{ds}^{r} is changed from 0 A to -5 A under 0.5 N·m load torque.

In Fig. 5.6, the possibility of the flux-weakening region operation is simulated when i_{ds}^{r*} is changed from 0 A to -5 A at 0.125 second. Total simulation time in this case

is 0.3 second. As it can be seen in Fig. 5.6 that the shape of stator flux linkage trajectory is kept same, however its amplitude is smaller compared to the initial case which means that the flux in the machine is weakened to obtain maximum possible torque above the base speed. It is concluded that in the proposed control scheme flux-weakening operation is viable by properly selecting the *d*–axis current reference as in PMSM drives. As a result, there is no need to use position-varying stator flux linkage amplitude $|\varphi_s(\theta_e)|^*$ as a reference which is complicated to obtain especially in the field-weakening region. Proper selection of the *d*–axis current reference respective of speed for field-weakening region operation is not in the scope of this paper. This is left as a future research study.

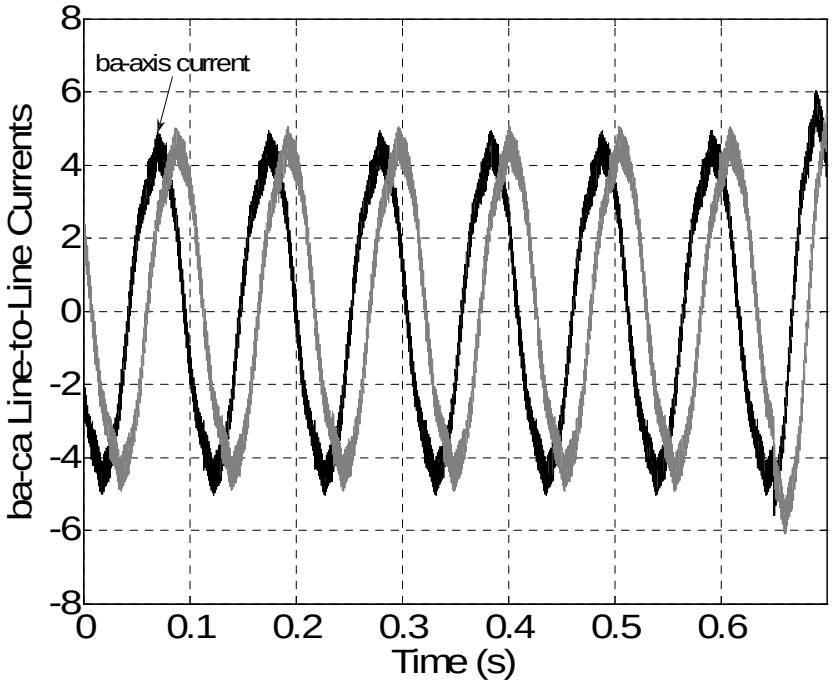

(a)

Fig. 5.7. Steady-state and transient behavior of (a) simulated *ba–ca* frame currents, (b) actual electromagnetic torque, and (c) estimated electromagnetic torque under 0.5 N·m load torque.

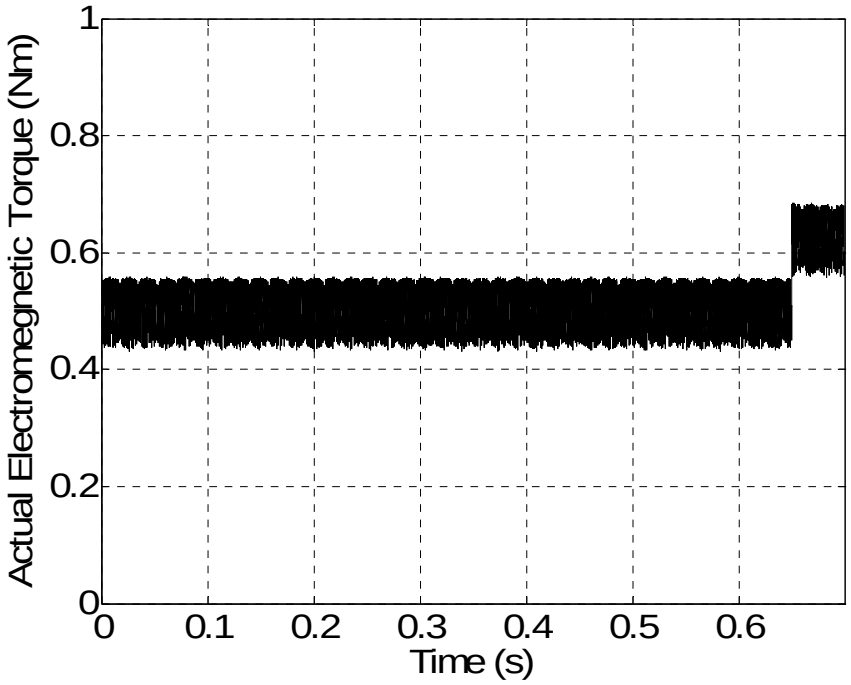

(b)

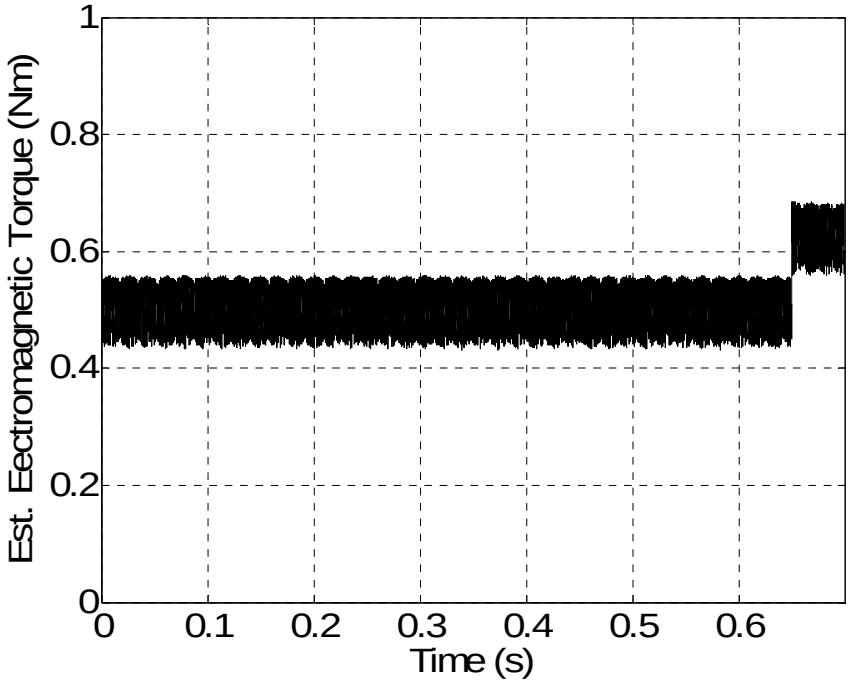

(c)

Fig. 5.7. Continued.

Steady-state and transient behavior of *ba–ca* axes line-to-line currents, actual and estimated electromagnetic torque are shown in Fig. 5.7(a), (b) and (c), respectively. The reference torque is suddenly increased 25 percent from 0.51 N·m to 0.6375 N·m at 0.65 s under 0.5 N·m load torque. Actual and estimated electrical rotor positions are illustrated in Fig. 5.8(a) and (b), respectively under the same control conditions. The estimated electrical rotor position tracks the actual electrical rotor position quite well as shown in Fig. 5.8(b). As it can be seen in Fig. 5.7(a) and (b), when the torque is suddenly increased the current amplitudes also increase and fast torque response is achieved. Also, the estimated torque follows the desired torque satisfactorily as seen in Fig. 5.7(c). The high frequency ripples observed in the torque and current are related to the sampling time, hysteresis bandwidth, winding inductance, and dc-link voltage. Those ripples can be minimized by properly selecting the dc-link voltage and torque hysteresis band size. It can be seen in Fig. 5.7(a) that the top of the *ba–ca* frame currents are reciprocal of the corresponding back-EMFs to generate smooth torque profile.

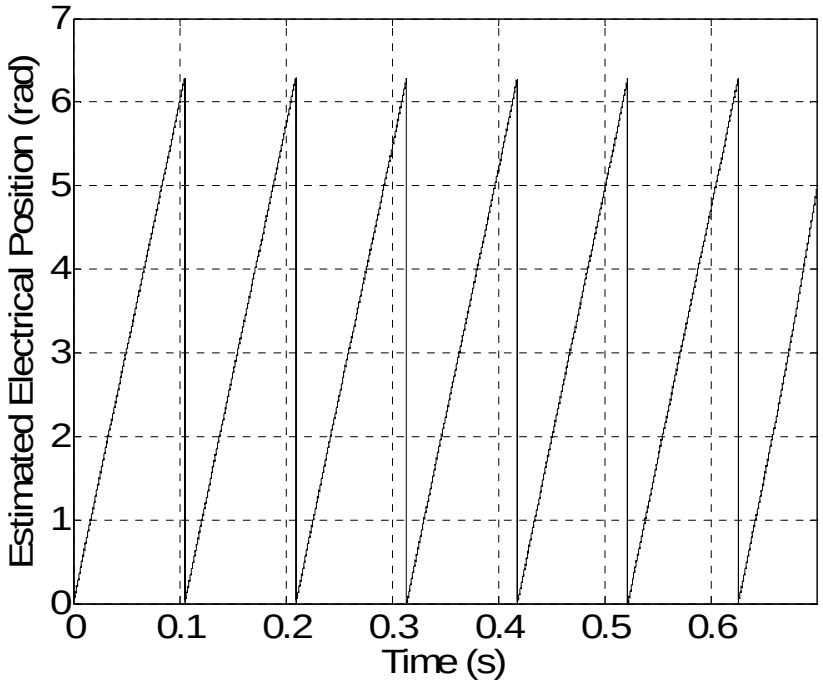

(a)

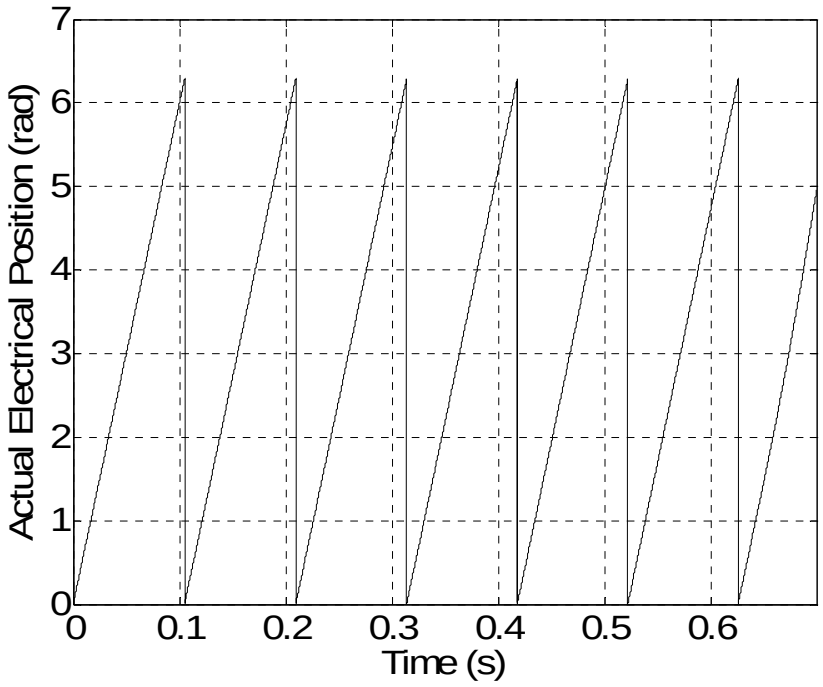

(b)

Fig. 5.8. Steady-state and transient behavior of (a) estimated electrical rotor position, (b) actual electrical rotor position under 0.5 N·m load torque.

Figs. 5.9 and 5.10 show the actual *ba–ca* frame back-EMF constants versus electrical rotor position ($k_{ba}(\theta_e)$ and $k_{ca}(\theta_e)$) obtained offline using the constant-speed test in generation mode. Line-to-line back-EMF constants according to the electrical rotor position are converted to the *dq* frame equivalents ($k_d(\theta_e)$ and $k_q(\theta_e)$) using (5.15) as shown in Fig. 5.10 and then they are set up in the look-up table for torque estimation.

q– and *d*–axis currents used in (5.32) are illustrated in Fig. 5.11 from top to bottom, respectively under 0.5 N·m load torque. At 0.65 second the torque reference is increased and the change in the *q*–axis frame current is noted in Fig. 5.11. In the same figure, *q*–axis current fluctuates around a dc offset to obtain smooth electromagnetic torque. It is seen in Fig. 5.11 that the *d*–axis current oscillates around the desired zero reference value which means that the stator flux amplitude equals the magnet flux.

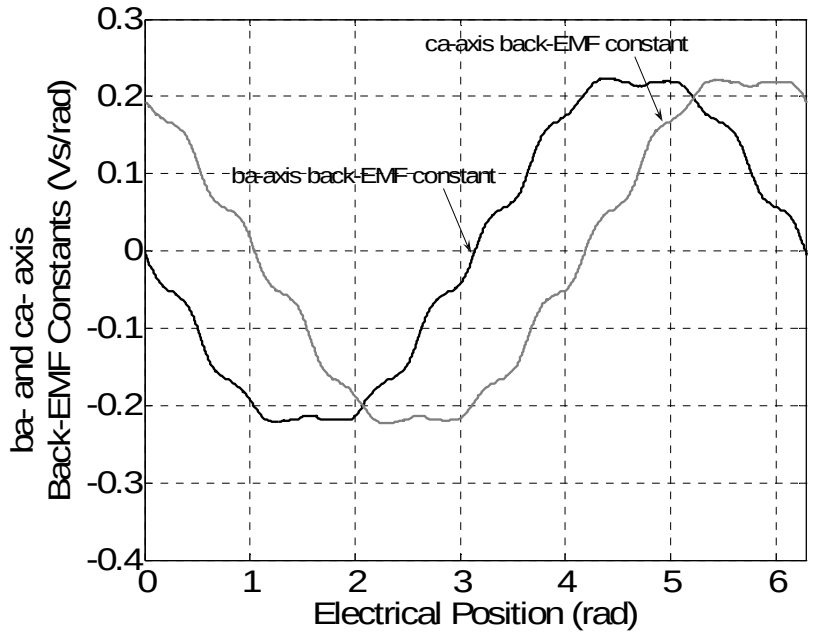

Fig. 5.9. Actual *ba–ca* frame back-EMF constants versus electrical rotor position ($k_{ba}(\theta_e)$ and $k_{ca}(\theta_e)$).

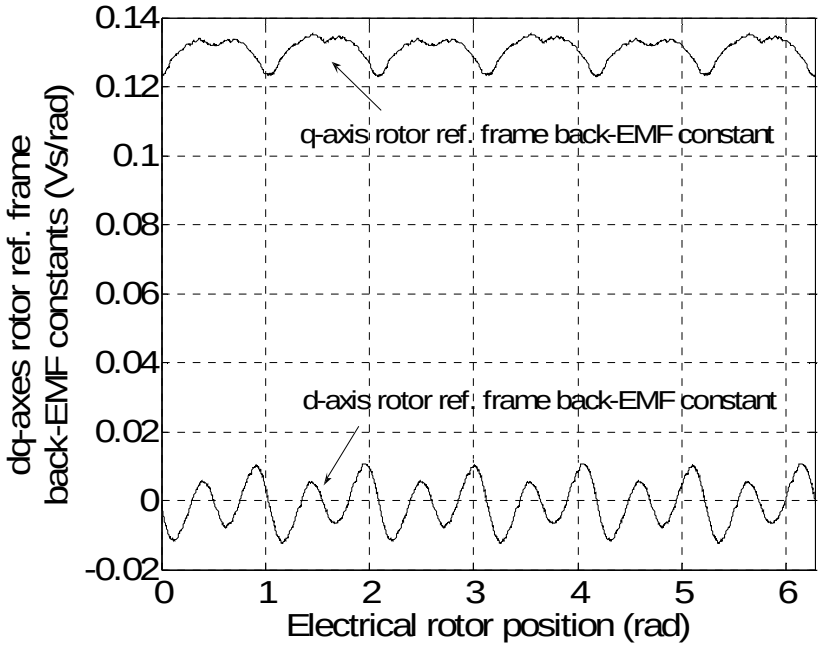

Fig. 5.10. Actual *q*– and *d*–axis rotor reference frame back-EMF constants versus electrical rotor position ($k_q(\theta_e)$ and $k_d(\theta_e)$).

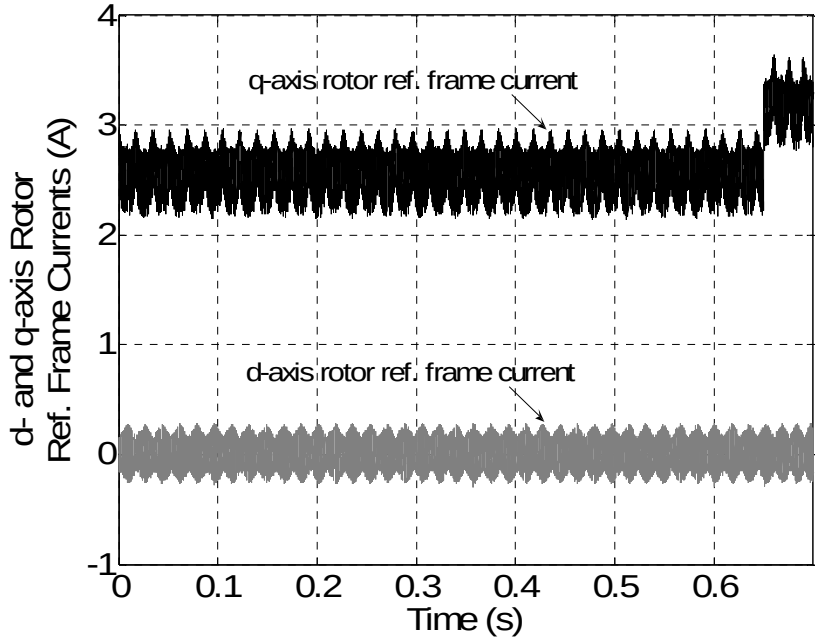

Fig. 5.11. Steady-state and transient behavior of the simulated *q*– and *d*–axis rotor reference frame currents when i_{ds}^{r*} = 0 under 0.5 N·m load torque.

5.5. Experimental Results

The feasibility and practical features of the proposed three-phase conduction DTC of a BLDC motor drive scheme have been evaluated using an experimental test-bed, as shown in Fig. 5.12. The proposed control algorithm is digitally implemented using the eZdsp^{TM} board from Spectrum Digital, Inc. based on TMS320F2812 DSP, as shown in Fig 5.12(a). In Fig. 5.12(b), the BLDC motor whose parameters are given in the Appendix A is coupled to the overall system. The sampling interval is 15 μs. The magnitudes of the torque and flux hysteresis bands are 0.001 N·m, and 0.001 Wb, respectively. The steady-state speed is 30 mechanical rad/s and the dc-link voltage V_{dc} equals $40\sqrt{2}$ V. The experimental results are obtained from the datalog (data logging) module in the Texas Instruments Code Composer Studio^{TM} IDE software.

Implementations of steady-state and transient torque and line-to-line current responses of the proposed DTC of a BLDC motor drive scheme are demonstrated in Fig. 5.13(a) and (b), respectively under 0.5 N·m load torque condition. The torque reference is changed abruptly from 0.52 N·m to 0.65 N·m at 0.425 second. As seen in Fig. 5.13(a) that fast torque response is obtained and the estimated torque tracks the reference torque closely. Reference torque value in experimental test is selected a little bit higher than the load torque to compensate the friction of the total experimental system such that the rotor speed is kept at steady-state level (30 mechanical rad/s). Since there was no torque-meter coupled to the system, actual torque value was not available for comparison purpose. The high frequency ripples observed in the torque and current are related to the sampling time, hysteresis bandwidth, winding inductance, and dc-link voltage. Those

ripples can be minimized by properly selecting the dc-link voltage and torque hysteresis band size. It can be seen in Fig. 5.13(b) that the top of the *ba–ca* frame currents are reciprocal of the corresponding back-EMFs to generate smooth torque profile.

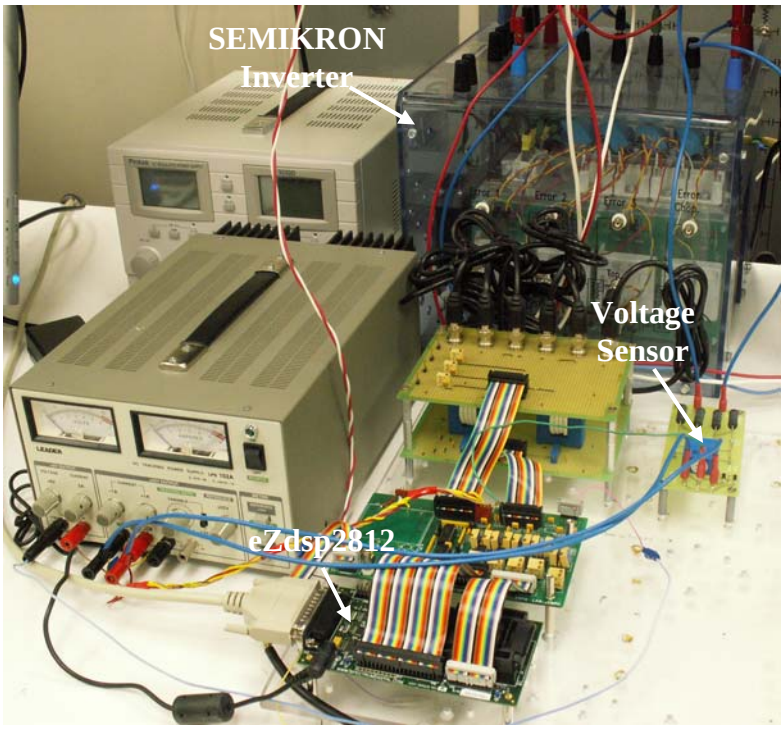

(a)

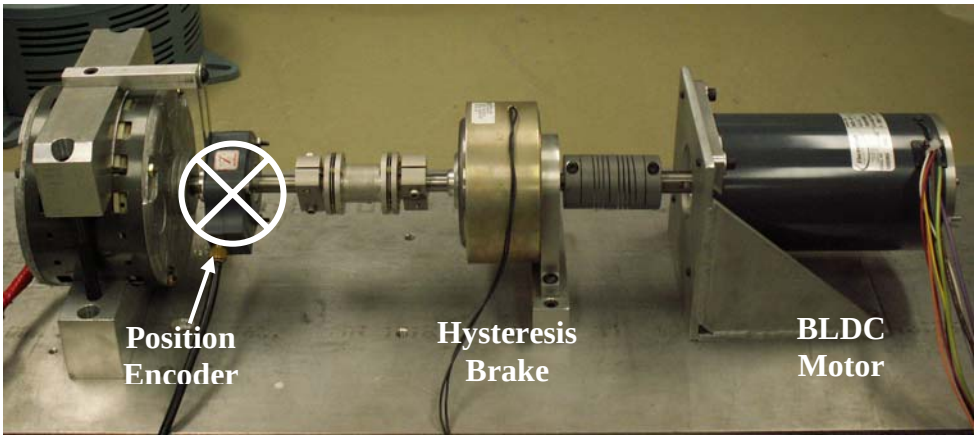

(b)

Fig. 5.12. Experimental test-bed. (a) Inverter and DSP control unit. (b) BLDC motor coupled to dynamometer and position encoder (2048 pulse/rev) is not used.

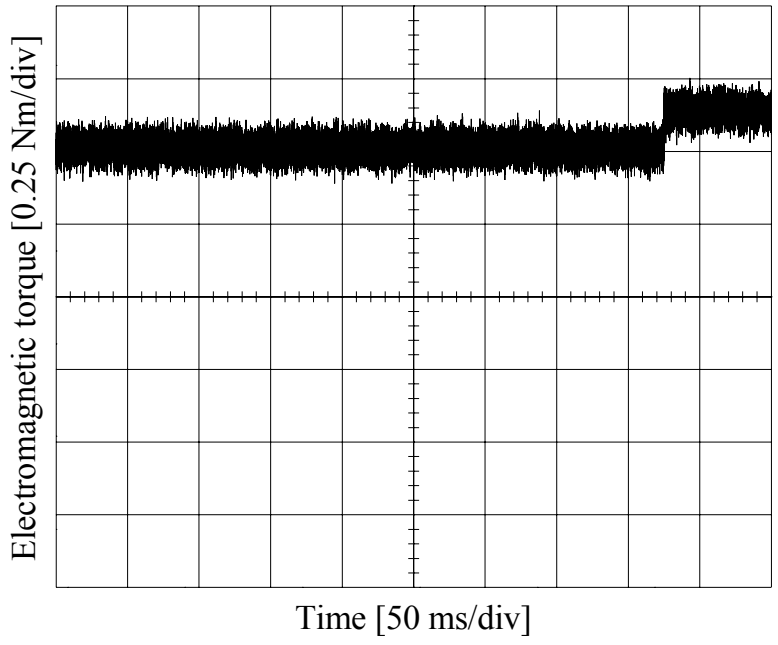

(a)

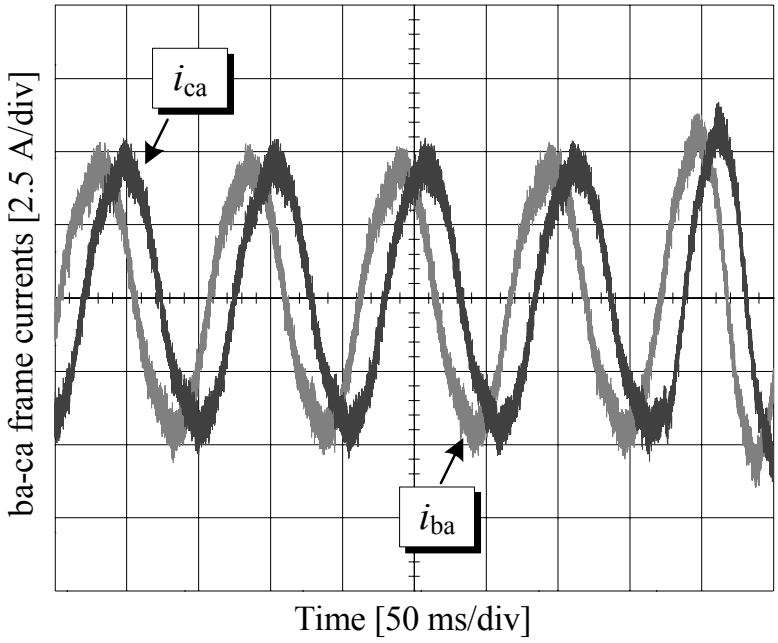

(b)

Fig. 5.13. Steady-state and transient behavior of the experimental (a) estimated electromagnetic torque and (b) *ba–ca* frame currents under 0.5 N·m load torque.

The $\alpha\beta$–axes stator flux linkages are estimated using (5.36) in which the $\alpha\beta$–axes voltages are measured using a dc-link voltage sensor and the estimated position of the stator flux linkage vector θ_s. The motor is initially locked at zero position (phase–a) for proper starting. Although stator flux linkage amplitude is not directly used in the control scheme, its position in the look-up table is quite important for proper voltage vector selection as shown in Fig. 5.4. However, the amplitudes of the $\alpha\beta$–axes stator flux linkages are required in the estimation for the electrical rotor position algorithm. Since the voltage model is used to estimate the stator flux linkages, eliminating any dc offsets generated by the measurement devices is quite important in the proposed control scheme. Therefore, the stator flux linkage is estimated using an effective integration algorithm with an amplitude limiter as shown in Fig. 5.3. The cut-off frequency ω_c in the stator flux linkage estimation algorithm is selected as 20 rad/s which is capable of accurately obtaining the stator flux over a wide speed range (0-100). Fig. 5.14 shows the experimental results of the indirectly controlled stator flux linkage locus by controlling the d–axis rotor reference frame current at 0 A when 0.5 N·m load torque is applied to the BLDC motor. The dodecagon shape in the stator flux locus is observed in Fig. 5.14 due to the non-sinusoidal waveform of the actual back-EMFs. Because the actual line-to-line back-EMF is not completely uniform over one electrical cycle, peak value of the stator flux linkage along the trajectory ($\alpha\beta$ frame) may vary slightly. It is seen in Fig. 5.14 that the amplitude of the stator flux linkage, which is the amplitude of the magnet flux linkage, is indirectly controlled quite well at its required value in the constant torque

region. In the same figure, it is noted that the amplitude of the magnet flux varies non-sinusoidally as expected.

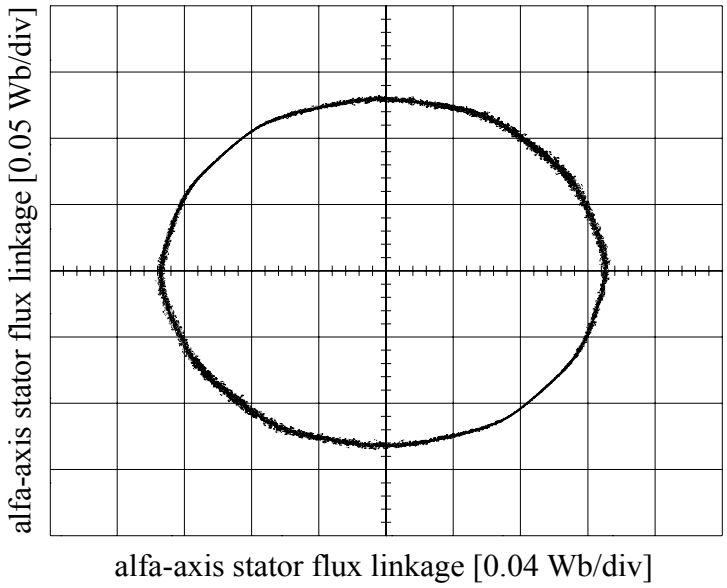

Fig. 5.14. Experimental indirectly controlled stator flux linkage trajectory under the sensorless three-phase conduction DTC of a BLDC motor drive when $i_{ds}^{r*} = 0$ at 0.5 N·m load torque.

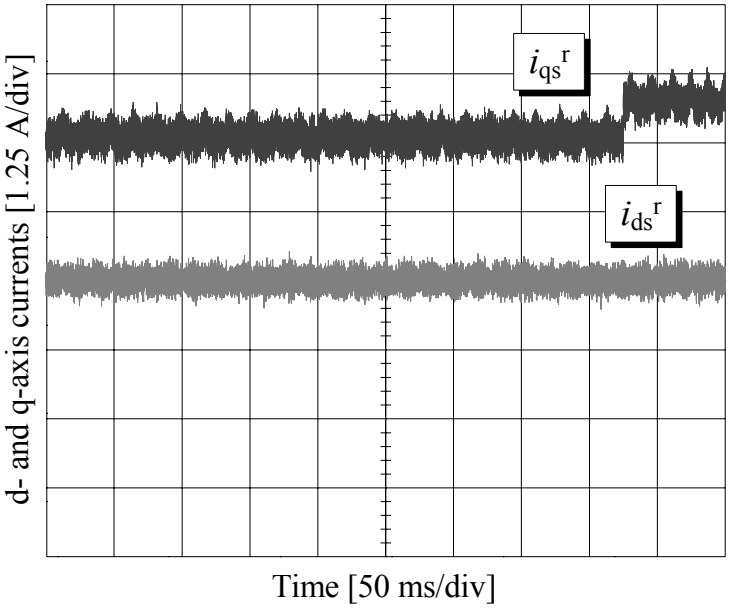

Fig. 5.15. Steady-state and transient behavior of the experimental *q*– and *d*–axis rotor reference frame currents when $i_{ds}^{r*} = 0$ under 0.5 N·m load torque.

q– and *d*–axis currents used in (5.32) are illustrated in Fig. 5.15 from top to bottom, respectively under 0.5 N·m load torque. At 0.425 second the torque reference is increased and the change in the *q*–axis frame current is noted in Fig. 5.15. In the same figure, *q*–axis current fluctuates around a dc offset to obtain smooth electromagnetic torque. It is seen in Fig. 5.15 that the *d*–axis current oscillates around the desired zero reference value which means that the stator flux amplitude equals the magnet flux.

Actual and estimated electrical rotor positions are shown in Fig. 5.16 from top to bottom, respectively. Experimental estimated electrical rotor position is capable of tracking the actual position quite well. Because the estimation algorithm depends on the winding inductance as well as resistance, their variations should be considered. However, this is left as a future research study.

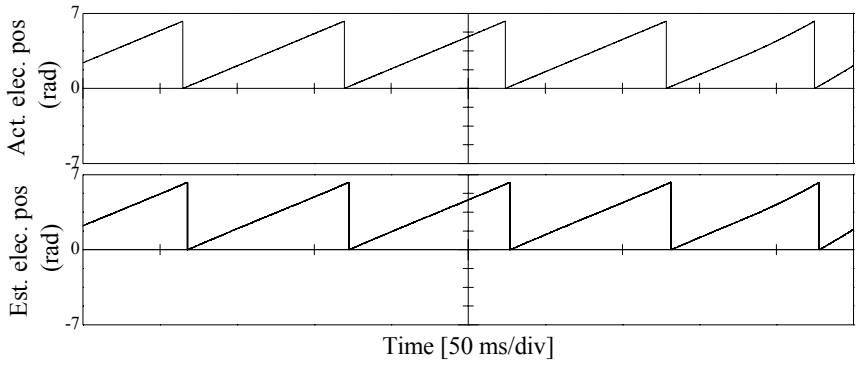

Fig. 5.16. Steady-state and transient behavior of the actual and estimated electrical rotor positions from top to bottom under 0.5 N·m load torque.

26143 data for each line-to-line back-EMF (e_{ba} and e_{ca}) is obtained using an oscilloscope. Then, it is converted to back-EMF constant (k_d and k_q) and down sampled to 252 data in Matlab/Simulink for real-time DSP implementation. Moreover, to obtain a

much realistic result linear interpolation technique is performed on the 252 data in the DSP implementation.

5.6. Conclusion

This study has successfully demonstrated application of the proposed position sensorless three-phase conduction direct torque control (DTC) scheme for BLDC motor drives. It is shown that the BLDC motor could also operate in the field-weakening region by properly selecting the *d*–axis current reference in the proposed DTC scheme. First, practically available actual two line-to-line back-EMF constants (k_{ba} and k_{ca}) versus electrical rotor position are obtained using generator test and converted to the *dq* frame equivalents using the new Line-to-Line Park Transformation in which only two input variables are required. Then, they are used in the torque estimation algorithm. Electrical rotor position required in the torque estimation is obtained using winding inductance, stationary reference frame currents and stator flux linkages.

Since the actual back-EMF waveforms are used in the torque estimation, low-frequency torque oscillations can be reduced convincingly compared to the one with the ideal-trapezoidal waveforms having 120 electrical degree flat top. A look-up table for the three-phase voltage vector selection is designed similar to a DTC of PMSM drive to provide fast torque and flux control. Because the actual rotor flux linkage is not sinusoidal, stator flux control with constant reference is not viable anymore. Therefore, indirect stator flux control is performed by controlling the flux related *d*–axis current using bang-bang (hysteresis) control which provides acceptable control of time-varying signals (reference and/or feedback) quite well. Since the proposed DTC scheme does not

involve any PWM strategies, PI controllers as well as inverse Park and Clarke Transformations to drive the motor, much simpler overall control is achieved.

CHAPTER VI

SUMMARY AND FUTURE WORK

This work presented the direct torque control (DTC) techniques, implemented in four- and six-switch inverter, for brushless dc (BLDC) motors with non-sinusoidal back-EMF using two and three-phase conduction modes.

In Chapter II, the proposed two-phase conduction mode for DTC of BLDC motors is introduced as opposed to the conventional three-phase conduction DTC of PMSM drives in the constant torque region. Much faster torque response is achieved compared to conventional PWM current and especially voltage control techniques. It is also shown that in the constant torque region under the two-phase conduction DTC scheme, the amplitude of the stator flux linkage cannot easily be controlled due to the sharp changes and the curved shape of the flux vector between two consecutive commutation points in the stator flux linkage locus. Furthermore, to eliminate the low-frequency torque oscillations caused by the non-ideal trapezoidal shape of the actual back-EMF waveform of the BLDC motor, pre-stored back-EMF constants in $\alpha\beta$–axes versus electrical rotor position look-up tables are designed and used in the torque estimation algorithm.

In Chapter III, the avarege current controlled boost power factor correction (PFC) method is applied to the previously discussed proposed DTC of BLDC motor drive in the constant torque region. The duty cycle of the boost converter is determined

by a control algorithm. This control algorithm is based on the input voltage, output voltage which is the dc-link of the BLDC motor drive, and the inductor current using the average current control method with input voltage feed-forward compensation during each sampling period of the drive system. The test results verify that the proposed PFC for DTC of BLDC motor drive improves the power factor from 0.77 to about 0.9997 irrespective of the load.

In Chapter IV, the DTC technique for BLDC motor using four-switch inverter in the constant torque region is studied. The results show that the direct torque controlled four-switch three-phase BLDC motor drive could be a good alternative to the conventional six-switch counterpart with respect to low cost and high performance. Since the flux control and PWM generation are removed in the above two methods, fewer algorithms are required for the proposed control schemes.

Finally, the position sensorless direct torque and indirect flux control (DTIFC) of BLDC motor with non-sinusoidal (non-ideal trapezoidal) back-EMF has been extensively investigated using three-phase conduction scheme with six-switch inverter. In the literature, several methods have been proposed to eliminate the low-frequency torque pulsations for BLDC motor drives such as Fourier series analysis of current waveforms and either iterative or least-mean-square minimization techniques. Most methods do not consider the stator flux linkage control, therefore possible high-speed operations are not feasible. In this work, a novel and simple approach to achieve a low-frequency torque ripple-free direct torque control with maximum efficiency based on *dq* reference frame similar to permanent magnet synchronous motor (PMSM) drives is

presented. The electrical rotor position is estimated using winding inductance, and the stationary reference frame stator flux linkages and currents. The proposed sensorless DTC method controls the torque directly and stator flux amplitude indirectly using *d*–axis current. Since stator flux is controllable, flux-weakening operation is possible. Moreover, this method also permits to regulate the varying references. Simple voltage vector selection look-up table is designed to obtain fast torque and flux control. Furthermore, to eliminate the low-frequency torque oscillations, two actual and easily available line-to-line back-EMF constants (k_{ba} and k_{ca}) according to electrical rotor position are obtained offline and converted to the *dq* frame equivalents using the new Line-to-Line Park Transformation. Then, they are set up in the look-up table for torque estimation.

Theoretical concepts are developed, and the validity and effectiveness of the proposed three-phase conduction DTC of BLDC motor drive scheme discussed above are verified through the simulations and experimental results.

Possible future research of the previously explained DTC of BLDC motor drive techniques will be discussed in the following:

In Chapter II and IV, a position estimation technique can be used both in six- and four-switch DTC of BLDC motor drive instead of an expensive and bulky position encoder for a cost-effective system. When back-EMF estimation method is selected as a position sensorless technique, parameter variations should also be considered especially in low speed region. Because at very low speeds the back-EMF information is very weak and quite comparable with the supply voltage, any variation in resistance in conjunction

with current and voltage sensing errors (offset errors causing a drift in integration) will degrade the flux estimation and the overall system may become unstable.

In Chapter III, the power factor control technique can be coupled with the proposed two-phase conduction DTC of BLDC motor drive to improve the current and torque performance at high dc-link voltage conditions while keeping the dc-link voltage fluctuations at minimum and power factor at maximum level.

In Chapter IV, the control of phase torque (T_{ea} and T_{eb}) can be replaced with the line-to-line torque control which eliminates the need for phase back-EMFs, therefore easily available line-to-line back-EMFs can be used in the torque control scheme.

In Chapter V, resistance, inductance and even back-EMF constant variations can be updated online for adaptive control to improve the efficiency and controllability of the overall system in any conditions. Back-EMF used in the torque estimation algorithm can be obtained in real-time instead of the offline look-up table method. Accuracy of the real-time back-EMF information which is used in the torque equation can be analyzed and compared with the look-up table method. Results of the overall control when torque is estimated with online back-EMF and with look-up table can be compared under low speed and saturation conditions. Effects of the back-EMF constant variations can also be studied in both cases.

When the motor speed is above the rated (base) speed, the motor torque decreases very quickly since the back-EMF rapidly approaches the dc-link voltage if the small switch voltage drops are ignored. Eventually, the current (torque) regulators saturate, losing the ability to force the commanded current into the motor phase. In order

to solve this problem, the flux-weakening technique can be developed for the proposed DTC of BLDC motor drive in which the properly selected negative *d*–axis current should be applied to weaken the field produced by the permanent magnet rotor considering the voltage and current limitations of the BLDC machine.

Moreover, SVPWM technique can be combined with the proposed sensorless direct torque and indirect flux control (DTIFC) method to reduce the current and torque ripples while keeping the robustness in the torque control. Also, instead of six-switch inverter four-switch one as in Chapter IV can be used to minimize the cost of the overall system.

Because the possible mechanical/magnetic discrepancy of the rotor magnets over one mechanical rotation using actual back-EMF data containing one complete mechanical cycle will be more effective to eliminate the low-frequency torque ripples in the proposed DTC of BLDC motor drives. If the pole number of the machine is high more data is required to obtain the back-EMF in one mechanical cycle. Therefore, the memory requirement will be increased.

REFERENCES

[1] K. Hasse, “Drehzahlgelverfahren für schnelle umkehrantriebe mit stromrichtergespeisten asynchron-kurzschlusslaufer-motoren,” *Reglungstechnik*, vol. 20, pp. 60–66, 1972.

[2] S. P. Waikar, “A low-cost low-loss brushless permanent magnet motor drive.” Ph.D. dissertation, Texas A&M University, College Station, TX, 2001.

[3] J. Luukko, “Direct torque control of permanent magnet synchronous machines - analysis and implementation.” Ph.D. dissertation, Lappeenranta University of Technology, Lappeenranta , Finland, 2000.

[4] I. Takahashi and T. Noguchi, “A new quick-response and high efficiency control strategy of an induction machine,” *IEEE Trans. Ind. Appl.*, vol. IA–22, pp. 820–827, Sep./Oct. 1986.

[5] U. Baader, M. Depenbrock, and G. Gierse, “Direct self control (DSC) of inverter-fed-induction machine—A basis for speed control without speed measurement,” *IEEE Trans. Ind. Appl.*, vol. 28, pp. 581–588, May/Jun. 1992.

[6] M. Depenbrock, “Direct self control of inverter-fed induction machines,” *IEEE Trans. Power Electron.*, vol. 3, pp. 420–429, Oct. 1988.

[7] M. Depenbrock, “Direct self-control of the flux and rotary moment of a rotary-field machine,” U.S. Patent 4 678 248, Jul. 7, 1987.

[8] P. Vas, *Vector Control of AC Machines*. London, U.K.: Oxford Univ. Press, 1990.

[9] C. French and P. Acarnley, “Direct torque control of permanent magnet drives,” *IEEE Trans. Ind. Appl.*, vol. IA–32, pp. 1080–1088, Sep./Oct. 1996.

[10] L. Zhong, M. F. Rahman, W. Y. Hu, and K. W. Lim, “Analysis of direct torque control in permanent magnet synchronous motor drives,” *IEEE Trans. Power Electron.*, vol. 12, pp. 528–536, May 1997.

[11] I. Takahashi and T. Noguchi, “Take a look back upon the past decade of direct torque control,” in *Proc. IEEE-IECON Annu. Meeting*, vol. 2, 1997, pp. 546–551.

[12] D. Casadei, G. Serra, and A. Tani, “Implementation of a direct torque control algorithm for induction motors based on discrete space vector modulation,” *IEEE Trans. Power Electron.*, vol. 15, pp. 769–777, Jul. 2000.

[13] C. G. Mei, S. K. Panda, J. X. Xu, and K. W. Lim, “Direct torque control of induction motor-variable switching sectors,” in *Proc. IEEE-PEDS Annu. Meeting*, Hong Kong, Jul. 1999, pp. 80–85.

[14] A. Tripathi, A. M. Khambadkone, and S. K. Panda, “Space-vector based, constant frequency, direct torque control and dead beat stator flux control of ac machines,” in *Proc. IEEE-IECON Annu. Meeting*, Nov. 2001, pp. 1219–1224.

[15] C. Lascu, I. Boldea, and F. Blaabjerg, “A modified direct torque control for induction motor sensorless drive,” *IEEE Trans. Ind. Appl.*, vol. 36, pp. 122–130, Jan./Feb. 2000.

[16] D. Swierczynski, M. Kazmierkowski, and F. Blaabjerg, “DSP based direct torque control of permanent magnet synchronous motor (PMSM) using space vector modulation (DTC-SVM),” in *Proc. IEEE-ISIE Annu. Meeting*, vol. 3, May 2002, pp. 723–727.

[17] L. Tang , L. Zhong, M. F. Rahman, and Y. Hu “A novel direct torque control for interior permanent-magnet synchronous machine drive with low ripple in torque and flux-a speed-sensorless approach,” in *Proc. IEEE Trans. Ind. Appl.*, vol. 39, pp. 1748–1756, Nov./Dec. 2003.

[18] C. Martins, X. Roboam, T. A. Meynard, and A. S. Caryalho, “Switching frequency imposition and ripple reduction in DTC drives by using a multilevel converter,” *IEEE Trans. Power Electron.*, vol. 17, pp. 286–297, Mar. 2002.

[19] Y. A. Chapuis, D. Roye, and J. Davoine, “Principles and implementation of direct torque control by stator flux orientation of an induction motor,” in *Conf. Rec. IEEE-IAS Annu. Meeting*, vol. 1, 1995, pp. 185–191.

[20] B. K. B. And and N. R. Patel, “A programmable cascaded low-pass filter-based flux synthesis for a stator flux-oriented vector-controlled induction motor drive,” *IEEE Trans. Ind. Electron.*, vol. 44, pp. 140–143, Feb. 1997.

[21] M. R. Zolghadri and D. Roye, “A fully digital sensorless direct torque control system for synchronous machine,” *Elect. Mach. Power Syst.*, vol. 26, pp. 709–721, 1998.

[22] P. Vas. *Sensorless Vector and Direct Torque Control*. London, U.K.: Oxford Univ. Press, 1998.

[23] M. F. Rahman, Md. E. Haque, L. Tang, and L. Zhong, “Problems associated with the direct torque control of an interior permanent-magnet synchronous motor drive and their remedies,” *IEEE Trans. Ind. Electron.*, vol. 51, pp. 799–809, Aug. 2004.

[24] S. Mir, M. E. Elbuluk, and D. S. Zinger, “PI and fuzzy estimators for tuning the stator resistance in direct torque control of induction machines,” *IEEE Trans. Power Electron.*, vol. 13, pp. 279–287, Mar. 1998.

[25] L. Zhong, M. F. Rahman, K. W. Lim, Y. Hu, and Y. Xu, “A fuzzy observer for induction motor stator resistance for application in direct torque control,” in *Proc. IEEE-PEDS Annu. Meeting*, 1997, pp. 91–96.

[26] B. S. Lee and R. Krishnan, “Adaptive stator resistance compensator for high performance direct torque controlled induction motor drive,” in *Conf. Rec. IEEE-IAS Annu. Meeting*, St. Louis, MO, 1998, pp. 423–423.

[27] M. E. Haque and M. F. Rahman, “Influence of stator resistance variation on direct torque controlled interior permanent magnet synchronous motor drive performance and its compensation,” in *Proc. IEEE-IAS Annu. Meeting*, 2001, pp. 2563–2569.

[28] R. Dhaouadi, N. Mohan, and L. Norum, “Design and implementation of an extended Kalman filter for the state estimation of a permanent magnet synchronous motor,” *IEEE Trans. Power Electron.*, vol. 6, no. 3, pp. 491–497, 1991.

[29] M. Schroedl, “Sensorless control of ac machines at low speed and standstill based on the “INFORM” method,” in *Proc. IEEE-IAS Annu. Meeting*, San Diego, CA, Oct. 6–10, 1996, pp. 270–277.

[30] M. Schroedl, “Sensorless control of permanent magnet synchronous motors,” *Elect. Mach. Power Syst.*, vol. 22, no. 2, pp. 173–185, Mar./Apr. 1994.

[31] R. B. Sepe and J. H. Lang, “Real-Time observer-based (adaptive) control of a permanent-magnet synchronous motor without mechanical sensors,” *IEEE Trans. Ind. Appl.*, vol. 28, pp. 1345–1352, Nov./Dec. 1992.

[32] A. B. Kulkarni and M. Ehsani, “A novel position sensor elimination technique for the interior permanent magnet synchronous motor drive,” *IEEE Trans. Ind. Appl.*, vol. 28, pp. 144–150, Jan./Feb. 1992.

[33] S. Ogasawara and H. Akagi, “An approach to real time position estimation at zero and low speed for a PM motor based on saliency,” in *Proc. IEEE-IAS Annu. Meeting*, San Diego, CA, Oct. 6–10, 1996, pp. 29–35.

[34] S. Ostlund and M. Brokemper, “Sensorless rotor-position detection from zero to rated speed for an integrated PM synchronous motor drive,” *IEEE Trans. Ind. Appl.*, vol. 32, pp. 1158–1165, Sep./Oct. 1996.

[35] P. B. Schmidt, M. L. Gasperi, G. Ray, and A. H. Wijenayake, “Initial rotor angle detection of a nonsalient pole permanent magnet synchronous machine,” in *Proc. IEEE-IAS Annu. Meeting*, New Orleans, LA, Oct. 5–9, 1997, pp. 549–463.

[36] T. Noguchi, K. Yamada, S. Kondo, and I. Takahashi, “Initial rotor position estimation method of sensorless PM motor with no sensitivity to armature resistance,” *IEEE Trans. Ind. Electron.*, vol. 45, pp. 118–125, Feb. 1998.

[37] M. W. Degner and R. D. Lorenz, “Using multiple saliencies for the estimation of flux, position, and velocity in ac machines,” in *Proc. IEEE-IAS Annu. Meeting*, New Orleans, LA, Oct. 5–9, 1997, pp. 760–767.

[38] M. J. Corley and R. D. Lorenz, “Rotor position and velocity estimation for a salient-pole permanent magnet synchronous machine at standstill and high speeds,” *IEEE Trans. Ind. Appl.*, vol. 34, pp. 784–789, Jul./Aug. 1998.

[39] A. Consoli, G. Scarcella, and A. Testa, “Sensorless control of ac motors at zero speed,” in *Proc. IEEE-ISIE Annu. Meeting*, vol. 1, Bled, Slovenia, Jul. 1999, pp. 373–379.

[40] B. K. Bose. *Modern Power Electronics and AC Drives*. Upper Saddle River, NJ: Prentice Hall PTR., 2002.

[41] L. Hao, H. A. Toliyat, “BLDC motor full-speed operation using hybrid sliding mode observer,” in *Proc. IEEE-APEC Annu. Meeting*, Miami, FL, Feb. 9-13, 2003, vol. 1, pp. 286-293.

[42] P. Pillay and R. Krishnan, “Application characteristics of permanent magnet synchronous and brushless dc motors for servo drives,” *IEEE Trans. Ind. Appl.*, vol. 27, no. 5, pp. 986–996, Sep./Oct. 1991.

[43] P. J. Sung,W. P. Han, L. H. Man, and F. Harashima, “A new approach for minimum-torque-ripple maximum-efficiency control of BLDC motor,” *IEEE Trans. Ind. Electron.*, vol. 47, no. 1, pp. 109–114, Feb. 2000.

[44] C. French and P. Acarnley, “Direct torque control of permanent magnet drives,” *IEEE Trans. Ind. Appl.*, vol. 32, no. 5, pp. 1080–1088, Sep./Oct. 1996.

[45] S. J. Kang and S. K. Sul, “Direct torque control of brushless dc motor with nonideal trapezoidal back-EMF,” *IEEE Trans. Power Electron.*, vol. 10, no. 6, pp. 796–802, Nov. 1995

[46] S. K. Chung, H. S. Kim, C. G. Kim, and M. J. Youn, “A new instantaneous torque control of PM synchronous motor for high-performance direct-drive applications,” *IEEE Trans. Power Electron.*, vol. 13, no. 3, pp. 388–400, May 1998.

[47] T. S. Low, K. J. Tseng, T. H. Lee, K. W. Lim, and K. S. Lock, “Strategy for the instantaneous torque control of permanent-magnet brushless dc drives,” in *Proc. IEE Elect. Power Appl.*, vol. 137, no. 6, pp. 355–363, Nov. 1990.

[48] T. S. Low, T. H. Lee, K. J. Tseng, and K. S. Lock, “Servo performance of a BLDC drive with instantaneous torque control,” *IEEE Trans. Ind. Appl.*, vol. 28, no. 2, pp. 455–462, Mar./Apr. 1992.

[49] K. Y. Cho, J. D. Bae, S. K. Chung, and M. J. Youn, “Torque harmonics minimization in permanent magnet synchronous motor with back-EMF estimation,” in *Proc IEE Elec. Power Appl.*, vol. 141, no. 6, pp. 323–330, 1994.

[50] D. Grenier, L. A. Dessaint, O. Akhrif, J. P. Louis, “A park-like transformation for the study and the control of a nonsinusoidal brushless dc motor,” in *Proc. IEEE-IECON Annu. Meeting*, Orlando, FL, Nov. 6-10, 1995, vol. 2, pp. 836–843.

[51] F. Bodin, S. Siala, “New reference frame for brushless dc motor drive,” in *Proc. IEE-PEVD Annu. Meeting*, London, UK, Sep. 21-23, 1998, pp. 554-559.

[52] D. Grenier, S. Yala, O. Akhrif, L. A. Dessaint, “Direct torque control of pm ac motor with non-sinusoidal flux distribution using state-feedback linearization techniques,” in *Proc. IEEE-IECON Annu. Meeting*, Aachen, Germany, Aug. 31-Sep. 4, 1998, vol. 3, pp. 1515–1520.

[53] I. Takahashi and T. Noguchi, “A new quick-response and high-efficiency control strategies of an induction motor,” *IEEE Trans. Ind. Appl.*, vol. 22, no. 5, pp. 820–827, Sep./Oct. 1986.

[54] M. Depenbrock, “Direct self-control of inverter-fed induction machine,” *IEEE Trans. Power Electron.*, vol. 3, no. 4, pp. 420–429, Oct. 1988.

[55] L. Zhong, M. F. Rahman, W. Y. Hu, and K. W. Lim, “Analysis of direct torque control in permanent magnet synchronous motor drives,” *IEEE Trans. Power Electron.*, vol. 12, no. 3, pp. 528–536, May 1997.

[56] Y. Liu, Z. Q. Zhu, and D. Howe, “Direct torque control of brushless dc drives with reduced torque ripple,” *IEEE Trans. Ind. Appl.*, vol. 41, no. 2, pp. 599–608, Mar./Apr. 2005.

[57] W. S. H. Wong, D. Holliday, “Constant inverter switching frequency direct torque control,” in *Proc. IEE-PEMD Annu. Meeting*, Bath, UK, Jun. 4-7, 2002, pp. 104–109.

[58] M. Ehsani, R. C. Becerra, “High-speed torque control of brushless permanent magnet motors,” *IEEE Trans. Ind. Electron.*, vol. 35, no. 3, pp. 402–406, Aug. 1988.

[59] P. C. Todd, “UC3854 controlled power factor correction circuit design,” *U-134, Unitrode Application Note*, pp. 3-269–3-288.

[60] R. Redl and B. P. Erisman, “Reducing distortion in peak-current-controlled boost power-factor correctors,” in *Proc. IEEE-APEC Annu. Meeting*, Orlando, FL, Feb. 13-17, 1994, vol. 2, pp. 576–583.

[61] J. Spangler and A. Behera, “A comparison between hysteretic and fixed frequency boost converters used for power factor correction,” in *Proc. IEEE-APEC Annu. Meeting*, San Diego, CA, Mar. 7-11, 1993, pp. 281–286.

[62] R. Zane and D. Maksimovic, “Nonlinear-carrier control for high-power factor rectifiers based on up-down switching converters,” *IEEE Trans. Power Electron.*, vol. 13, no. 2, pp. 213–221, Mar. 1998.

[63] W. Zhang, G. Feng, Y.-F. Liu, and B. Wu, “A digital power factor correction (PFC) control strategy optimized for DSP,” *IEEE Trans. Power Electron.*, vol. 19, no. 6, pp. 1474–1485, Nov. 2004.

[64] M. Fu and Q. Chen, “A DSP based controller for power factor correction in a rectifier circuit,” in *Proc. IEEE-APEC Annu. Meeting*, Anaheim, CA, Mar. 4-8, 2001, pp. 144–149.

[65] S. Buso et al., “Simple digital control improving dynamic performance of power factor pre-regulators,” *IEEE Trans. Power Electron.*, vol. 13, no. 5, pp. 814–823, Sep. 1998.

[66] J. Zhou et al., “Novel sampling algorithm for DSP controlled 2 kW PFC converter,” *IEEE Trans. Power Electron.*, vol. 16, no. 2, pp. 217–222, Mar. 2001.

[67] S. Choudhury, “Average current mode controlled power factor correction converter using TMS320LF2407A,” *Texas Instruments Application Note SPRA902A*, Jul. 2005, pp. 1–14.

[68] H.W. Van Der Broeck and J. D. Van Wyk, “A comparative investigation of a tree-phase induction machine drive with a component minimized voltage-fed inverter under different control options,” *IEEE Trans. Ind. Appl.*, vol. 20, no. 2, pp. 309–320, Mar./Apr. 1984.

[69] B-K. Lee, T-K. Kim and M. Ehsani, “On the feasibility of four-switch three-phase BLDC motor drives for low cost commercial applications: topology and control,” *IEEE Trans. Power. Electron.*, vol. 18, no. 1, pp. 164–172, Jan. 2003.

[70] S-H. Park, T-S. Kim, S-C. Ahn, D-S. Hyun, “A simple current control algorithm for torque ripple reduction of brushless dc motor using four-switch three-phase inverter,” in *Proc. IEEE-PESC Annu. Meeting*, Jun. 15-19, 2003, vol. 2, pp. 574–579.

[71] J-H. Lee, S-C. Ahn, D-S. Hyun, “A BLDCM drive with trapezoidal back EMF using four-switch three phase inverter,” in *Proc. IEEE-IAS Annu. Meeting*, Oct. 8-12, 2000, vol. 3, pp. 1705–1709.

[72] S. B. Ozturk and H. A. Toliyat, “Direct torque control of brushless dc motor with non-sinusoidal back-EMF,” in *Proc. IEEE-IEMDC Biennial Meeting*, Antalya, Turkey, May 3-5, 2007.

[73] H. R. Bolton and R. A. Ashen, “Influence of motor design and feedcurrent waveform on torque ripple in brushless dc drives,” in *Proc. IEE Elect. Power Appl.*, vol. 131, no. 3, pp. 82–90, 1984.

[74] B. H. Ng, M. F. Rahman, and T. S. Low, “An investigation into the effects of machine parameters on torque pulsation in a brushless dc drive,” in *Proc. IEEE-IECON*, 1988, pp. 749–754.

[75] H. L. Huy, R. Perret, and R. Feuillet, “Minimization of torque ripple in brushless dc motor drives,” *IEEE Trans. Ind. Appl.*, vol. 22, no. 4, pp. 748–755, 1986.

[76] F. Piriou, A. Razek, R. Perret, and H. L. Huy, “Torque characteristics of brushless dc motors with imposed current waveform,” in *Proc. IEEE-IAS Annu. Meeting*, 1986, pp. 176–181.

[77] D. Hanselman, “Minimum torque ripple, maximum efficiency excitation of brushless permanent magnet motors,” *IEEE Trans. Ind. Electron.*, vol. 41, no. 3, pp. 292–300, 1994.

[78] N. Matsui, T. Makino, and H. Satoh, “Auto-compensation of torque ripple of DD motor by torque observer,” *IEEE Trans. Ind. Appl.*, vol. 29, no. 1, pp. 187–194, 1993.

[79] T. Kim, H-W Lee, L. Parsa, and M. Ehsani, “Optimal power and torque control of a brushless dc (BLDC) motor/generator drive in electric and hybrid electric vehicles,” in *Proc. IEEE-IAS Annu. Meeting*, 8-12 Oct. 2006, vol. 3, pp. 1276–1281.

[80] P. L. Chapman, S.D. Sudhoff, and C.A. Whitcomb, “Multiple reference frame analysis of non-sinusoidal brushless dc drives,” *IEEE Trans. Eng. Convers.* vol. 143, pp. 440 –446. Sep. 1999.

[81] R. H. Park, “Two-reaction theory of synchronous machines, generalized method of analysis - Part I” *AIEE Trans.*, vol. 48, pp. 716–730, Jul. 1929.

[82] C. M. Ong. *Dynamic Simulation of Electric Machinery Using MATLAB / SIMULINK*. Upper Saddle River, NJ: Prentice Hall PTR, 1998.

[83] J. Hu, B. Wu, “New integration algorithms for estimating motor flux over a wide speed range,” *IEEE Trans. Power Electrons.*, vol. 13, pp. 969–977, Sep. 1998.

APPENDIX A

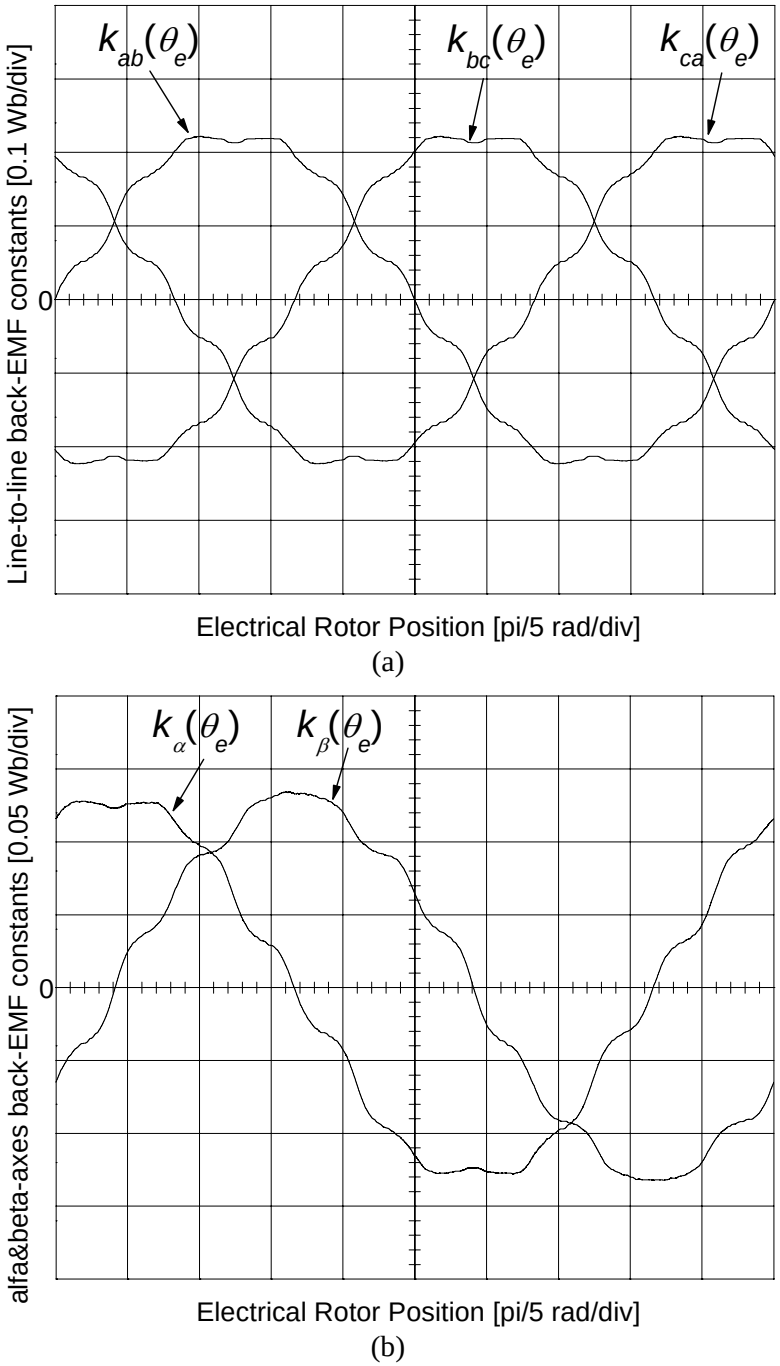

Fig. A.1. (a) Actual line-to-line back-EMF constants ($k_{ab}(\theta_e)$, $k_{bc}(\theta_e)$, and $k_{ca}(\theta_e)$) and (b) stationary reference frame back-EMF constants ($k_{\alpha}(\theta_e)$ and $k_{\beta}(\theta_e)$).

SPECIFICATIONS AND PARAMETERS OF THE BLDC MOTOR

Symbol	Quantity	Value
P	Number of poles	4
V_{LL}	Maximum line-to-line voltage (V_{rms})	115
I_{pk}	Maximum peak current (A)	24
I_{rated}	Rated current (A)	5.6
T_{rated}	Rated torque (N·m)	1.28352
L_s	Winding inductance (mH)	1.4
M	Mutual inductance (mH)	0.3125
R_s	Winding resistance (ohm)	0.315
λ_f	Rotor magnetic flux linkage (Wb)	0.1146
λ_{fmax}	Maximum rotor magnetic flux linkage (Wb)	0.1304

APPENDIX B

The electromagnetic torque equation for a BLDC motor consisting of *ba–ca* reference frame variables can be derived as follows:

The line-to-line components constituting the electromagnetic torque equation can be obtained by using Clarke Transformation which is given by

$$\begin{pmatrix} X_\alpha \\ X_\beta \end{pmatrix} = \frac{2}{3}\begin{pmatrix} 1 & -\frac{1}{2} & -\frac{1}{2} \\ 0 & \frac{\sqrt{3}}{2} & -\frac{\sqrt{3}}{2} \end{pmatrix}\begin{pmatrix} X_a \\ X_b \\ X_c \end{pmatrix} \tag{B.1}$$

where X_α and X_β are the stationary reference frame components, and X_a, X_b, and X_c are the *abc* frame components. X in (B.1) represents currents and/or rotor flux linkages in the electromagnetic torque equation.

If X_α and X_β are expanded and algebraically manipulated, the line-to-line representations of X_α and X_β in *ba–ca* reference frame are attained respectively as

$$\begin{aligned} X_\alpha &= \frac{2X_a - X_b - X_c}{3} = \frac{X_a - X_b + X_a - X_c}{3} \\ &= \frac{-X_{ba} - X_{ca}}{3} \end{aligned} \tag{B.2}$$

and

$$\begin{aligned} X_\beta &= \frac{\sqrt{3}}{3}\left(X_b - X_c\right) = \frac{\sqrt{3}}{3}\left(X_b - X_a + X_a - X_c\right) \\ &= \frac{\sqrt{3}}{3}\left(X_{ba} - X_{ca}\right) \end{aligned} \tag{B.3}$$

where $X_{ba} = X_b - X_a$ and $X_{ca} = X_c - X_a$.

Using the results obtained in (B.2) and (B.3), X_α and X_β can be rewritten in matrix form as

$$\begin{pmatrix} X_\alpha \\ X_\beta \end{pmatrix} = \begin{pmatrix} -\frac{1}{3} & -\frac{1}{3} \\ \frac{\sqrt{3}}{3} & -\frac{\sqrt{3}}{3} \end{pmatrix} \begin{pmatrix} X_{ba} \\ X_{ca} \end{pmatrix} \tag{B.4}$$

If the matrix in (B.4) is used in (2.16), the electromagnetic torque equation in terms of *ba–ca* frame line-to-line components can be expressed as follows:

$$T_{em} = \frac{3}{2}\frac{P}{2}\left\{ \frac{d\left(-1/3\varphi_{rba} - 1/3\varphi_{rca}\right)}{d\theta_e}(-1/3i_{ba} - 1/3i_{ca}) + \frac{d\left(\sqrt{3}/3\varphi_{rba} - \sqrt{3}/3\varphi_{rca}\right)}{d\theta_e}(\sqrt{3}/3i_{ba} - \sqrt{3}/3i_{ca}) \right\} \tag{B.5}$$

After algebraically simplifying (B.5), the electromagnetic torque equation is obtained as

$$T_{em} = \frac{P}{6}\left[\left(\frac{2d\varphi_{rba}}{d\theta_e} - \frac{d\varphi_{rca}}{d\theta_e} \right) i_{ba} + \left(\frac{2d\varphi_{rca}}{d\theta_e} - \frac{d\varphi_{rba}}{d\theta_e} \right) i_{ca} \right] \tag{B.6}$$

where P is the pole number, $d\varphi_{rba}/d\theta_e$ and $d\varphi_{rca}/d\theta_e$ are the derivatives of the *ba*– and *ca*–axis rotor flux linkages over electrical rotor position, $i_{ba} = i_b - i_a$, and $i_{ca} = i_c - i_a$.

If (B.6) is rewritten in terms of line-to-line back-EMFs the torque equation can be given in the following:

$$T_{em} = \frac{P}{6}\left[\left(\frac{2e_{ba} - e_{ca}}{\omega_e} \right) i_{ba} + \left(\frac{2e_{ca} - e_{ba}}{\omega_e} \right) i_{ca} \right] \tag{B.7}$$

where $e_{ba} = e_b - e_a$, $e_{ca} = e_c - e_a$, and ω_e is the electrical rotor speed. As a result, two line-to-line back-EMFs (e_{ba}, e_{ca}) and currents (i_{ba}, i_{ca}) are enough to estimate the electromagnetic torque. The problematic electrical rotor speed ω_e in (B.7) can be removed if the two electrical rotor position dependant line-to-line back-EMF constants are used in the electromagnetic torque equation which is given by

$$T_{em} = \frac{P}{6}\left[\left(2k_{ba}(\theta_e) - k_{ca}(\theta_e)\right)i_{ba} + \left(2k_{ca}(\theta_e) - k_{ba}(\theta_e)\right)i_{ca}\right] \tag{B.8}$$

Another torque equation similar to (2.16) using line-to-line model in *ab–bc–ca* reference frame can be obtained as

$$T_{em} = \frac{P}{2}\left(\frac{e_{ab}i_{ab} + e_{bc}i_{bc} + e_{ca}i_{ca}}{3\omega_e}\right) \tag{B.9}$$

where $e_{bc} = e_b - e_c$, and $i_{bc} = i_b - i_c$.

Even though (B.9) has fewer components compared to (B.8), there are additional line-to-line back-EMF and current components in *bc*–axis. Equation (B.9) can further be simplified by removing the electrical rotor speed ω_e in the denominator allowing zero and near zero speed torque estimation possible as follows:

$$T_{em} = \frac{P}{6}\left(k_{ab}(\theta_e)i_{ab} + k_{bc}(\theta_e)i_{bc} + k_{ca}(\theta_e)i_{ca}\right) \tag{B.10}$$

As a result, the electromagnetic torque equations given in (B.8) and (B.10) avoid the use of the line-to-neutral back-EMF components. They only require line-to-line back-EMFs which can be measured directly even if the motor neutral connection is not accessible.

APPENDIX C

Switching functions of the six non-zero voltage space vectors V_1, V_2, ..., V_6 of the six-switch DTC of BLDC motor drive, which are represented in stationary reference frame ($V_{x\alpha}$ and $V_{x\beta}$), can be derived as follows:

Six non-zero voltage space vectors which are used in six-switch DTC of BLDC motor drive can be shown in the following form:

$$V_x(S_1\ S_2\ S_3\ S_4\ S_5\ S_6) \tag{C.1}$$

where x is between 1 and 6, and S_1, S_2,…, S_6 are the switch states. “1” represents on state and “0” is off state of the corresponding switch.

$\alpha\beta$–axes six-switch voltage vectors ($V_{x\alpha}$ and $V_{x\beta}$) can be obtained using Fig. 2.1 as follows:

$$V_1(1\ 0\ 0\ 0\ 0\ 1) \Rightarrow V_{1\alpha} = \frac{\sqrt{3}V_{dc}}{2}, V_{1\beta} = \frac{V_{dc}}{2} \tag{C.2}$$

$$V_2(0\ 0\ 1\ 0\ 0\ 1) \Rightarrow V_{2\alpha} = 0, V_{2\beta} = \frac{V_{dc}}{2} \tag{C.3}$$

$$V_3(0\ 1\ 1\ 0\ 0\ 0) \Rightarrow V_{3\alpha} = -\frac{\sqrt{3}V_{dc}}{2}, V_{3\beta} = \frac{V_{dc}}{2} \tag{C.4}$$

$$V_4(0\ 1\ 0\ 0\ 1\ 0) \Rightarrow V_{4\alpha} = -\frac{\sqrt{3}V_{dc}}{2}, V_{4\beta} = -\frac{V_{dc}}{2} \tag{C.5}$$

$$V_5(0\ 0\ 0\ 1\ 1\ 0) \Rightarrow V_{5\alpha} = 0, V_{5\beta} = -\frac{V_{dc}}{2} \tag{C.6}$$

$$V_6(1\ 0\ 0\ 1\ 0\ 0) \Rightarrow V_{6\alpha} = \frac{\sqrt{3}V_{dc}}{2}, V_{6\beta} = -\frac{V_{dc}}{2} \tag{C.7}$$

By performing some algebraic manipulations on (C.1) through (C.7), the final switching function of $\alpha\beta$–axes four-switch voltage vectors ($V_{x\alpha}$ and $V_{x\beta}$) can be given respectively as

$$V_{x\alpha} = \frac{\sqrt{3}}{2} V_{dc} \left[S_1 \left(S_6 + S_4 \right) - S_2 \left(S_3 + S_5 \right) \right] \tag{C.8}$$

$$V_{x\beta} = \frac{V_{dc}}{2} \left[S_6 \left(S_1 + S_3 \right) + S_2 \left(S_3 - S_5 \right) - S_4 \left(S_5 + S_1 \right) \right] \tag{C.9}$$

APPENDIX D

Switching functions of the eight voltage space vectors V_0, V_1, ..., V_7 of four-switch DTC of BLDC motor drive, which are represented in stationary reference frame ($V_{x\alpha}$ and $V_{x\beta}$), can be derived as follows:

Eight voltage space vectors which are used in four-switch DTC of BLDC motor drive can be shown in the following form:

$$V_x(S_1\ S_2\ S_3\ S_4) \tag{D.1}$$

where x is between 0 and 7, and S_1, S_2,…, S_4 are the switch states. “1” represents on state and “0” is off state of the corresponding switch.

$\alpha\beta$–axes four-switch voltage vectors ($V_{x\alpha}$ and $V_{x\beta}$) can be obtained using Fig. 4.3 as follows:

$$V_1(1\ 0\ 0\ 0) \Rightarrow V_{1\alpha} = \frac{\sqrt{3}V_{dc}}{4}, V_{1\beta} = \frac{V_{dc}}{4} \tag{D.2}$$

$$V_2(0\ 0\ 1\ 0) \Rightarrow V_{2\alpha} = \frac{V_{dc}}{2}, V_{2\beta} = 0 \tag{D.3}$$

$$V_3(0\ 1\ 1\ 0) \Rightarrow V_{3\alpha} = -\frac{\sqrt{3}V_{dc}}{2}, V_{3\beta} = \frac{V_{dc}}{2} \tag{D.4}$$

$$V_4(0\ 1\ 0\ 0) \Rightarrow V_{4\alpha} = -\frac{\sqrt{3}V_{dc}}{4}, V_{4\beta} = -\frac{V_{dc}}{4} \tag{D.5}$$

$$V_5(0\ 0\ 0\ 1) \Rightarrow V_{5\alpha} = -\frac{V_{dc}}{2}, V_{5\beta} = 0 \tag{D.6}$$

$$V_6(1\ 0\ 0\ 1) \Rightarrow V_{6\alpha} = \frac{\sqrt{3}V_{dc}}{2}, V_{6\beta} = -\frac{V_{dc}}{2} \tag{D.7}$$

$$V_0(0\ 1\ 0\ 1) \Rightarrow V_{0\alpha} = \frac{V_{dc}}{6}, V_{0\beta} = \frac{\sqrt{3}V_{dc}}{6} \tag{D.8}$$

$$V_7(1\ 0\ 1\ 0) \Rightarrow V_{7\alpha} = -\frac{V_{dc}}{6}, V_{7\beta} = -\frac{\sqrt{3}V_{dc}}{6} \tag{D.9}$$

By performing some algebraic manipulations on (D.1) through (D.9), the final switching function of $\alpha\beta$–axes four-switch voltage vectors ($V_{x\alpha}$ and $V_{x\beta}$) can be given respectively as

$$V_{x\alpha} = \frac{\sqrt{3}}{4}V_{dc}\left[S_1 - S_2 - S_2S_3 + S_1S_4 + S_2S_4 - S_1S_3 + \frac{2}{3\sqrt{3}}\left(S_2S_4 + S_1S_3\right)\right] \tag{D.10}$$

$$\begin{aligned} V_{x\beta} = \Bigg(&\frac{1}{4}V_{dc}S_1 + 2S_3 + 2S_2S_3 - S_2 - 2S_4 - 2S_1S_4 + 3\left(S_2S_4 - S_1S_3\right) \\ &+ \frac{2\sqrt{3}}{3}\left(S_2S_4 - S_1S_3\right)\Bigg) \end{aligned} \tag{D.11}$$

APPENDIX E

Peak value of the rotor flux linkage in stationary reference frame ($\varphi_{r\alpha\beta(pk)}$) can be derived for a BLDC motor with an ideal trapezoidal back-EMF using easily accessible line-to-line back-EMF waveforms as follows:

Ideal line-to-line back-EMF waveforms (e_{ab}, e_{bc}, e_{ca}) can be illustrated in Fig. E.1 below:

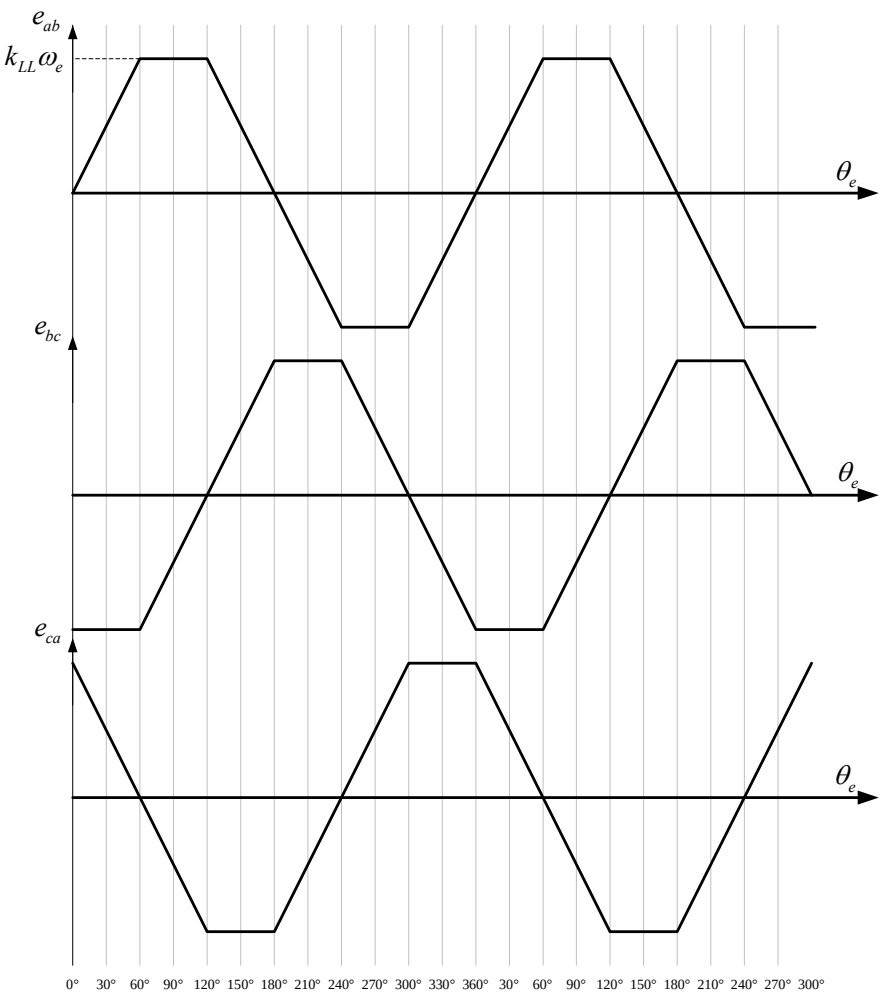

Fig. E.1. Line-to-line back-EMF waveforms (e_{ab}, e_{bc}, and e_{ca}).

Line-to-line back-EMF waveforms (e_{ab}, e_{bc}, e_{ca}) shown in Fig. E.1 are converted to $\alpha\beta$–axes equivalents (e_α, and e_β) using Line-to-Line Clarke Transformation given by

$$\begin{bmatrix} e_\alpha \\ e_\beta \end{bmatrix} = \begin{bmatrix} \frac{2}{3\sqrt{3}} & -\frac{1}{3\sqrt{3}} & -\frac{1}{3\sqrt{3}} \\ 0 & \frac{1}{3} & -\frac{1}{3} \end{bmatrix} \begin{bmatrix} e_{ab} \\ e_{bc} \\ e_{ca} \end{bmatrix} \tag{E.1}$$

Every 60°, e_α, and e_β values can be obtained using (E.1) as follows:

$$\text{At } 0^\circ \Rightarrow \; e_\alpha = 0, \; e_\beta = -\frac{2}{3} k_{LL} \omega_e \tag{E.2}$$

$$\text{At } 60^\circ \Rightarrow \; e_\alpha = \frac{1}{\sqrt{3}} k_{LL} \omega_e, \; e_\beta = -\frac{1}{3} k_{LL} \omega_e \tag{E.3}$$

$$\text{At } 120^\circ \Rightarrow \; e_\alpha = \frac{1}{\sqrt{3}} k_{LL} \omega_e, \; e_\beta = \frac{1}{3} k_{LL} \omega_e \tag{E.4}$$

$$\text{At } 180^\circ \Rightarrow \; e_\alpha = 0, \; e_\beta = \frac{2}{3} k_{LL} \omega_e \tag{E.5}$$

$$\text{At } 240^\circ \Rightarrow \; e_\alpha = -\frac{1}{\sqrt{3}} k_{LL} \omega_e, \; e_\beta = \frac{1}{3} k_{LL} \omega_e \tag{E.6}$$

$$\text{At } 300^\circ \Rightarrow \; e_\alpha = -\frac{1}{\sqrt{3}} k_{LL} \omega_e, \; e_\beta = -\frac{1}{3} k_{LL} \omega_e \tag{E.7}$$

$$\text{At } 360^\circ \Rightarrow \; e_\alpha = 0, \; e_\beta = -\frac{2}{3} k_{LL} \omega_e \tag{E.8}$$

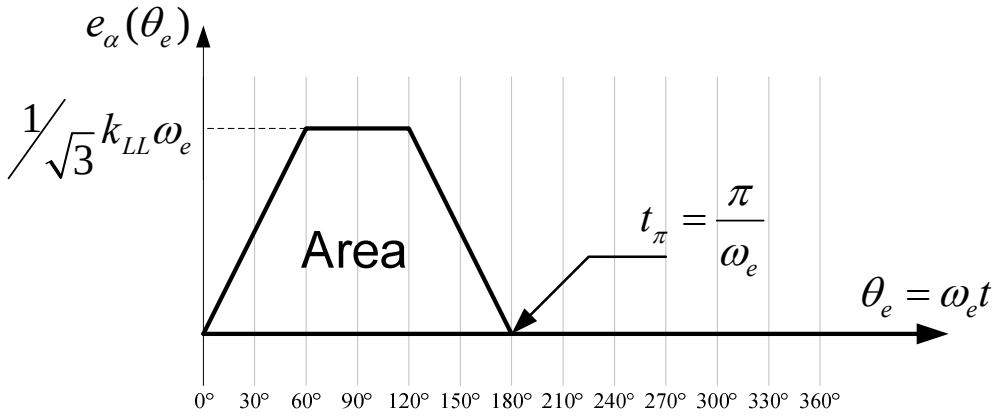

Fig. E.2. α–axis back-EMF (e_α) waveform.

α–axis back-EMF (e_α) can be drawn using (E.2) through (E.8) as shown in Fig. E.2. Finally, the stationary reference frame peak value of the rotor flux linkage $\varphi_{r\alpha\beta(pk)}$ can be found by integrating the α-axis back-EMF (e_α) over time as

$$\varphi_{r\alpha\beta(pk)} = \frac{2\pi k_{LL}}{3\sqrt{3}} \text{ [Wb]} \tag{E.9}$$

The same result in (E.9) can be obtained using only two line-to-line back-EMFs (e_{ba} and e_{ca}) and the proposed Line-to-Line Clarke Transformation with two input variables which is given in (5.10).

VITA

Salih Baris Ozturk received the B.S. degree (Hons.) in electrical engineering from Istanbul Technical University, Istanbul, Turkey, in June 2000. In January 2002, he joined the Electrical Machines and Power Electronics Laboratory research group at Texas A&M University, College Station, TX, where he received the M.S. degree in electrical engineering in December 2005. Prof. Hamid A. Toliyat was his advisor.

Since January 2002, Ozturk has been a graduate researcher and teaching assistant, as well as a lecturer in the Department of Electrical and Computer Engineering at Texas A&M University, and he has served as the EMPE lab manager since 2006. In 2004, he was also with the Whirlpool R&D Center, Benton Harbor, MI.

In May 2008, Ozturk received the Ph.D. degree in electrical engineering at Texas A&M University under the supervision of Prof. Toliyat. His current research interests include power factor correction for ac motor drives, fault diagnosis of electric machinery, electric machine design, and digital signal processor-based advanced control of ac drives, in particular sensorless and direct torque control of permanent magnet assisted synchronous reluctance, permanent magnet synchronous and brushless dc motors.

Ozturk also is one of the contributing authors of the book “DSP-Based Electromagnetic Motion Control,” (Boca Raton, FL: CRC Press, 2003).

Salih Baris Ozturk is a member of the IEEE.

He may be reached in c/o

Prof. Hamid A. Toliyat
Electrical Machines & Power Electronics Laboratory
Department of Computer and Electrical Engineering
TAMU 3128
Texas A&M University
College Station, Texas 77843-3128